The Astrophysical Journal, 997:141 (37pp), 2026 February 1 https://doi.org/10.3847/1538-4357/ae2c4e

Prompt Searches for Very-high-energy γ-Ray Counterparts to IceCube Astrophysical Neutrino Alerts

J. Abhir[1], A. Biland[1], K. Brand[2], T. Bretz[1,175], D. Dorner[2], L. Eisenberger[2], D. Elsaesser[3], P. Günther[2], S. Hasan[1], D. Hildebrand[1], K. Mannheim[2], M. Linhoff[3], F. Pfeifle[2], W. Rhode[3], B. Schleicher[2,176], V. Sliusar[4], M. Vorbrugg[2], R. Walter[4], (FACT Collaboration),
F. Aharonian[5,6,7], F. Ait Benkhali[8], J. Aschersleben[9], H. Ashkar[10], M. Backes[11,12], V. Barbosa Martins[13], R. Batzofin[14], Y. Becherini[15,16], D. Berge[13,17], M. Böttcher[12], C. Boisson[18], J. Bolmont[19], J. Borowska[17], R. Brose[14], A. Brown[20], F. Brun[21], B. Bruno[22], S. Casanova[23], J. Celic[22], M. Cerruti[15], A. Chen[24], M. Chernyakova[5], J. Chibueze[12], O. Chibueze[12], B. Cornejo[21], G. Cotter[20], G. Cozzolongo[22], J. Damascene Mbarubucyeye[13], J. de Assis Scarpin[10], A. Delgado Giles[17], A. Djannati-Ataï[15], J. Djuvsland[6], A. Dmytriiev[12], K. Egberts[14], K. Egg[22], S. Einecke[25], J.-P. Ernenwein[26], C. Escañuela Nieves[6], K. Feijen[15], M. Filipovic[27], G. Fontaine[10], S. Funk[22], S. Gabici[15], J.F. Glicenstein[21], P. Goswami[15], G. Grolleron[19], B. Hess[28], J.A. Hinton[6], M. Holler[29], M. Jamrozy[30], F. Jankowsky[8], I. Jung-Richardt[22], E. Kasai[11], K. Katarzyński[31], H. Katjaita[11], D. Kerszberg[19], R. Khatoon[12], B. Khélifi[15], W. Kluźniak[32], Nu. Komin[24,33], R. Konno[13], K. Kosack[21], D. Kostunin[13], G. Kukec Mezek[16], R.G. Lang[22], A. Lemière[15], M. Lemoine-Goumard[34], J.-P. Lenain[19], A. Luashvili[12], J. Mackey[5], V. Marandon[21], G. Martí-Devesa[29], R. Marx[8], M. Mayer[22], A. Mehta[13], A. Mitchell[22], R. Moderski[32], M.O. Moghadam[14], L. Mohrmann[6], E. Moulin[21], M. de Naurois[10], J. Niemiec[23], E. de Ona Wilhelmi[13], S. Panny[29], M. Panter[6], R.D. Parsons[17], U. Pensec[19], P. Pichard[15], G. Pühlhofer[28], M. Punch[15], A. Quirrenbach[8], M. Regeard[15], O. Reimer[29], H. Ren[6], F. Rieger[6], G. Rowell[25], B. Rudak[32], K. Sabri[33], V. Sahakian[35], H. Salzmann[28], M. Sasaki[22], J. Schäfer[22], F. Schüssler[21,177], H.M. Schutte[12], M. Senniappan[16,178], J.N.S. Shapopi[11], A. Sharma[15], H. Sol[18], S. Spencer[22], Ł. Stawarz[30], R. Steenkamp[11], S. Steinmassl[6], C. Steppa[14], T. Takahashi[36], T. Tanaka[37], A.M. Taylor[13], M. Tsirou[13], C. van Eldik[22], M. Vecchi[9], C. Venter[12], J. Vink[38], T. Wach[22], S.J. Wagner[8], A. Wierzcholska[8,23], M. Zacharias[8,12], A.A. Zdziarski[32], A. Zech[18], N. Żywucka[12], (H.E.S.S. Collaboration),
S. Abe[39], J. Abhir[1], A. Abhishek[40], A. Aguasca-Cabot[41], I. Agudo[42], T. Aniello[43], S. Ansoldi[44,45], L. A. Antonelli[43], A. Arbet Engels[46], C. Arcaro[47], M. Artero[48], K. Asano[39], A. Babić[49], C. Bakshi[50], U. Barres de Almeida[51], J. A. Barrio[52], L. Barrios-Jiménez[53], I. Batković[47], J. Baxter[39], J. Becerra González[53], W. Bednarek[54], E. Bernardini[47], J. Bernete[55], A. Berti[46], J. Besenrieder[46], C. Bigongiari[43], A. Biland[1], O. Blanch[48], H. Bökenkamp[3], G. Bonnoli[43], Ž. Bošnjak[49], E. Bronzini[43], I. Burelli[48], A. Campoy-Ordaz[56], A. Carosi[43], R. Carosi[57], M. Carretero-Castrillo[41], A. J. Castro-Tirado[42], D. Cerasole[58], G. Ceribella[46], Y. Chai[39], A. Chilingarian[59], A. Cifuentes[55], J. L. Contreras[52], J. Cortina[55], S. Covino[43,60], G. D'Amico[61], P. Da Vela[43], F. Dazzi[43], A. De Angelis[47], B. De Lotto[44], M. Delfino[48,62], C. Delgado Mendez[55], F. Di Pierro[63], R. Di Tria[58], L. Di Venere[58], A. Dinesh[52], D. Dominis Prester[64], A. Donini[43], D. Dorner[2], M. Doro[47], L. Eisenberger[2], D. Elsaesser[3], J. Escudero[42], L. Fariña[48], A. Fattorini[3], L. Foffano[43], L. Font[56], S. Fröse[3], Y. Fukazawa[65], S. Gasparyan[66], M. Gaug[56], J. G. Giesbrecht Paiva[51], N. Giglietto[58], F. Giordano[58], P. Gliwny[54], N. Godinović[67], T. Gradetzke[3], R. Grau[48], D. Green[46], J. G. Green[46], P. Günther[2], D. Hadasch[39], A. Hahn[46], T. Hassan[55], L. Heckmann[46,68], D. Hrupec[69], R. Imazawa[65], D. Israyelyan[66], I. Jiménez Martínez[46], J. Jiménez Quiles[48], J. Jormanainen[70], S. Kankkunen[70], T. Kayanoki[65], D. Kerszberg[48], J. Konrad[3], P. M. Kouch[70], H. Kubo[39], J. Kushida[71], M. Láinez[52], A. Lamastra[43], E. Lindfors[70], S. Lombardi[43], F. Longo[44,72], R. López-Coto[42], M. López-Moya[52], A. López-Oramas[53], S. Loporchio[58], L. Lulić[64], E. Lyard[4], P. Majumdar[50], M. Makariev[73], M. Mallamaci[74], G. Maneva[73], M. Manganaro[64], S. Mangano[55], S. Marchesi[43], M. Mariotti[47], M. Martínez[48], P. Maruševec[49], A. Mas-Aguilar[52], D. Mazin[39,46], S. Menchiari[42], J. Méndez Gallego[42], D. Miceli[47], J. M. Miranda[40], R. Mirzoyan[46], M. Molero González[53], E. Molina[53], H. A. Mondal[39], A. Moralejo[48], T. Nakamori[75], C. Nanci[43], V. Neustroev[76], M. Nievas Rosillo[53], C. Nigro[48], L. Nikolić[40], K. Nilsson[70], K. Nishijima[71], K. Noda[77], S. Nozaki[39], A. Okumura[78], J. Otero- Santos[47], S. Paiano[43], D. Paneque[46], J. M. Paredes[41], M. Peresano[46], M. Persic[44,179], M. Pihet[42], F. Podobnik[40], P. G. Prada Moroni[57], E. Prandini[47], M. Ribó[41], J. Rico[48], T. Saito[39], S. Sakurai[39], K. Satalecka[79], F. G. Saturni[43], K. Schmitz[3], F. Schmuckermaier[46], J. L. Schubert[3], A. Sciaccaluga[43], G. Silvestri[47], J. Sitarek[54], V. Sliusar[4], D. Sobczynska[54], A. Stamerra[43], J. Strišković[69], D. Strom[46], M. Strzys[39], Y. Suda[65], H. Tajima[78], M. Takahashi[78], R. Takeishi[39], P. Temnikov[73], K. Terauchi[80], T. Terzić[64], A. Tutone[43], S. Ubach[56], J. van Scherpenberg[46], M. Vazquez Acosta[53], S. Ventura[40], G. Verna[40], I. Viale[63,180], A. Vigliano[44], C. F. Vigorito[63], E. Visentin[63], V. Vitale[81], I. Vovk[39], R. Walter[4], F. Wersig[3], M. Will[46], T. Yamamoto[82], P. K. H. Yeung[39], S. Yoo[80], (MAGIC Collaboration),
A. Acharyya[83], A. Archer[84], P. Bangale[85], J. T. Bartkoske[86], W. Benbow[87], J. H. Buckley[88], Y. Chen[89], J. L. Christiansen[90], A. J. Chromey[87], M. Errando[88], S. Feldman[89], Q. Feng[86], S. Filbert[86], L. Fortson[91], A. Furniss[92],

W. Hanlon[87], O. Hervet[92], C. E. Hinrichs[93], J. Holder[94], Z. Hughes[88], T. B. Humensky[95], W. Jin[89,181], M. N. Johnson[92], P. Kaaret[96], M. Kertzman[84], M. Kherlakian[97], D. Kieda[86], T. K. Kleiner[98], N. Korzoun[94], M. J. Lang[99], M. Lundy[100], G. Maier[98], M. J. Millard[96], J. Millis[101,102], P. Moriarty[99], R. Mukherjee[103], W. Ning[89], R. A. Ong[89], A. Pandey[86], M. Pohl[104], J. Quinn[105], P. L. Rabinowitz[88], K. Ragan[100], P. T. Reynolds[106], D. Ribeiro[91], E. Roache[87], I. Sadeh[98], A. C. Sadun[107], L. Saha[87], M. Santander[108], G. H. Sembroski[109], R. Shang[103], D. Tak[110], A. K. Talluri[91], J. V. Tucci[111], J. Valverde[112], V. V. Vassiliev[89], D. A. Williams[92], S. L. Wong[100],
(VERITAS Collaboration),
S. Buson[13,113],
(Fermi-LAT Collaboration),
R. Abbasi[114], M. Ackermann[115], J. Adams[116], S. K. Agarwalla[117,182], J. A. Aguilar[118], M. Ahlers[119], J.M. Alameddine[120], S. Ali[121], N. M. Amin[122], K. Andeen[123], C. Argüelles[124], Y. Ashida[86], S. Athanasiadou[115], S. N. Axani[122], R. Babu[125], X. Bai[126], J. Baines-Holmes[117], A. Balagopal V.[117,122], S. W. Barwick[127], S. Bash[128], V. Basu[86], R. Bay[129], J. J. Beatty[130,131], J. Becker Tjus[97,183], P. Behrens[132], J. Beise[133], C. Bellenghi[128], B. Benkel[115], S. BenZvi[134], D. Berley[135], E. Bernardini[136,184], D. Z. Besson[121], E. Blaufuss[135], L. Bloom[108], S. Blot[115], I. Bodo[117], F. Bontempo[137], J. Y. Book Motzkin[124], C. Boscolo Meneguolo[136,184], S. Böser[138], O. Botner[133], J. Böttcher[132], J. Braun[117], B. Brinson[139], Z. Brisson-Tsavoussis[140], R. T. Burley[141], D. Butterfield[117], M. A. Campana[142], K. Carloni[124], J. Carpio[143,144], S. Chattopadhyay[117,182], N. Chau[118], Z. Chen[145], D. Chirkin[117], S. Choi[86], B. A. Clark[135], A. Coleman[133], P. Coleman[132], G. H. Collin[146], D. A. Coloma Borja[136], A. Connolly[130,131], J. M. Conrad[146], D. F. Cowen[147,148], C. De Clercq[149], J. J. DeLaunay[147], D. Delgado[124], T. Delmeulle[118], S. Deng[132], P. Desiati[117], K. D. de Vries[149], G. de Wasseige[150], T. DeYoung[125], J. C. Díaz-Vélez[117], S. DiKerby[125], T. Ding[143,144], M. Dittmer[151], A. Domi[152], L. Draper[86], L. Dueser[132], D. Durnford[153], K. Dutta[138], M. A. DuVernois[117], T. Ehrhardt[138], L. Eidenschink[128], A. Eimer[152], P. Eller[128], E. Ellinger[154], D. Elsässer[120], R. Engel[137,155], H. Erpenbeck[117], W. Esmail[151], S. Eulig[124], J. Evans[135], P. A. Evenson[122], K. L. Fan[135], K. Fang[117], K. Farrag[156], A. R. Fazely[157], A. Fedynitch[158], N. Feigl[159], C. Finley[160], L. Fischer[115], D. Fox[147], A. Franckowiak[97], S. Fukami[115], P. Fürst[132], J. Gallagher[161], E. Ganster[132], A. Garcia[124], M. Garcia[122], G. Garg[117,182], E. Genton[124,150], L. Gerhardt[162], A. Ghadimi[108], C. Glaser[133], T. Glüsenkamp[133], J. G. Gonzalez[122], S. Goswami[143,144], A. Granados[125], D. Grant[163], S. J. Gray[135], S. Griffin[117], S. Griswold[134], K. M. Groth[119], D. Guevel[117], C. Günther[132], P. Gutjahr[120], C. Ha[164], C. Haack[152], A. Hallgren[133], L. Halve[132], F. Halzen[117], L. Hamacher[132], M. Ha Minh[128], M. Handt[132], K. Hanson[117], J. Hardin[146], A. A. Harnisch[125], P. Hatch[140], A. Haungs[137], J. Häussler[132], K. Helbing[154], J. Hellrung[97], B. Henke[125], L. Hennig[152], F. Henningsen[163], L. Heuermann[132], R. Hewett[116], N. Heyer[133], S. Hickford[154], A. Hidvegi[160], C. Hill[156], G. C. Hill[141], R. Hmaid[156], K. D. Hoffman[135], D. Hooper[117], S. Hori[117], K. Hoshina[117,185], M. Hostert[124], W. Hou[137], M. Hrywniak[160], T. Huber[137], K. Hultqvist[160], K. Hymon[120,158], A. Ishihara[156], W. Iwakiri[156], M. Jacquart[119], S. Jain[117], O. Janik[152], M. Jansson[150], M. Jeong[86], M. Jin[124], N. Kamp[124], D. Kang[137], W. Kang[142], X. Kang[142], A. Kappes[151], L. Kardum[120], T. Karg[115], M. Karl[128], A. Karle[117], A. Katil[153], M. Kauer[117], J. L. Kelley[117], M. Khanal[86], A. Khatee Zathul[117], A. Kheirandish[143,144], H. Kimku[164], J. Kiryluk[145], C. Klein[152], S. R. Klein[129,162], Y. Kobayashi[156], A. Kochocki[125], R. Koirala[122], H. Kolanoski[159], T. Kontrimas[128], L. Köpke[138], C. Kopper[152], D. J. Koskinen[119], P. Koundal[122], M. Kowalski[115,159], T. Kozynets[119], A. Kravka[86], N. Krieger[97], J. Krishnamoorthi[117,182], T. Krishnan[124], K. Kruiswijk[150], E. Krupczak[125], A. Kumar[115], E. Kun[97], N. Kurahashi[142], N. Lad[115], C. Lagunas Gualda[128], L. Lallement Arnaud[118], M. Lamoureux[150], M. J. Larson[135], F. Lauber[154], J. P. Lazar[150], K. Leonard DeHolton[148], A. Leszczyńska[122], J. Liao[139], C. Lin[122], Y. T. Liu[148], M. Liubarska[153], C. Love[142], L. Lu[117], F. Lucarelli[165], W. Luszczak[130,131], Y. Lyu[129,162], M. Macdonald[124], J. Madsen[117], E. Magnus[149], Y. Makino[117], E. Manao[128], S. Mancina[136,186], A. Mand[117], I. C. Mariş[118], S. Marka[166], Z. Marka[166], L. Marten[132], I. Martinez-Soler[124], R. Maruyama[167], J. Mauro[150], F. Mayhew[125], F. McNally[168], J. V. Mead[119], K. Meagher[117], S. Mechbal[115], A. Medina[131], M. Meier[156], Y. Merckx[149], L. Merten[97], J. Mitchell[157], L. Molchany[126], S. Mondal[86], T. Montaruli[165], R. W. Moore[153], Y. Morii[156], A. Mosbrugger[152], M. Moulai[117], D. Mousadi[115], E. Moyaux[150], T. Mukherjee[137], R. Naab[115], M. Nakos[117], U. Naumann[154], J. Necker[115], L. Neste[160], M. Neumann[151], H. Niederhausen[125], M. U. Nisa[125], K. Noda[156], A. Noell[132], A. Novikov[122], A. Obertacke[160], V. O'Dell[117], A. Olivas[135], R. Orsoe[128], J. Osborn[117], E. O'Sullivan[133], V. Palusova[138], H. Pandya[122], A. Parenti[118], N. Park[140], V. Parrish[125], E. N. Paudel[108], L. Paul[126], C. Pérez de los Heros[133], T. Pernice[115], T. C. Petersen[119], J. Peterson[117], M. Plum[126], A. Pontén[133], V. Poojyam[108], Y. Popovych[138], M. Prado Rodriguez[117], B. Pries[125], R. Procter- Murphy[135], G. T. Przybylski[162], L. Pyras[86], C. Raab[150], J. Rack-Helleis[138], N. Rad[115], M. Ravn[133], K. Rawlins[169], Z. Rechav[117], A. Rehman[122], I. Reistroffer[126], E. Resconi[128], S. Reusch[115], C. D. Rho[170], W. Rhode[120], L. Ricca[150], B. Riedel[117], A. Rifaie[154], E. J. Roberts[141], M. Rongen[152], A. Rosted[156], C. Rott[86], T. Ruhe[120], L. Ruohan[128], D. Ryckbosch[171], J. Saffer[155], D. Salazar-Gallegos[125], P. Sampathkumar[137], A. Sandrock[154], G. Sanger-Johnson[125], M. Santander[108], S. Sarkar[172], J. Savelberg[132], M. Scarnera[150], P. Schaile[128], M. Schaufel[132], H. Schieler[137], S. Schindler[152], L. Schlickmann[138], B. Schlüter[151], F. Schlüter[118], N. Schmeisser[154], T. Schmidt[135], F. G. Schröder[122,137], L. Schumacher[152], S. Schwirn[132], S. Sclafani[135], D. Seckel[122], L. Seen[117],

M. Seikh[121], S. Seunarine[173], P. A. Sevle Myhr[150], R. Shah[142], S. Shefali[155], N. Shimizu[156], B. Skrzypek[129], R. Snihur[117], J. Soedingrekso[120], A. Sègaard[119], D. Soldin[86], P. Soldin[132], G. Sommani[97], C. Spannfellner[128], G. M. Spiczak[173], C. Spiering[115], J. Stachurska[171], M. Stamatikos[131], T. Stanev[122], T. Stezelberger[162], T. Stürwald[154], T. Stuttard[119], G. W. Sullivan[135], I. Taboada[139], S. Ter-Antonyan[157], A. Terliuk[128], A. Thakuri[126], M. Thiesmeyer[117], W. G. Thompson[124], J. Thwaites[117], S. Tilav[122], K. Tollefson[125], S. Toscano[118], D. Tosi[117], A. Trettin[115], A. K. Upadhyay[117,182], K. Upshaw[157], A. Vaidyanathan[123], N. Valtonen-Mattila[97,133], J. Valverde[123], J. Vandenbroucke[117], T. Van Eeden[115], N. van Eijndhoven[149], L. Van Rootselaar[120], J. van Santen[115], J. Vara[151], F. Varsi[155], M. Venugopal[137], M. Vereecken[150], S. Vergara Carrasco[116], S. Verpoest[122], D. Veske[166], A. Vijai[135], J. Villarreal[146], C. Walck[160], A. Wang[139], E. H. S. Warrick[108], C. Weaver[125], P. Weigel[146], A. Weindl[137], J. Weldert[138], A. Y. Wen[124], C. Wendt[117], J. Werthebach[120], M. Weyrauch[137], N. Whitehorn[125], C. H. Wiebusch[132], D. R. Williams[108], L. Witthaus[120], M. Wolf[128], G. Wrede[152], X. W. Xu[157], J. P. Yanez[153], Y. Yao[117], E. Yildizci[117], S. Yoshida[156], R. Young[121], F. Yu[124], S. Yu[86], T. Yuan[117], A. Zander Jurowitzki[128], A. Zegarelli[97], S. Zhang[125], Z. Zhang[145], P. Zhelnin[124], P. Zilberman[117,187], F. D'Ammando[174], and
(IceCube Collaboration)

[1] ETH Zürich, CH-8093 Zürich, Switzerland
[2] Universität Würzburg, D-97074 Würzburg, Germany
[3] Technische Universität Dortmund, D-44221 Dortmund, Germany
[4] University of Geneva, Chemin d'Ecogia 16, CH-1290 Versoix, Switzerland
[5] Dublin Institute for Advanced Studies, 31 Fitzwilliam Place, Dublin 2, Ireland
[6] Max-Planck-Institut für Kernphysik, Saupfercheckweg 1, 69117 Heidelberg, Germany
[7] Yerevan State University, 1 Alek Manukyan St, Yerevan 0025, Armenia
[8] Landessternwarte, Universität Heidelberg, Königstuhl, D 69117 Heidelberg, Germany
[9] Kapteyn Astronomical Institute, University of Groningen, Landleven 12, 9747 AD Groningen, The Netherlands
[10] Laboratoire Leprince-Ringuet, École Polytechnique, CNRS, Institut Polytechnique de Paris, F-91128 Palaiseau, France
[11] University of Namibia, Department of Physics, Private Bag 13301, Windhoek 10005, Namibia
[12] Centre for Space Research, North-West University, Potchefstroom 2520, South Africa
[13] Deutsches Elektronen-Synchrotron DESY, Platanenallee 6, 15738 Zeuthen, Germany
[14] Institut für Physik und Astronomie, Universität Potsdam, Karl-Liebknecht-Strasse 24/25, D 14476 Potsdam, Germany
[15] Université Paris Cité, CNRS, Astroparticule et Cosmologie, F-75013 Paris, France
[16] Department of Physics and Electrical Engineering, Linnaeus University, 351 95 Växjö, Sweden
[17] Institut für Physik, Humboldt-Universität zu Berlin, Newtonstr. 15, D 12489 Berlin, Germany
[18] LUX, Observatoire de Paris, Université PSL, Sorbonne Université, CNRS, 92190 Meudon, France
[19] Sorbonne Université, CNRS/IN2P3, Laboratoire de Physique Nucléaire et de Hautes Energies, LPNHE, 4 place Jussieu, 75005 Paris, France
[20] University of Oxford, Department of Physics, Denys Wilkinson Building, Keble Road, Oxford OX1 3RH, UK
[21] IRFU, CEA, Université Paris-Saclay, F-91191 Gif-sur-Yvette, France
[22] Friedrich-Alexander-Universität Erlangen-Nürnberg, Erlangen Centre for Astroparticle Physics, Nikolaus-Fiebiger-Str. 2, 91058 Erlangen, Germany
[23] Instytut Fizyki Jądrowej PAN, ul. Radzikowskiego 152, 31-342 Kraków, Poland
[24] School of Physics, University of the Witwatersrand, 1 Jan Smuts Avenue, Braamfontein, Johannesburg, 2050, South Africa
[25] School of Physical Sciences, University of Adelaide, Adelaide 5005, Australia
[26] Aix Marseille Université, CNRS/IN2P3, CPPM, Marseille, France
[27] School of Science, Western Sydney University, Locked Bag 1797, Penrith South DC, NSW 2751, Australia
[28] Institut für Astronomie und Astrophysik, Universität Tübingen, Sand 1, D 72076 Tübingen, Germany
[29] Universität Innsbruck, Institut für Astro- und Teilchenphysik, Technikerstraße 25, 6020 Innsbruck, Austria
[30] Obserwatorium Astronomiczne, Uniwersytet Jagielloński, ul. Orla 171, 30-244 Kraków, Poland
[31] Institute of Astronomy, Faculty of Physics, Astronomy and Informatics, Nicolaus Copernicus University, Grudziadzka 5, 87-100 Torun, Poland
[32] Nicolaus Copernicus Astronomical Center, Polish Academy of Sciences, ul. Bartycka 18, 00-716 Warsaw, Poland
[33] Laboratoire Univers et Particules de Montpellier, Université Montpellier, CNRS/IN2P3, CC 72, Place Eugène Bataillon, F-34095 Montpellier Cedex 5, France
[34] Université Bordeaux, CNRS, LP2I Bordeaux, UMR 5797, F-33170 Gradignan, France
[35] Yerevan Physics Institute, 2 Alikhanian Brothers Street, 0036 Yerevan, Armenia
[36] Kavli Institute for the Physics and Mathematics of the Universe (WPI), The University of Tokyo Institutes for Advanced Study (UTIAS), The University of Tokyo, 5-1-5 Kashiwa-no-Ha, Kashiwa, Chiba, 277-8583, Japan
[37] Department of Physics, Konan University, 8-9-1 Okamoto, Higashinada, Kobe, Hyogo 658-8501, Japan
[38] GRAPPA, Anton Pannekoek Institute for Astronomy, University of Amsterdam, Science Park 904, 1098 XH Amsterdam, The Netherlands
[39] Japanese MAGIC Group: Institute for Cosmic Ray Research (ICRR), The University of Tokyo, Kashiwa, 277-8582 Chiba, Japan
[40] Università di Siena and INFN Pisa, I-53100 Siena, Italy
[41] Universitat de Barcelona, ICCUB, IEEC-UB, E-08028 Barcelona, Spain
[42] Instituto de Astrofísica de Andalucía-CSIC, Glorieta de la Astronomía s/n, 18008, Granada, Spain
[43] National Institute for Astrophysics (INAF), I-00136 Rome, Italy
[44] Università di Udine and INFN Trieste, I-33100 Udine, Italy
[45] also at International Center for Relativistic Astrophysics (ICRA), Rome, Italy
[46] Max-Planck-Institut für Physik, D-85748 Garching, Germany
[47] Università di Padova and INFN, I-35131 Padova, Italy
[48] Institut de Física d'Altes Energies (IFAE), The Barcelona Institute of Science and Technology (BIST), E-08193 Bellaterra (Barcelona), Spain
[49] Croatian MAGIC Group: University of Zagreb, Faculty of Electrical Engineering and Computing (FER), 10000 Zagreb, Croatia
[50] Saha Institute of Nuclear Physics, A CI of Homi Bhabha National Institute, Kolkata 700064, West Bengal, India
[51] Centro Brasileiro de Pesquisas Físicas (CBPF), 22290-180 URCA, Rio de Janeiro (RJ), Brazil
[52] IPARCOS Institute and EMFTEL Department, Universidad Complutense de Madrid, E-28040 Madrid, Spain
[53] Instituto de Astrofísica de Canarias and Dpto. de Astrofísica, Universidad de La Laguna, E-38200, La Laguna, Tenerife, Spain
[54] University of Lodz, Faculty of Physics and Applied Informatics, Department of Astrophysics, 90-236 Lodz, Poland
[55] Centro de Investigaciones Energéticas, Medioambientales y Tecnológicas, E-28040 Madrid, Spain
[56] Departament de Física, and CERES-IEEC, Universitat Autònoma de Barcelona, E-08193 Bellaterra, Spain

[57] Università di Pisa and INFN Pisa, I-56126 Pisa, Italy
[58] INFN MAGIC Group: INFN Sezione di Bari and Dipartimento Interateneo di Fisica dell'Università e del Politecnico di Bari, I-70125 Bari, Italy
[59] Armenian MAGIC Group: A. Alikhanyan National Science Laboratory, 0036 Yerevan, Armenia
[60] also at Como Lake centre for AstroPhysics (CLAP), DiSAT, Università dell?Insubria, via Valleggio 11, 22100, Como, Italy
[61] Department for Physics and Technology, University of Bergen, Norway
[62] also at Port d'Informació Cientà-fica (PIC), E-08193 Bellaterra (Barcelona), Spain
[63] INFN MAGIC Group: INFN Sezione di Torino and Università degli Studi di Torino, I-10125 Torino, Italy
[64] Croatian MAGIC Group: University of Rijeka, Faculty of Physics, 51000 Rijeka, Croatia
[65] Japanese MAGIC Group: Physics Program, Graduate School of Advanced Science and Engineering, Hiroshima University, 739-8526 Hiroshima, Japan
[66] Armenian MAGIC Group: ICRANet-Armenia, 0019 Yerevan, Armenia
[67] Croatian MAGIC Group: University of Split, Faculty of Electrical Engineering, Mechanical Engineering and Naval Architecture (FESB), 21000 Split, Croatia
[68] now at Université Paris Cité, CNRS, Astroparticule et Cosmologie, F-75013 Paris, France
[69] Croatian MAGIC Group: Josip Juraj Strossmayer University of Osijek, Department of Physics, 31000 Osijek, Croatia
[70] Finnish MAGIC Group: Finnish Centre for Astronomy with ESO, Department of Physics and Astronomy, University of Turku, FI-20014 Turku, Finland
[71] Japanese MAGIC Group: Department of Physics, Tokai University, Hiratsuka, 259-1292 Kanagawa, Japan
[72] also at Dipartimento di Fisica, Università di Trieste, I-34127 Trieste, Italy
[73] Inst. for Nucl. Research and Nucl. Energy, Bulgarian Academy of Sciences, BG-1784 Sofia, Bulgaria
[74] INFN MAGIC Group: INFN Sezione di Catania and Dipartimento di Fisica e Astronomia, University of Catania, I-95123 Catania, Italy
[75] Japanese MAGIC Group: Department of Physics, Yamagata University, Yamagata 990-8560, Japan
[76] Finnish MAGIC Group: Space Physics and Astronomy Research Unit, University of Oulu, FI-90014 Oulu, Finland
[77] Japanese MAGIC Group: Chiba University, ICEHAP, 263-8522 Chiba, Japan
[78] Japanese MAGIC Group: Institute for Space-Earth Environmental Research and Kobayashi-Maskawa Institute for the Origin of Particles and the Universe, Nagoya University, 464-6801 Nagoya, Japan
[79] Deutsches Elektronen-Synchrotron (DESY), D-15738 Zeuthen, Germany
[80] Japanese MAGIC Group: Department of Physics, Kyoto University, 606-8502 Kyoto, Japan
[81] INFN MAGIC Group: INFN Roma Tor Vergata, I-00133 Roma, Italy
[82] Japanese MAGIC Group: Department of Physics, Konan University, Kobe, Hyogo 658-8501, Japan
[83] CP3-Origins, University of Southern Denmark, Campusvej 55, 5230 Odense M, Denmark
[84] Department of Physics and Astronomy, DePauw University, Greencastle, IN 46135-0037, USA
[85] Department of Physics, Temple University, Philadelphia, PA 19122, USA
[86] Department of Physics and Astronomy, University of Utah, Salt Lake City, UT 84112, USA
[87] Center for Astrophysics | Harvard & Smithsonian, Cambridge, MA 02138, USA
[88] Department of Physics, Washington University, St. Louis, MO 63130, USA
[89] Department of Physics and Astronomy, University of California, Los Angeles, CA 90095, USA
[90] Physics Department, California Polytechnic State University, San Luis Obispo, CA 94307, USA
[91] School of Physics and Astronomy, University of Minnesota, Minneapolis, MN 55455, USA
[92] Santa Cruz Institute for Particle Physics and Department of Physics, University of California, Santa Cruz, CA 95064, USA
[93] Center for Astrophysics | Harvard & Smithsonian, Cambridge, MA 02138, USA and Department of Physics and Astronomy, Dartmouth College, 6127 Wilder Laboratory, Hanover, NH 03755, USA
[94] Department of Physics and Astronomy and the Bartol Research Institute, University of Delaware, Newark, DE 19716, USA
[95] Department of Physics, University of Maryland, College Park, MD, USA and NASA GSFC, Greenbelt, MD 20771, USA
[96] Department of Physics and Astronomy, University of Iowa, Van Allen Hall, Iowa City, IA 52242, USA
[97] Fakultät für Physik & Astronomie, Ruhr-Universität Bochum, D-44780 Bochum, Germany
[98] DESY, Platanenallee 6, 15738, Zeuthen, Germany
[99] School of Natural Sciences, University of Galway, University Road, Galway, H91 TK33, Ireland
[100] Physics Department, McGill University, Montreal, QC H3A 2T8, Canada
[101] Department of Physics and Astronomy, Ball State University, Muncie, IN 47306, USA
[102] Department of Physics, Anderson University, 1100 East 5th Street, Anderson, IN 46012, USA
[103] Department of Physics and Astronomy, Barnard College, Columbia University, NY 10027, USA
[104] Institute of Physics and Astronomy, University of Potsdam, 14476, Potsdam-Golm, Germany and DESY, Platanenallee 6, 15738, Zeuthen, Germany
[105] School of Physics, University College Dublin, Belfield, Dublin 4, Ireland
[106] Department of Physical Sciences, Munster Technological University, Bishopstown, Cork, T12 P928, Ireland
[107] Department of Physics, University of Colorado Denver, Campus Box 157, P.O. Box 173364, Denver, CO 80217, USA
[108] Department of Physics and Astronomy, University of Alabama, Tuscaloosa, AL 35487, USA
[109] Department of Physics and Astronomy, Purdue University, West Lafayette, IN 47907, USA
[110] SNU Astronomy Research Center, Seoul National University, Seoul 08826, Republic of Korea
[111] Department of Physics, Indiana University Indianapolis, Indianapolis, IN 46202, USA
[112] Department of Physics, University of Maryland, Baltimore County, Baltimore MD 21250, USA and NASA GSFC, Greenbelt, MD 20771, USA
[113] Julius-Maximilians-Universität Würzburg, Fakultät für Physik und Astronomie, Institut für Theoretische Physik und Astrophysik, Lehrstuhl für Astronomie, Emil-Fischer-Str. 31, D-97074 Würzburg, Germany
[114] Department of Physics, Loyola University Chicago, Chicago, IL 60660, USA
[115] Deutsches Elektronen-Synchrotron DESY, Platanenallee 6, D-15738 Zeuthen, Germany
[116] Department of Physics and Astronomy, University of Canterbury, Private Bag 4800, Christchurch, New Zealand
[117] Departmentof Physics and Wisconsin IceCube Particle Astrophysics Center, University of Wisconsin–Madison, Madison, WI 53706, USA
[118] Université Libre de Bruxelles, Science Faculty CP230, B-1050 Brussels, Belgium
[119] Niels Bohr Institute, University of Copenhagen, DK-2100 Copenhagen, Denmark
[120] Department of Physics, TU Dortmund University, D-44221 Dortmund, Germany
[121] Department of Physics and Astronomy, University of Kansas, Lawrence, KS 66045, USA
[122] Bartol Research Institute and Dept. of Physics and Astronomy, University of Delaware, Newark, DE 19716, USA
[123] Department of Physics, Marquette University, Milwaukee, WI 53201, USA
[124] Department of Physics and Laboratory for Particle Physics and Cosmology, Harvard University, Cambridge, MA 02138, USA
[125] Department of Physics and Astronomy, Michigan State University, East Lansing, MI 48824, USA
[126] Physics Department, South Dakota School of Mines and Technology, Rapid City, SD 57701, USA
[127] Department of Physics and Astronomy, University of California, Irvine, CA 92697, USA
[128] Physik-department, Technische Universität München, D-85748 Garching, Germany
[129] Department of Physics, University of California, Berkeley, CA 94720, USA

[130] Department of Astronomy, Ohio State University, Columbus, OH 43210, USA
[131] Department of Physics and Center for Cosmology and Astro-Particle Physics, Ohio State University, Columbus, OH 43210, USA
[132] III. Physikalisches Institut, RWTH Aachen University, D-52056 Aachen, Germany
[133] Department of Physics and Astronomy, Uppsala University, Box 516, SE-75120 Uppsala, Sweden
[134] Department of Physics and Astronomy, University of Rochester, Rochester, NY 14627, USA
[135] Department of Physics, University of Maryland, College Park, MD 20742, USA
[136] Dipartimento di Fisica e Astronomia Galileo Galilei, Università Degli Studi di Padova, I-35122 Padova PD, Italy
[137] Karlsruhe Institute of Technology, Institute for Astroparticle Physics, D-76021 Karlsruhe, Germany
[138] Institute of Physics, University of Mainz, Staudinger Weg 7, D-55099 Mainz, Germany
[139] School of Physics and Center for Relativistic Astrophysics, Georgia Institute of Technology, Atlanta, GA 30332, USA
[140] Department of Physics, Engineering Physics, and Astronomy, Queen's University, Kingston, ON K7L 3N6, Canada
[141] Department of Physics, University of Adelaide, Adelaide, 5005, Australia
[142] Department of Physics, Drexel University, 3141 Chestnut Street, Philadelphia, PA 19104, USA
[143] Department of Physics & Astronomy, University of Nevada, Las Vegas, NV 89154, USA
[144] Nevada Center for Astrophysics, University of Nevada, Las Vegas, NV 89154, USA
[145] Department of Physics and Astronomy, Stony Brook University, Stony Brook, NY 11794-3800, USA
[146] Department of Physics, Massachusetts Institute of Technology, Cambridge, MA 02139, USA
[147] Department of Astronomy and Astrophysics, Pennsylvania State University, University Park, PA 16802, USA
[148] Department of Physics, Pennsylvania State University, University Park, PA 16802, USA
[149] Vrije Universiteit Brussel (VUB), Dienst ELEM, B-1050 Brussels, Belgium
[150] Centre for Cosmology, Particle Physics and Phenomenology—CP3, Université catholique de Louvain, Louvain-la-Neuve, Belgium
[151] Institut für Kernphysik, Universität Münster, D-48149 Münster, Germany
[152] Erlangen Centre for Astroparticle Physics, Friedrich-Alexander-Universität Erlangen-Nürnberg, D-91058 Erlangen, Germany
[153] Department of Physics, University of Alberta, Edmonton, Alberta, T6G 2E1, Canada
[154] Department of Physics, University of Wuppertal, D-42119 Wuppertal, Germany
[155] Karlsruhe Institute of Technology, Institute of Experimental Particle Physics, D-76021 Karlsruhe, Germany
[156] Department of Physics and The International Center for Hadron Astrophysics, Chiba University, Chiba 263-8522, Japan
[157] Department of Physics, Southern University, Baton Rouge, LA 70813, USA
[158] Institute of Physics, Academia Sinica, Taipei, 11529, Taiwan
[159] Institut für Physik, Humboldt-Universität zu Berlin, D-12489 Berlin, Germany
[160] Oskar Klein Centre and Dept. of Physics, Stockholm University, SE-10691 Stockholm, Sweden
[161] Department of Astronomy, University of Wisconsin–Madison, Madison, WI 53706, USA
[162] Lawrence Berkeley National Laboratory, Berkeley, CA 94720, USA
[163] Department of Physics, Simon Fraser University, Burnaby, BC V5A 1S6, Canada
[164] Department of Physics, Chung-Ang University, Seoul 06974, Republic of Korea
[165] Département de physique nucléaire et corpusculaire, Université de Genève, CH-1211 Genève, Switzerland
[166] Columbia Astrophysics and Nevis Laboratories, Columbia University, New York, NY 10027, USA
[167] Department of Physics, Yale University, New Haven, CT 06520, USA
[168] Department of Physics, Mercer University, Macon, GA 31207-0001, USA
[169] Department of Physics and Astronomy, University of Alaska Anchorage, 3211 Providence Dr., Anchorage, AK 99508, USA
[170] Department of Physics, Sungkyunkwan University, Suwon 16419, Republic of Korea
[171] Department of Physics and Astronomy, University of Gent, B-9000 Gent, Belgium
[172] Department of Physics, University of Oxford, Parks Road, Oxford OX1 3PU, UK
[173] Department of Physics, University of Wisconsin, River Falls, WI 54022, USA
[174] INAF-IRA Bologna, Via P. Gobetti 101, I-40129 Bologna, Italy
Received 2025 October 2; revised 2025 December 4; accepted 2025 December 10; published 2026 January 20

[175] Also at GSI Darmstadt, Germany.
[176] Corresponding author, contact@fact-project.org.
[177] Corresponding author, contact.hess@hess-experiment.eu.
[178] Now at Khalifa University of Science and Technology, Department of Physics, PO Box 127788, Abu Dhabi, United Arab Emirates.
[179] Also at INAF Padova.
[180] Corresponding author, contact.magic@mpp.mpg.de.
[181] Corresponding author, wjin@astro.ucla.edu.
[182] Also at Institute of Physics, Sachivalaya Marg, Sainik School Post, Bhubaneswar 751005, India.
[183] Also at Department of Space, Earth and Environment, Chalmers University of Technology, 412 96 Gothenburg, Sweden.
[184] Also at INFN Padova, I-35131 Padova, Italy.
[185] Also at Earthquake Research Institute, University of Tokyo, Bunkyo, Tokyo 113-0032, Japan.
[186] Now at INFN Padova, I-35131 Padova, Italy.
[187] Corresponding author, analysis@icecube.wisc.edu.

Abstract

The search for sources of high-energy astrophysical neutrinos can be significantly advanced through a multimessenger approach, which seeks to detect the γ-rays that accompany neutrinos as they are produced at their sources. Multimessenger observations have so far provided the first evidence for a neutrino source, illustrated by the joint detection of the flaring blazar TXS 0506+056 in high-energy ($E > 1$ GeV) and very-high-energy (VHE; $E > 100$ GeV) γ-rays in coincidence with the high-energy neutrino IceCube-170922A, identified by IceCube. Imaging atmospheric Cherenkov telescopes (IACTs), namely FACT, H.E.S.S., MAGIC, and VERITAS, continue to conduct extensive neutrino target-of-opportunity follow-up programs. These programs have two components: follow-up observations of single astrophysical neutrino candidate events (such as IceCube-170922A), and observation of known γ-ray sources after the identification of a cluster of neutrino events by IceCube. Here we present a comprehensive analysis of follow-up observations of high-energy neutrino events observed by the four IACTs between 2017 September (after the IceCube-170922A event) and 2021 January. Our study found no associations between γ-ray sources and the observed neutrino events. We provide a detailed overview of each neutrino event and its potential counterparts. Furthermore, a joint analysis of all IACT data is included, yielding combined upper limits on the VHE γ-ray flux.

Unified Astronomy Thesaurus concepts: Particle astrophysics (96); High energy astrophysics (739); Gamma-rays (637); Cosmological neutrinos (338)

1. Introduction

The detection of high-energy astrophysical neutrinos at hundreds of TeV is an important step toward understanding the origin of cosmic rays (CRs). During their acceleration and/or propagation, hadronic CRs interact with ambient matter or radiation fields, producing high-energy neutrinos through the decay of secondary particles. As such, high-energy neutrinos serve as a distinctive signature of hadronic acceleration processes (A. Atoyan & C. D. Dermer 2001; C. D. Dermer et al. 2007; M. Ahlers & F. Halzen 2018).

In 2013, the IceCube Neutrino Observatory (M. G. Aartsen et al. 2017a) announced the discovery of a diffuse flux of cosmic neutrinos (M. G. Aartsen et al. 2013), which is now well established through additional measurements (R. Abbasi et al. 2021a). The astrophysical neutrino flux shows an isotropic distribution, favoring an extragalactic origin. This is also supported by recent evidence for neutrino emission from active galactic nuclei (AGNs; M. G. Aartsen et al. 2018a, 2018b; R. Abbasi et al. 2022a).

The contributions of transient and steady extragalactic sources to the diffuse astrophysical neutrino flux have been significantly constrained (R. Abbasi et al. 2023a), while those of identified sources remain minimal: TXS 0506+056 and NGC 1068 each would account for no more than $\sim$1% of the total flux (M. G. Aartsen et al. 2018a, 2018b; R. Abbasi et al. 2022a), while the Galactic plane contributes approximately 10% at 30 TeV (R. Abbasi et al. 2023b). Consequently, the sources responsible for the bulk of the diffuse neutrino flux are still to be identified (e.g., S. Buson et al. 2022).

The challenge in identifying sources is caused by low signal statistics: only $\mathcal{O}(10)$ high-energy neutrino events with a high probability of being astrophysical are singled out by IceCube each year, and their angular localization is uncertain to 1° or more (M. G. Aartsen et al. 2017b).

In this context, simultaneous electromagnetic (EM) observations are essential for identifying neutrino sources. A particularly important role is played by very-high-energy (VHE; $E > 100$ GeV) γ-rays, which are produced together with neutrinos in the same hadronic (pp) or photo-hadronic ($p\gamma$) interactions. These interactions produce charged and neutral pions that decay into neutrinos and γ-rays, respectively. Thus, the observation of γ-rays in coincidence with high-energy neutrinos may dramatically increase the significance of any detections and pinpoint genuine hadronic accelerators, giving us valuable insights into the CR acceleration mechanisms in the observed sources. However, unlike neutrinos, VHE γ-rays may lose energy or be absorbed within their source environment or during propagation over cosmological distances due to their interactions with the extragalactic background light (E. Dwek & F. Krennrich 2013; A. Reimer et al. 2019). In such scenarios, VHE γ-ray telescopes may not be able to detect the source. In any case, combining multiwavelength (MWL) and VHE observations provides essential information on the emission mechanisms occurring within sources as well as the characteristics of their emission environments (C. D. Dermer et al. 2007; S. Ansoldi et al. 2018; M. Cerruti et al. 2019; X. Rodrigues et al. 2019).

The efficacy of following up neutrino events with EM observations was demonstrated with the 2017 September 22 report of a high-energy neutrino (IceCube-170922A, $\sim$290 TeV) that was spatially and temporally coincident with the flaring γ-ray blazar TXS 0506+056 (M. G. Aartsen et al. 2018a). This is one of the most compelling pieces of evidence for a neutrino point source so far. The significance of this correlation is estimated to be at the 3σ level. The MWL follow-up of this alert was key for establishing this coincidence and constraining the subsequent theoretical modeling for the emission.

Another recent example is the detection of excess astrophysical neutrino events associated with the nearby active galaxy NGC 1068. This association came out from the search for neutrinos from a list of 110 known gamma-ray sources selected a priori from the Fermi-LAT 4FGL-DR2 catalog. A new analysis improves upon the previous results, with the significance increasing from 2.9σ (M. G. Aartsen et al. 2020a) to 4.2σ (R. Abbasi et al. 2022a).

The four imaging atmospheric Cherenkov telescopes (IACTs) systems—FACT (A. Biland et al. 2014), H.E.S.S. (F. Aharonian et al. 2006), MAGIC (J. Aleksić et al. 2012), and VERITAS (J. Holder et al. 2006)—conduct neutrino event follow-up observations in cooperation with IceCube, with the aim of identifying potential γ-ray counterparts. These target-of-opportunity (ToO) programs can be broadly categorized according to two observing strategies, depending on whether they are triggered by neutrino event clusters or single high-energy neutrino events.

The first strategy involves the follow-up observation of clusters of candidate neutrino events with energies above $\sim$1 TeV detected by IceCube around a hypothetical source

location and within a limited time window. The cluster alerts are privately distributed by IceCube to individual IACTs under a memorandum of understanding in the framework of the Gamma-ray follow-up (GFU) program, in operation since 2012 (M. G. Aartsen et al. 2016)

The second strategy involves the follow-up observation of *single high-energy neutrino events* (>60 TeV), which are likely of astrophysical origin. Single-neutrino alerts are publicly distributed, with a typical localization uncertainty radius of $\sim 1^\circ$ (i.e., $\sim 2^\circ$ diameter containment region), which matches well with current IACT fields of view (FOVs) of $3.^\circ 5$–5°. If a promising neutrino source candidate, such as an AGN (e.g., TXS 0506+056) identified using the Large Area Telescope (LAT) on board the Fermi Gamma-ray Space Telescope and IACT catalogs, or a transient source identified by one of the many EM observatories worldwide, falls within the region of interest (ROI) defined by the neutrino's localization uncertainty, observations are usually focused on these specific objects. If no promising source candidates can be identified a priori, the search typically covers the whole ROI defined by the neutrino localization uncertainty.

The MAGIC and VERITAS results from the first stage of the GFU program (up to 2016) are presented in M. G. Aartsen et al. (2016), while those referring to alerts issued from 2016 up to the photon–neutrino coincidence in 2017 September are reported in M. Santander (2017), F. Schüssler et al. (2017), and M. G. Aartsen et al. (2018a; see their Appendix). Results from observations of high-energy neutrino event positions, under the hypothesis of steady or long-term source emission, have been presented in M. Santander et al. (2017).

In this paper, we present a retrospective analysis of follow-up of real-time IceCube neutrino alerts using both strategies during the period from 2017 September (i.e., after the IceCube-170922A and TXS 0506+056 detection) to 2021 January. The paper is organized as follows: in Section 2, we give a brief overview of the alert channels distributed by IceCube. Section 3 provides a description of the neutrino follow-up programs conducted by the IACTs, including an overview of the VHE γ-ray observations that have been performed (Section 3.5) and a description of the methods used to combine IACT data (Section 3.6). In Section 4, we describe the complementary observations performed by MWL instruments and the respective analysis techniques. Sections 5 and 6, respectively present the results from the IACT and MWL observations for each neutrino alert, whether cluster or single neutrino, that was followed up. We conclude with a discussion in Section 7. Appendices A and B summarize additional details of the observations and results.

2. IceCube Neutrino Alerts

The IceCube Neutrino Observatory (M. G. Aartsen et al. 2017a) is a cubic-kilometer neutrino telescope located at the South Pole and designed to search for astrophysical sources of neutrinos and study fundamental neutrino physics. It is currently the most sensitive neutrino telescope in the TeV–PeV range. It consists of 5160 spherically shaped optical sensors called digital optical modules (DOMs) that are deployed below the surface of the ice between 1450 m and 2450 m. Cherenkov light is produced by secondary charged particles when neutrinos interact in or near the active detector volume. This light can be detected by the DOMs. The signals are digitized and sent to the IceCube Laboratory at the surface of the ice sheet. Here, key information is reconstructed in real time, such as the energy, direction, and time sequence of arriving neutrinos.

The construction of the IceCube detector was completed in 2010, and the discovery of an astrophysical neutrino flux in the TeV–PeV energy range was first announced in 2013 (M. G. Aartsen et al. 2013). The properties of the diffuse neutrino flux are measured in different analyses, sensitive to various event topologies (i.e., the characteristic light patterns observed by the detector's optical modules), flavor composition, and sky regions (see, e.g., M. G. Aartsen et al. 2020b; R. Abbasi et al. 2021a, 2022b). We note that, as IceCube cannot distinguish between neutrinos and antineutrinos, we refer to both as *neutrinos* in the following.

In the search for astrophysical neutrinos, the primary backgrounds are atmospheric muon neutrinos and atmospheric muons that are misidentified as neutrinos, both originating from cosmic-ray interactions in the Earth's atmosphere. For event geometries corresponding to downgoing trajectories—as observed by IceCube—the muon background dominates, particularly affecting observations of the Southern sky. In contrast, observations of the Northern sky are primarily limited by atmospheric neutrinos alone, enabling more sensitive searches for astrophysical neutrinos in that direction.

The atmospheric neutrino background can be discriminated thanks to its soft spectrum ($\propto E^{-3.7}$) and known zenith-angle dependence.

On the one hand, taking advantage of the isotropy of the atmospheric neutrino background, an astrophysical neutrino emission can be probed by searching for clusters of neutrino events. This search can be performed over the entire sky, or at the location of potential neutrino emitters, and different timescales are tested. This is the basis for most point-source searches in IceCube and for the real-time GFU program, which produces the *GFU-cluster* alert stream, described in Section 2.1.

On the other hand, at energies above 150 TeV, the harder spectrum of the astrophysical neutrino flux dominates the background of muons and neutrinos arising from CR interactions in the atmosphere. This allows for selection, in near real time, of single-neutrino events that are likely astrophysical, based on their energy. This selection feeds the *single high-energy neutrino* alert stream described in Section 2.2.

2.1. GFU-cluster Alert Stream

The real-time GFU event reconstruction and selection chain is designed to yield a sample of well-pointing candidate neutrino events, suitable for searching for point sources in both space and time by identifying localized event excesses above the expected background over time (i.e., neutrino flares; T. Kintscher 2020; R. Abbasi et al. 2025).

This scheme follows an earlier work implemented in 2006 for the AMANDA-II and MAGIC experiments, which later evolved into the GFU program between the IceCube, MAGIC and VERITAS instruments (M. G. Aartsen et al. 2016, 2017b). In its most recent version, developed in 2019, a time-dependent point-source analysis is applied in real time to the GFU event sample to monitor the locations of known γ-ray emitters as well as the whole sky (T. Kintscher 2019; C. Boscolo Meneguolo et al. 2024). The sources monitored by the GFU program are mostly BL Lac objects and FSRQs. They are selected from the Fermi-LAT 3FGL (F. Acero et al. 2015) and 3FHL (M. Ajello et al. 2017) catalogs, with selection criteria on redshift ($z \leqslant 1$), flux variability, spectral index, and a high γ-ray flux with energy up to 100 GeV (see M. G. Aartsen et al. 2016 for the detailed

definition of these quantities). These criteria maximize the probability for VHE gamma-ray detection by IACTs.

The search for neutrino flares from hypothetical sources is conducted by running a likelihood analysis across multiple sliding time windows. Different timescales are tested with increasingly larger time windows: starting from the latest recorded event (the trigger), a set of significant preceding events (defined in T. Kintscher 2020) is picked for building retroactive time windows to be tested, up to a maximum duration of 180 days, with the trigger serving as the endpoint of each window. Within each possible time window, a likelihood ratio test is performed. The likelihood accounts for the angular distance between observed neutrinos and the hypothetical source direction, estimates of the angular reconstruction uncertainty, the energy spectra of both potential sources and background, and the detector live-time during the time window being tested. Two parameters are fitted: the spectral index and the most likely number of signal events within the given time window.

A test statistic (TS) is calculated for each tested time window by comparing the best-fit result versus the null hypothesis (i.e., the ratio between the likelihood value corresponding to the best-fit spectral index and number of signal events, and the likelihood assuming no signal events). The time window yielding the overall largest TS is selected as the candidate cluster. The pre-trials significance is evaluated by comparing the observed TS with the distribution of TSs obtained from repeated background-only pseudo-experiments.

The outcome of the likelihood scan for every triggering event therefore includes the duration of the most likely cluster time window, the corresponding fitted spectral index and number of signal events, and the significance of the resulting candidate neutrino cluster.

When pre-trials significant excess above a predetermined threshold is registered, an alert is privately sent to partner IACTs, allowing them to rapidly re-point their telescopes to acquire γ-ray observations from the direction of the candidate source. Alerts are issued only once the significance threshold is exceeded and are not updated afterwards. New alerts for the same source can only be generated after the significance level falls back below the threshold.

It is likely that some alerts are given by background fluctuations. Hence, we calculate the false-alert rate (FAR; C. Boscolo Meneguolo et al. 2024) in order to quantify the frequency at which a cluster is found from some particular direction with a significance surpassing the pre-defined threshold, being produced by chance in the background-only scenario. For each source, the FAR is estimated by applying the cluster search algorithm to 1 yr of time-scrambled data at the same source decl. For the all-sky scan, the FAR is estimated from 1 yr of time-scrambled data at sampled declinations.

The significance threshold for alert issuing was pre-set to 3σ for individual sources and 4.2σ for the whole sky, in order to obtain a total FAR of 10 alerts per year per each IACT, from monitoring their respective full source catalogs, and one all-sky alert per year to be shared with all partners. Indeed, a higher threshold was set for all-sky alerts to take into account the larger trials arising from testing multiple sky pixels.

No post-trials significance is reported for alerts, as the real-time analyses are continuously updated with the arrival of new events. Trial corrections for neutrino alerts are only applied retrospectively in a posteriori checks to the best pre-trials p-value recorded. This calculation of the trial factors accounts for the total exposure time at the time of evaluation since the program was started and, in the case of pre-defined source hypotheses, the total number of monitored sources.

The complete information on the GFU-cluster alerts used in this paper is provided in Table 16.

2.2. Single High-energy Neutrino Alert Streams

Since 2016, IceCube has been promptly broadcasting the positions of single potential astrophysical neutrino events to the wider astronomical community after detecting them at the South Pole, encouraging timely follow-up observations (M. G. Aartsen et al. 2017b). Two alert streams were first defined to select astrophysical neutrino candidates based on their energy and the geometry of the Cherenkov light deposition in the IceCube detector.

The High-Energy Starting Events (HESE) stream uses a vetoing technique to reject atmospheric background and select only events with an interaction vertex inside the detector. This guarantees a very good signal purity at the expense of a low event rate, due to a reduced sensitive volume, and a moderate angular resolution ($1.^{\circ}89$ for 90% containment), due to limited track lengths.

The Extreme High-Energy (EHE) event selection features a two-dimensional cut on the quality of the directional reconstruction and the total amount of measured Cherenkov light (a proxy for the energy of the incoming muon). A better angular resolution can be achieved ($0.^{\circ}81$ for 90% containment), thanks to the long selected muon tracks.

In 2019 May, the two separate streams were replaced by a unified algorithm selecting candidate astrophysical neutrinos from three channels: the existing EHE selection, an improved version of the HESE selection, and the GFU-GOLD/BRONZE selection (i.e., high-energy muon track events selected from the GFU event sample based on their reconstructed energy and signal purity) constituting the majority (86%) of the issued alerts. More details about the above alert streams can be found in E. Blaufuss et al. (2019).

For each event that passes these selections, a quantity called "signalness" is calculated to quantify the probability that it is of astrophysical origin. Two alert streams, dubbed "GOLD" and "BRONZE," are defined with different event rates and an average astrophysical signalness value of 50% and 30%, respectively.

The sky coordinates, angular uncertainty, energy, signalness, and FAR values of selected events are publicly distributed through the NASA General Coordinates Network (GCN) as a "GCN Notice."[188] The median delay between the event detection at the South Pole and the successful dissemination via a GCN Notice was 41.8 s for GOLD and BRONZE alerts during the period under consideration in this work.

More advanced reconstruction algorithms are applied to the event once the data have been transferred to computing clusters in the Northern Hemisphere, and updated position and angular uncertainty estimates are circulated in a revised GCN Notice accompanied by a GCN Circular.[189] This updated position can be used by follow-up instruments to revise their observing strategy with respect to the first notice or identify alternative potential counterparts. The median delay between

[188] An example GCN Notice for the Gold alert IceCube-190730A is available in https://gcn.gsfc.nasa.gov/notices_amon_g_b/132910_57145925.amon.

[189] An example GCN Circular for the Gold alert IceCube-190730A is available in https://gcn.nasa.gov/circulars/25225.

the initial event detection and the dissemination of the second notice was 3.35 hr over the period covered by this work.

For more details on the alert streams and a recent, refined reconstruction of the single high-energy neutrino events triggering alerts, see *IceCat-1*: The IceCube Event Catalog of Alert Tracks (R. Abbasi et al. 2023c).

For completeness, we mention that since 2020, IceCube has been issuing alerts also for cascade-like events,[190] showing a different topology compared to the track-like GFU event sample (R. Abbasi et al. 2021b). However, they are not part of the neutrino ToO programs reported in this work.

3. IACT Neutrino Follow-up Programs

The MAGIC, FACT, H.E.S.S., and VERITAS IACT instruments operate ToO programs designed to search for the VHE γ-rays that are expected to be emitted in association with astrophysical neutrinos. We present here a brief overview of the main characteristics of these observatories and describe the evolution of their neutrino ToO programs.

3.1. MAGIC

MAGIC is a system of two IACTs located at the Observatorio del Roque de Los Muchachos (28°45.70′N, 17°53.42′ W; 2200 m above sea level) in La Palma, Canary Islands, Spain. The two telescopes each have a reflector with a diameter of 17 m and are situated 85 m apart, comprising a system capable of achieving an energy threshold as low as 50 GeV (∼20 GeV using the Sum-Trigger-II analog trigger; F. Dazzi et al. 2021a). MAGIC can detect γ-rays up to ∼50 TeV with an integral sensitivity of ∼0.7% of the Crab Nebula flux above 220GeV in 50 h of observation (J. Aleksić et al. 2016a).

Together with other IACTs, MAGIC has conducted follow-up observations of neutrino triggers from IceCube since 2012. As soon as IceCube started delivering single high-energy neutrino alerts via the GCN in 2016, they were added to the MAGIC transient alert system, and automatic reaction was implemented in 2017 December. The MAGIC neutrino ToO follow-up program was upgraded after the IceCube transition from the HESE/EHE to the GOLD/BRONZE channels. Currently, MAGIC automatically repoints to any GOLD alert position that is visible during the night, with a zenith angle smaller than 60° and with an angular distance to the Moon larger than 30°. BRONZE and GFU-cluster alerts are scheduled manually. The final decision to perform follow-up observations typically relies on a combination of several factors like the intrinsic parameters of the neutrino alert (e.g., signalness, FAR, and duration of the flare), the available visibility window, weather conditions, or the presence of a candidate electromagnetic counterpart. MAGIC allocates approximately 40 hr of dark time and 20 hr of Moon time per year for the follow-up of neutrino events and their potential counterparts.

The majority of observations presented here were performed using the standard stereo trigger (R. Paoletti et al. 2007; J. Aleksić et al. 2016b), except for the observations of the AGNs OP 313 and PKS 1502+106. Those two distant sources ($z \gtrsim 1.0$) were observed using the Sum-Trigger-II analog trigger, which is optimized for a low-energy threshold and delivers improved sensitivity in the <200 GeV energy range (F. Dazzi et al. 2021b). All observations were performed in wobble mode with an offset of 0.°4 from the source, allowing for a simultaneous background measurement in the telescope's FOV (V. P. Fomin et al. 1994; D. Berge et al. 2007). MAGIC data were analyzed using the MARS (*MAGIC Analysis and Reconstruction Software*) proprietary package (R. Zanin et al. 2013). When necessary, the flux values were corrected for atmospheric extinction due to clouds and aerosols, using the LIDAR system at the MAGIC site (F. Schmuckermaier et al. 2022, 2023). For the observations performed during moonlight, the analysis method described in M. L. Ahnen et al. (2017) was applied.

3.2. FACT

The first Geiger-mode avalanche photodiode (G-APD) Cherenkov telescope (FACT) is an imaging atmospheric Cherenkov telescope located at the Observatorio del Roque de los Muchachos next to the two MAGIC telescopes. It has a mirror surface of 9.51 m^2 and a camera with an FOV of 4.°5 (H. Anderhub et al. 2013). While the main focus of the project is the monitoring of bright TeV blazars, a follow-up program for multimessenger and multiwavelength alerts has been set up. Thanks to the use of silicon-based photosensors (A. Biland et al. 2014), the duty cycle of the instrument is maximized. The ability to operate the telescope even in bright moonlight (M. L. Knoetig et al. 2013) not only minimizes gaps in the long-term light curves of monitored sources, but also allows for follow-up observations during light conditions in which other IACTs are not available. From the beginning, the project was targeted toward robotic operation, and automating the operations further increased the duty cycle of the instrument (D. Dorner et al. 2019).

Up to 2019 May, FACT followed up multiwavelength and multimessenger alerts on a best-effort basis, adding the observations manually to the schedule. Then, an automatic follow-up mode was introduced for alerts received via GCN. Additional alerts received by email and extensions of interesting follow-ups are handled manually. For automatic follow-ups, the following strategy is applied: alerts for γ-ray bursts (from, e.g., INTEGRAL, Swift/BAT, Agile, Fermi-GBM, HAWC), neutrino alerts (e.g., IceCube single high-energy events and multimessenger coincidences) and transient Fermi-LAT sources are followed-up for 1 hr. Automatic follow-up observations are carried out if the following conditions are satisfied: (1) the observation occurs during astronomical night (Sun elevation $< -18°$); (2) the zenith distance of the source's position is <45°; (3) the angular distance between the source and the Moon is between 10° and 170°; (4) the currents in the photosensors are predicted from moonlight to be <110 μA (see T. Bretz et al. 2013); and (5) the predicted energy threshold is not more than 10 times higher than for the best observing conditions (see T. Bretz et al. 2013). In case these conditions are not met when the alert arrives, but at any time within the ongoing or following observing night (for alerts arriving during day), an automatic call to the alert expert is issued, who decides on how to proceed and schedules a follow-up manually if needed.

So far, FACT has followed up 62 multiwavelength and multimessenger alerts, of which 24 were observed in automatic mode since 2019 May. Of the latter, four were following up neutrino alerts, three of which occurred between 2019 May and November. Before 2019 May, six neutrino alerts were followed up, of which two were after 2017 September. For this paper, we therefore study five neutrino alerts followed up by FACT.

All observations were performed in wobble mode with an offset of 0.°6 from the source location. The data were analyzed

[190] https://gcn.gsfc.nasa.gov/amon_icecube_cascade_events.html

using the open-source Modular Analysis and Reconstruction Software (MARS; T. Bretz & D. Dorner 2010). The details of the analysis are described in D. Dorner et al. (2015), and the background suppression cuts can be found in M. Beck et al. (2019). Integral-flux upper limits are determined using the "light-curve cuts," yielding an energy threshold of 810 GeV, assuming a power-law spectral index of $\Gamma = 2.5$. For the differential-flux upper limits, the "spectrum cuts" were used with an energy threshold of 490 GeV, using the same assumption for the spectrum as for the integral-flux upper limits. The dependence of the γ-ray rate on the zenith angle and the trigger threshold (which changes according to the level of ambient light) was determined and corrected for using the γ-ray rate measured from the Crab Nebula, a standard source at TeV energies. More details on the correction and spectral analysis can be found in A. Arbet-Engels et al. (2021) and B. Schleicher et al. (2022), respectively.

To reject data taken with bad atmospheric conditions, the observed cosmic-ray rate ($R750_{\rm cor}$) is extracted by applying an artificial trigger of 750 DAQ counts to the data and correcting it for the effect of zenith angle (M. Mahlke et al. 2017; T. Bretz 2019). Seasonal variations of the cosmic-ray rate due to changes in the Earth's atmosphere are considered by determining a monthly reference value $R750_{\rm ref}$. Good-quality data were selected using a cut of $0.93 < R750_{\rm cor}/R750_{\rm ref} < 1.3$.

3.3. H.E.S.S.

The High Energy Stereoscopic System (H.E.S.S.) consists of four 12 m IACTs that have been operating since 2004, and one 28 m telescope that was added in 2012. The telescopes are located in the Khomas Highlands, about 100 km southwest of Windhoek, Namibia (23°16.18′ S, 16°; 30.00′ *E*; 1800 m above sea level). Currently, H.E.S.S. is the only IACT-array in the Southern Hemisphere. The original four telescopes are placed in the corners of a square of side length 120 m, and the fifth telescope is placed at the center of this square. The initial four-telescope configuration is sensitive to γ-rays with energies between ∼100 GeV and ∼100 TeV and has an FOV equivalent to $5.^{\circ}0$ in the sky (F. Aharonian et al. 2006). The fifth telescope has a mirror area of 614 m^2, making it the largest optical instrument in the world. Its mirror is segmented into 875 hexagonal facets. The addition of this telescope enables the energy threshold of H.E.S.S. to be lowered to a few tens of GeV.

Since 2012, H.E.S.S. has conducted a neutrino ToO program, searching for spatial and temporal correlation between neutrinos and VHE γ-ray emission. While observations were initially triggered by real-time alerts from the ANTARES neutrino telescope (M. Ageron et al. 2012; A. Albert et al. 2024), observations of archival and real-time neutrino detections by IceCube have been an integral part of the H.E.S.S. multimessenger program since 2015.

The H.E.S.S. Collaboration joined the GFU program in 2018 December (F. Schüssler et al. 2019) when IceCube extended the search for neutrino clusters to an a priori defined list of known γ-ray sources in the Southern Hemisphere. H.E.S.S. observation time is awarded by an Observations Committee in a competitive process every year. Over the past few years, the typical amount of time allocated for neutrino-related observations was about 20 hr yr^{-1}. This time is mostly devoted to deep observations of particularly interesting events that enable not only the detection but also the characterization of possible VHE γ-ray emission. ToO observations are usually triggered fully automatically via the H.E.S.S. Transient alert system (C. Hoischen et al. 2022), which is connected to a large variety of brokers and alert channels, including a dedicated link to the IceCube computing center at the University of Wisconsin–Madison.

Focusing primarily on high-energy sensitivity, the H.E.S.S. results presented in this work make use of data collected by the four 12 m telescopes, except for the GFU-cluster alert associated with the source 1ES 1312-423 where data from all five telescopes are included. All observations are performed in wobble mode, where the telescopes are pointed with an offset of $0.^{\circ}5$ from the source position. The results are derived using the semianalytical Model Analysis (M. de Naurois & L. Rolland 2009) with loose cuts and cross-checked by the independent calibration and analysis procedure described in R. Parsons & J. Hinton (2014) for all of the neutrino ROIs.

3.4. VERITAS

VERITAS (J. Holder et al. 2006) consists of an array of four 12 m IACTs located at the Fred Lawrence Whipple Observatory in Southern Arizona, USA (31°40.50′ N, 110°57.11′ W, 1300 m above sea level). Each telescope is equipped with a camera containing 499 photomultiplier tubes covering an FOV of $3.^{\circ}5$. It reaches its best sensitivity in the 100 GeV to 30 TeV energy range. The angular resolution of VERITAS is $\sim 0.^{\circ}1$ at 1 TeV (for 68% containment), and the energy resolution is 15%–25% at the same energy. In its current configuration, VERITAS can detect a source with a VHE flux of 1% of the Crab Nebula above an energy threshold of 240 GeV in <25 hr at a statistical significance of 5σ (N. Park et al. 2015).

First efforts within VERITAS to study potential correlations between VHE γ-rays and IceCube neutrinos date back to 2007 and involved a neutrino search associated with flares of the known VHE blazar Markarian 421 (M. Bayer et al. 2007). Subsequent efforts concentrated on follow-ups of GFU-cluster alerts (M. G. Aartsen et al. 2016), which, following the IceCube announcement of the discovery of an astrophysical neutrino flux in 2013, were complemented by a broad program of deep exposures on archival IceCube neutrino positions of likely astrophysical origin (M. Santander 2016; M. Santander & VERITAS Collaboration 2016; M. Santander et al. 2017). This program later transitioned to the real-time efforts described in this paper where, as part of its long-term scientific program, VERITAS allocates approximately 45 hr of dark time observations per year to follow up neutrino alerts from IceCube or to perform deep exposures of potential VHE γ-ray counterparts of neutrino events.

Through its ToO program, VERITAS initiates automatic follow-up observations after receiving an alert from IceCube through GCN and will accumulate a 3 hr initial exposure as long as the target's zenith angle is smaller than 50°. Assuming that VERITAS is operating at the time of the alert, the total delay between the detection of the neutrino at the South Pole and the start of pointed observations by VERITAS is typically about a few minutes. For alerts that occur during local daytime, longer delays of up to 24 hr until the start of observations may be considered if the neutrino event has high astrophysical probability (>90%) and is well localized (<1°), or if a promising γ-ray counterpart (such as a source in the Fermi-LAT 3FHL or 4FGL catalogs) is identified within the neutrino uncertainty region. In the latter case, a long exposure

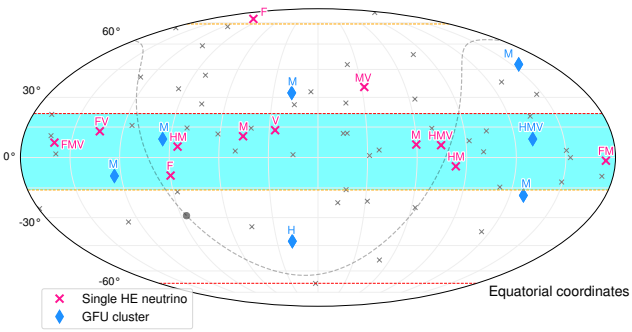

Figure 1. Skymap in equatorial coordinates showing IceCube alert positions in the period from 2017 September to 2021 January. Alerts followed up by IACTs are shown in color (according to the alert type), and those not followed up are shown in gray. Letters indicate which IACTs participated in the observations (F—FACT, H—H.E.S.S., M—MAGIC, V—VERITAS). The latitude band between two dashed orange lines and two dashed red lines indicates regions of the sky that are potentially observable at zenith angles $<45^\circ$ from the northern (FACT, MAGIC, VERITAS) and southern (H.E.S.S.) IACTs, respectively. The light-cyan band represents the overlapping visibility window for instruments in both hemispheres around the celestial equator, where the IceCube sensitivity to neutrinos in the ∼100 TeV energy range is at its best.

(up to tens of hours) is initiated, targeting a sensitivity level of a few percent of the Crab Nebula flux.

The analysis of VERITAS data presented here was performed using the standard VERITAS analysis tools (Eventdisplay; G. Maier & J. Holder 2017) with background-rejection cuts optimized for soft-spectrum sources ($\Gamma \geqslant 3.5$). The background was estimated through the standard "reflected regions" technique (V. P. Fomin et al. 1994). A cross-check analysis was performed with an independent software package (VEGAS; P. Cogan 2007).

3.5. Overview of VHE γ-ray Observations

Figure 1 provides a skymap of the direction of the alerts sent by IceCube as single high-energy neutrino events and GFU-clusters. The follow-up observations of different IACTs are indicated using letters (see figure caption). Tables 1 and 2 explicitly list the observed alerts and provide information on MWL data collected. The IACT delay and exposure times for all single events and GFU-clusters discussed here are presented in Figure 2. The delay is calculated from the neutrino event arrival time (single events) or the time at which the significance threshold is exceeded (clusters) up to the start of the IACT observation.

Already from this broad overview, we can deduce some general trends in the follow-up strategies. Reaction times of less than a day are achieved in 50% of the cases, and observations that began more than a week after the trigger are rare. The total time spent on following up public IceCube alerts is very similar for all collaborations (∼20 hr).

In detail, the IACTs followed 12 out of the 62 single high-energy event alerts sent by IceCube in the period between 2017 September and 2021 January.[191]

In the framework of the GFU program, for each IACT experiment, a separate list of possible follow-up sources was prepared. The numbers of sources and the corresponding total FAR (computed according to C. Boscolo Meneguolo et al. 2024) was 139 sources, 6.2 alerts per year for H.E.S.S.; 179 sources, 9.9 alerts per year for MAGIC; and 190 sources, 11.4 alerts per year for VERITAS. No private alert was sent to FACT.

From 2019 March until 2021 January (1.9 yr), IceCube issued 27 GFU-cluster alerts (17 for H.E.S.S., 12 for MAGIC, and 8 for VERITAS) from 17 sources, and a single all-sky alert. Some of the alerts have been issued simultaneously to multiple IACTs due to partial overlaps in the source catalogs, and in some cases when the source repeatedly went below and above the threshold, multiple correlated alerts were sent. During the first months of the online system's operation, it experienced inconsistent performance due to the development and testing phase, which caused the effective number of issued alerts to be lower than the expected FAR. Of the cluster alerts issued, seven were followed by at least one IACT (two H.E.S.S., six MAGIC, one VERITAS).

Seven of the single-event alerts and one GFU-cluster were followed by more than one IACT. We used the combined exposure to calculate joint upper limits, which are more constraining than single-instrument limits. For example, 4FGL J0955.1+3551, a possible counterpart to IceCube-200107, was observed by MAGIC and VERITAS, while the GFU-cluster alert on GB6 J0316+0904 was followed by all three large instruments. In the case of IceCube-201114A, a dedicated multiwavelength follow-up campaign (including H.E.S.S., MAGIC, and VERITAS) was organized for its potential counterpart 4FGL J0658.6+0636. The observation campaign and its results are discussed in more detail in a separate publication (R. de Menezes et al. 2022).

3.6. Calculation of Individual and Combined Upper Limits

For the upper limits (ULs) calculation, we used the Rolke method (W. A. Rolke et al. 2005; J. Lundberg et al. 2010) with a confidence level set to 95% and including a 30% global systematic uncertainty in the efficiency of the applied cuts. The upper limits were calculated considering an observed spectrum modeled by a power-law function, $dN/dE = KE^{-\Gamma}$, K being the normalization constant of the flux, and Γ the index. Following the slope of the IceCube spectrum for the astrophysical neutrino flux, Γ was set to 2.5 (R. Abbasi et al. 2024)—as the gamma-ray and neutrino emissions are expected to show the same spectral shape (M. Ahlers & F. Halzen 2018).

If the cluster alerts arrived from known sources or potential counterparts to the high-energy single-event alerts were found, both differential (and integral) flux upper limits above a given energy threshold (which varies for each alert and observatory) were calculated at the source or counterpart position.

Furthermore, the single-event public IceCube alerts are characterized by large localization uncertainties ($\sim 0.^\circ 5$ to a few degrees at 50% C.L.). As a consequence, the exact localization of the neutrino origin cannot be pinpointed to any point source with a high degree of accuracy. Therefore, we provide skymaps containing the integral γ-ray flux upper limits and covering the neutrino arrival localization error. The upper limits for those maps are calculated following the description above.

Whenever a cluster alert or a potential counterpart is observed by multiple IACTs, we use a method that combines individual likelihoods to produce combined flux upper limits, as described in H. Abe et al. (2022). All IACTs adopted the same energy binning with four bins per decade in the energy range of 71 GeV to 71 TeV. Therefore, the resulting spectra cover a subset of this range, depending on the energy threshold and maximum energy of the single instruments during each

[191] Full list available at: https://gcn.gsfc.nasa.gov/amon_icecube_gold_bronze_events.html and following links. IceCube-200107A was announced several hours after its detection, through a GCN Circular (see GCN #26655).

Table 1
List of GFU-cluster Alerts Followed Up by IACTs in the Years 2019–2020

Source	Duration (days)	Pre-trials Significance	H.E.S.S	MAGIC	VERITAS	MWL
1ES 1312-423	0.26	3.4σ	2.6 hr	⋯	⋯	Swift
MG1 J181841+0903	Multiple alerts	$>3.3\sigma$	⋯	1.6 hr	⋯	Swift
PMN J2016-0903	0.01	3.6σ	⋯	0.9 hr	⋯	⋯
OP 313	Multiple alerts	$> 3.0\sigma$	⋯	3.2 hr	⋯	Swift
OC 457	0.30	3.3σ	⋯	2.5 hr	⋯	Swift
GB6 J0316+0904	2.25	3.1σ	6.0 hr	1.9 hr	1.0 hr	⋯
All-sky alert (PMN J0325-1843)	3.67	5.1σ	⋯	2.0 hr	⋯	⋯

Note. The all-sky alert is shown separately. IACT-named columns give the total exposure time (in hours) for each instrument. Information on the available MWL data is also provided. Complete information on the GFU-cluster alerts is shown in Table 16.

Table 2
List of IceCube Single High-energy Neutrino Alerts Followed Up by at Least One IACT

Name (GCN Circular)		Energy (TeV)	Signalness	FACT	H.E.S.S.	MAGIC	VERITAS	Pot. Count.	MWL
IC-171106A	E	230	0.75	4.0 hr	⋯	4.5 hr	2.5 hr	87 GB 223537.9+070825	⋯
IC-181023A	E	120	0.28	1.0 hr	⋯	⋯	⋯	⋯	⋯
IC-190503A	E	100	0.36	⋯	⋯	0.5 hr	⋯	⋯	⋯
IC-190529A[a]	H	⋯	⋯	1.0 hr	⋯	⋯	⋯	⋯	⋯
IC-190730A	G	299	0.67	⋯	⋯	3.1 hr	⋯	PKS 1502+106	Swift
IC-190922B	G	187	0.50	2.0 hr	⋯	2.2 hr	⋯	AT2019pqh	⋯
IC-191001A	G	217	0.59	5.4 hr	⋯	⋯	1.0 hr	AT2019dsg	⋯
IC-200107A[b]	⋯	⋯	⋯	⋯	⋯	2.7 hr	9.5 hr	4FGL J0955.1+3551	Swift
IC-200926A	G	670	0.44	⋯	1.3 hr	1.0 hr	⋯	⋯	⋯
IC-201007A	G	683	0.88	⋯	3.0 hr	0.5 hr	⋯	⋯	⋯
IC-201114A	G	214	0.56	⋯	14.3 hr	6.0 hr	7.0 hr	4FGL J0658.6+0636	Swift
IC-201222A	G	186	0.53	⋯	⋯	⋯	1.0 hr	⋯	⋯

Notes. A link to the corresponding GCN Circular with updated coordinates (including information regarding the initial localization) released by IceCube is provided in the alert name. The alert nature is provided: E = EHE, H = HESE, G = GOLD. Energy and signalness estimates are not available for 200107A and 190529A. IACT-named columns give the total exposure time (in hours) for each instrument. The name of the potential counterpart and the available MWL data discussed in the text are also given. Complete information on the single high-energy neutrino alerts is shown in Table 17.
[a] Retracted.
[b] The high-energy starting track was not identified as either GOLD or BRONZE.

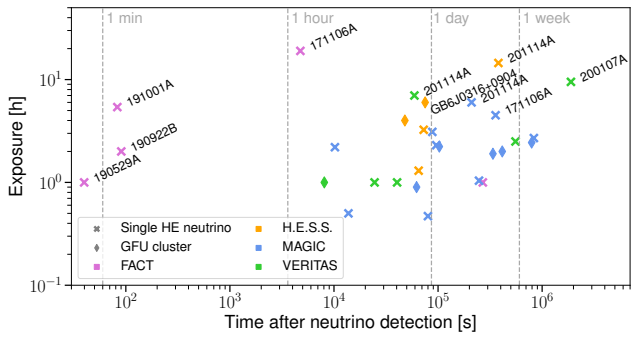

Figure 2. Delay times plotted against exposure times for IACT follow-up observations of neutrino alerts in the period from 2017 September to 2021 January. The delay is calculated from the neutrino event arrival time (single events) or the flare threshold-crossing time (clusters) up to the start of the IACT observation. Observations performed with delays of <100 s or total exposures longer than 4 hr are labeled by alert names. The marker color represents the IACT performing the observation while the marker type represents the alert type.

observation. The latter quantity, i.e., the maximum energy, is defined in a different way in the single experiments: H.E.S.S. and VERITAS use a Gaussian statistic for the estimation of the background, while FACT and MAGIC use a Poissonian approximation. This results in spectra whose maximum energy is computed only for $N_{\rm off} > 10$ in the first case, while in the second case, $N_{\rm off} < 10$ is also allowed. The combined-upper-limit calculation uses a profile maximum likelihood method to estimate the 95% containment for each experiment separately. For each energy bin, the likelihood function is calculated as

$$L = \frac{(\epsilon\mu + b)^{N_{\rm on}} e^{-(\epsilon\mu+b)}}{N_{\rm on}!} \cdot \frac{(\tau b)^{N_{\rm off}} e^{-\tau b}}{N_{\rm off}!} \cdot \frac{1}{\sigma_\epsilon \sqrt{2\pi}} \exp\left[-\frac{1}{2}\left(\frac{\epsilon - \epsilon_0}{\sigma_\epsilon}\right)^2\right], \quad (1)$$

where $N_{\rm on}$ and $N_{\rm off}$ are corresponding IACT-measured events in the signal and background regions, i.e., the ON and OFF

regions, μ and b are the expected gamma-ray signal and background events in the ON region, τ is the ratio between OFF and ON exposure, ϵ is the expected detector efficiency, ϵ_0 is the common efficiency of the detectors, which is set to 1. The efficiency systematic uncertainty, denoted by σ_ϵ, is conservatively taken as 0.3 in this study for all of the detectors. Thus, the derived upper limits based on this estimate are also conservative. The first term in Equation (1) describes the Poissonian signal, the second term describes the Poissonian background, and the third term describes the Gaussian detection efficiency.

The likelihood can be converted into a likelihood ratio test statistic λ after determining the maximum likelihood estimators $\hat{b}$ and $\hat{\epsilon}$:

$$\lambda_{\rm i}(\mu|N_{\rm on}, N_{\rm off}) = \frac{L(\mu, \hat{\varepsilon}, \hat{b}|N_{\rm on}, N_{\rm off})}{L(\hat{\mu}, \hat{\varepsilon}, \hat{b}|N_{\rm on}, N_{\rm off})}, \quad (2)$$

where i denotes different experiments. As the observations from different experiments are independent, the test statistics of individual experiments $-2\ln\lambda_{\rm i}$ can be added to extract a combined-upper-limit value:

$$-2\ln\lambda_{\rm comb} = \sum_{i=1}^{N} -2\ln\lambda_{\rm i}, \quad (3)$$

where, N is the number of experiments performing follow-up observations of the same event. The expected number of ON-region events, $N_{\rm on}$, is related to the differential flux $\Phi(E)$ through the instrument response functions (i.e., effective area, observation time, and energy dispersion) of each IACT, assuming a simple power-law spectral model with flux normalization K.

We note that FACT, H.E.S.S., and VERITAS use an upper-limit calculation that gives a particularly constraining limit when the number of events in the signal region is below the estimated background. The effect of these fluctuations is reduced by the combination of datasets from different instruments. The resulting, combined upper limits on the γ-ray flux can therefore be higher, i.e., less constraining, than the ones derived by the individual instruments.

4. Complementary Observations with Satellite Facilities

In this section, we describe complementary observations carried out by space-based observatories, i.e., the Fermi-LAT and the Neil Gehrels Swift Observatory.

4.1. Fermi Large Area Telescope Observations

The Fermi Large Area Telescope (LAT) is a pair-conversion telescope sensitive to γ-rays with energies from 20 MeV to >300 GeV (W. B. Atwood et al. 2009). It has a large FOV (>2 sr) and scans the entire sky every 3 hr during standard operation, making it well suited to monitor variable and transient γ-ray phenomena on different timescales, from seconds to years.

The real-time neutrino monitoring program carried out by the Fermi-LAT team started in mid-2016, i.e., when IceCube began distributing public alerts to the community (S. Garrappa et al. 2022). The potential and importance of the program was demonstrated with the detection of spatial and temporal coincidence of IceCube-170922A with the γ-ray flaring blazar TXS 0506+056. The prompt observations by the Fermi-LAT triggered a rich campaign, including follow-up by several multiwavelength ground- and space-based facilities, which led to the first identification of a compelling astrophysical counterpart to a source of IceCube neutrinos.

In this study, the LAT data analysis is performed using the Python package `fermipy` (M. Wood et al. 2018), adopting the same procedure for each source in the sample. We select photons of the `Pass 8 SOURCE` class, in an ROI of $15^\circ \times 15^\circ$ square, centered at the target. To minimize contamination from γ-rays produced in the Earth's upper atmosphere, a zenith-angle cut of $\theta < 90^\circ$ is applied. The standard data-quality cut (DATA_QUAL > 0) && (LAT_CONFIG == 1) is applied, and time periods coinciding with solar flares and γ-ray bursts detected by the LAT are removed. The ROI model includes all 4FGL catalog sources (J. Ballet et al. 2020) located within 20° from the ROI center, as well as the Galactic and isotropic diffuse backgrounds[192] (`gll_iem_v07.fits` and `iso_P8R3_SOURCE_V3_v1.txt`).

We perform a binned analysis in the energy range 0.1–800 GeV, using 10 bins per decade in energy and $0.^\circ1$ wide spatial bins and adopting the `P8R3_SOURCE_V3` instrument response functions. For each given target, a maximum likelihood analysis is performed over the time range of interest, ensuring overlap between Fermi data and IACT observations. When a candidate astrophysical counterpart to the neutrinos is available, we select this as the target of interest, and the analysis is centered at its position. For IceCube neutrino events with no candidate astrophysical counterparts, an analysis of the region centered at the best-fit position provided by IceCube was performed.

In the fit, the sources in the ROI are modeled by adopting the spectral shapes and parameters reported in 4FGL. The fit is performed using the "optimize" function, implemented in `fermipy`. The method performs an automatic optimization of the ROI by fitting all sources using an iterative strategy.

Since our data span a different integration time with respect to 4FGL, the results are checked for potential newly detected sources using the iterative procedure implemented in the `fermipy` function "find_sources." To this end, a TS map is produced. Following W. Cash (1979), the TS is defined as $2\log(L/L_0)$, where L is the likelihood of the model with a point source at a given position, and L_0 is the likelihood without the source. A TS value of 25 corresponds to a statistical significance of $\gtrsim 4.0\sigma$ (according to the prescription adopted in S. Abdollahi et al. 2020). A TS map is produced by including a putative point source at each pixel of the map and evaluating its significance over the current best-fit model. The test source is modeled with a power-law spectrum where only the normalization is allowed to vary in the fit, whereas the photon index is fixed at 2. We test whether there are significant peaks (TS > 25) in the TS map, with a minimum separation of $0.^\circ5$ from existing sources in the model, and add a new point source to the model at the position of the most significant peak found. Then, the ROI is fitted again, and a new TS map is produced. This process is iterated until no more significant excesses are found. Flux upper limits are computed if the TS of the target of interest is lower than 4 ($\sim 2\sigma$).

[192] https://fermi.gsfc.nasa.gov/ssc/data/access/lat/BackgroundModels.html

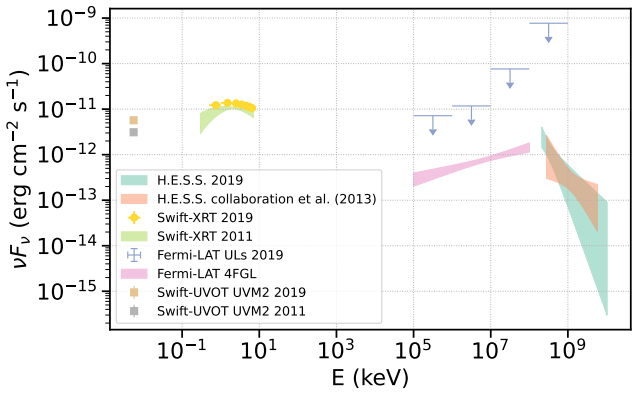

Figure 3. Shown here are 1ES 1312–423 MWL spectral energy distributions (SEDs), depicting both archival data and observations obtained during the period following the GFU neutrino alert (2019 March 12–13).

4.2. Swift

The *Neil Gehrels Swift* Observatory satellite (N. Gehrels et al. 2004) carried out observations of a few sources involved in the follow-up program described in the present paper (see Section 6). NVSS J065844+063711 (counterpart of IceCube-201114A). The observations were performed with all three instruments on board: the X-ray Telescope (XRT; D. N. Burrows et al. 2005; 0.2–10.0 keV), the Ultraviolet/Optical Telescope (UVOT; P. W. A. Roming et al. 2005; 170–600 nm), and the Burst Alert Telescope (BAT; S. D. Barthelmy et al. 2005; 15–150 keV).

All XRT observations were performed in photon-counting mode (for a description of the XRT read-out modes, see J. Hill et al. 2004). The XRT spectra were generated with the Swift-XRT data product generator tool at the UK Swift Science Data Center[193] (Version 1.10 of the product generator module was released as part of swifttools v3.0; for details, see P. A. Evans et al. 2009). Spectra having count rates higher than 0.5 counts s^{-1} may be affected by pile-up. To correct for this effect, the central region of the image has been excluded, and the source image has been extracted with an annular extraction region with an inner radius that depends on the level of pile-up (see, e.g., A. Moretti et al. 2005). We used the spectral redistribution matrices in the Calibration database maintained by HEASARC. The X-ray spectral analysis was performed using the `XSPEC 12.9.1` software package (K. A. Arnaud 1996). Data were grouped by single photons with `grppha` and the Cash statistic was used (W. Cash 1979). All XRT spectra are fitted with an absorbed power-law model `tbabs * pow` and an HI-column density set to the Galactic value in the direction of the source (N_H; taken from HI4PI Collaboration et al. 2016).

The hard X-ray flux of these sources is usually below the sensitivity of the BAT instrument for daily short exposures. Moreover, none of the sources were bright enough in the hard X-rays to be detected in the Swift/BAT 157 month catalog.[194] This reflects in a flux limit in the 14–195 keV energy range of $\sim 8.4 \times 10^{-12}$ erg s^{-1} cm^{-2}.

During the Swift pointings, the UVOT instrument observed the sources in its optical (v, b, and u) and UV ($w1$, $m2$, and $w2$) photometric bands (T. S. Poole et al. 2008; A. A. Breeveld et al. 2010). The UVOT data in all filters were analyzed with the `uvotimsum` and `uvotmaghist` tasks and the 20201215 CALDB-UVOTA release. Source counts were extracted from a circular region of 5″ radius centered on the source, while background counts were derived from a circular region with a 20″ radius in a nearby source-free region. All UVOT exposures were checked for possible small-scale sensitivity problems, which occur when the image of the source falls on small detector regions where the sensitivity is lower.[195] The UVOT magnitudes are corrected for Galactic extinction using the $E(B-V)$ value from E. F. Schlafly & D. P. Finkbeiner (2011) and the extinction laws from J. A. Cardelli et al. (1989) and converted to flux densities using the conversion factors from A. A. Breeveld et al. (2010).

5. Follow-up Results on GFU-cluster Alerts

A summary of the follow-up observation campaigns of GFU-cluster alerts is listed in Table 1 while details on the alerts including the cluster time window, duration, significance, and FAR are listed in Table 16.

No significant VHE emission is detected from any of the sources under study with the exception of blazar 1ES 1312-423 (see Section 5.1 and Figure 3). The flux upper limits are calculated as reported in Section 3.6.

Although for some sources a change of the X-ray spectrum or an enhancement of the X-ray activity has been detected during the period of the neutrino detection, X-rays alone are not sufficient to conclusively establish a correlation between neutrino emission and a specific blazar. Assuming that the neutrinos were produced in proton–photon interactions, the observed X-ray emission could come from the population of target photons in these processes. However, to better understand the mechanism(s) producing X-rays, a detailed modeling of the broadband spectra is needed.

The spectral energy distribution (SED) of each source, which includes MWL data covering the same observation time period and archival data, is shown in Figure 4, while the combined upper limits at VHE are shown in Figure 5(e) for the source GB6 J0316+0904, the only one observed by more than one IACT for the GFU-cluster alerts.

5.1. 1ES 1312-423

1ES 1312-423 is a blazar located at R.A.: 13°15′03.″39, decl.: −42°36′49.″75, i.e., about 2° from the Centaurus A (Cen A) radio galaxy, with a redshift of $z = 0.105 \pm 0.001$ (L. S. Mao 2011). The source was detected with H.E.S.S. in VHE γ-rays during the period from 2004 April to 2010 July using a total exposure time of 150.6 hr (HESS Collaboration et al. 2013). Based on this archival dataset, fitting the differential energy spectrum $\phi(E) = dN/dE$ of the VHE γ-ray emission above 280 GeV with a power-law function $\phi(E) = \phi(E_0) \times (E/E_0)^{-\Gamma}$ yields the best-fit parameters $\Gamma = 2.85 \pm 0.47(\text{stat}) \pm 0.20(\text{sys})$ and a differential flux at 1 TeV of $\phi(1\,\text{TeV}) = (1.91 \pm 0.59(\text{stat}) \pm 0.39(\text{sys})) \times 10^{-13}$ cm^{-2} s^{-1} TeV^{-1}.

On 2019 March 12, IceCube announced the detection of a neutrino cluster from the location. H.E.S.S. observed the source for a total of 2.6 hr divided over two nights: 2019 March 12 and 13. Applying a set of loose cuts (F. Aharonian et al. 2006), VHE emission from 1ES 1312-423 was observed

[193] http://www.swift.ac.uk/user_objects
[194] https://swift.gsfc.nasa.gov/results/bs157mon/
[195] https://swift.gsfc.nasa.gov/analysis/uvot_digest/sss_check.html

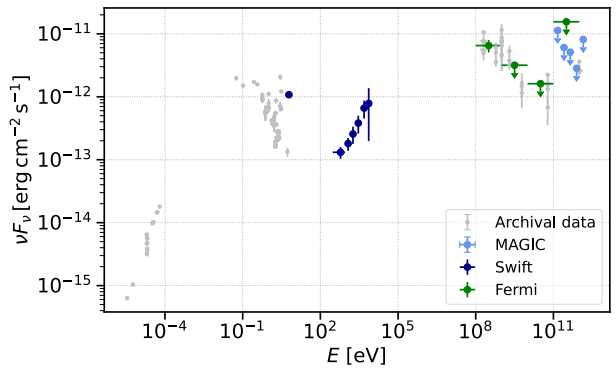

(a) MG1J181841+0903 (Section 5.2)

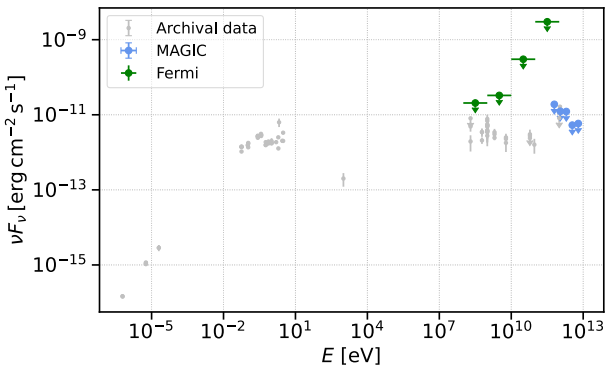

(b) PMNJ2016-0903 (Section 5.3)

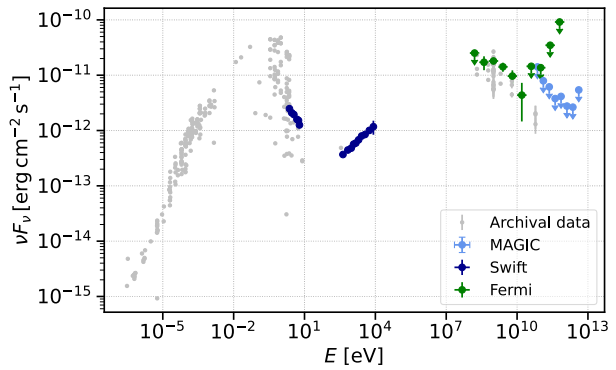

(c) OP313 (Section 5.4)

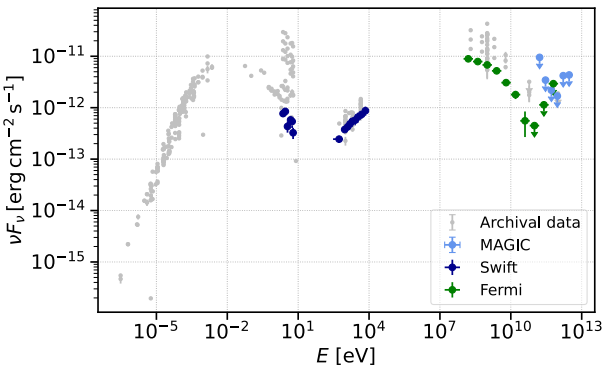

(d) OC457 (Section 5.5)

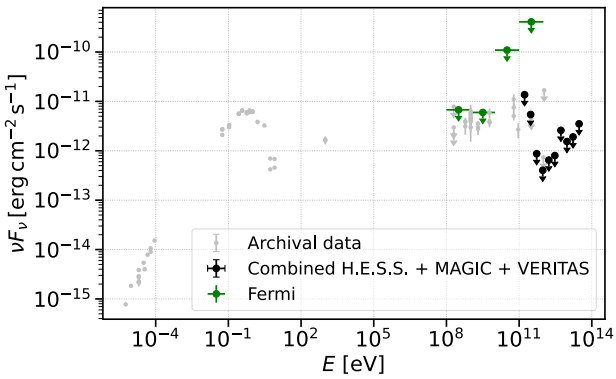

(e) GB6 J0316+0904 (Section 5.6)

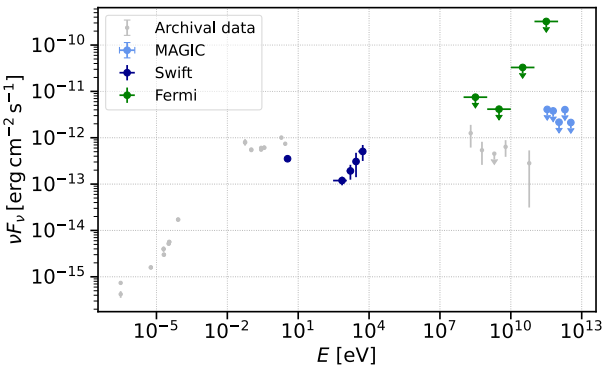

(f) PMN J0325+1843 (Section 5.7)

Figure 4. SEDs for the counterparts of the GFU-cluster alerts mentioned in the text. They comprise IACT ULs and simultaneous MWL data, together with archival data provided for comparison.

above 140 GeV with a significance of 4σ. For these observations, the best-fit parameters are $\Gamma = 3.57 \pm 0.60$ (stat) $\pm$ 0.20(sys) and $\phi(1\,\mathrm{TeV}) = (1.72 \pm 1.4(\mathrm{stat}) \pm 0.4(\mathrm{sys})) \times 10^{-13}\,\mathrm{cm^{-2}\,s^{-1}\,TeV^{-1}}$. A comparison of the SED with the archival dataset is given in Figure 3 together with the results obtained from dedicated ToO observations by Swift (UV + X-rays). The flux levels and energy spectra in the TeV domain are compatible, while some variations in the X-ray and UV bands can be seen in the figure. It is not clear whether this can be linked to a definite change in the state of 1ES 1312-423.

The source was observed six times by Swift during the period from 2011 January 25, to 2019 April 19, with five of these observations performed in 2019. The 0.3–10 keV spectrum can be fitted with an absorbed power-law model with N_H fixed to $7.25 \times 10^{20}\,\mathrm{cm^{-2}}$. No significant flux increase or spectral index change was found in the X-ray (see Table 3). The Swift/UVOT observation results can be found in Table 4.

5.2. MG1 J181841+0903

MG1 J181841+0903 is a flat-spectrum radio quasar (FSRQ) located at R.A.: 18°18′40.″06, decl.: +09°03′46.″20 at unknown redshift. On 2019 June 5, the MAGIC Collaboration received two GFU-cluster alerts related to this source. On 2019 June 7, the MAGIC telescopes observed MG1 J181841+0903 within a zenith-angle range of 25°−46° and collected 2.2 hr of good-

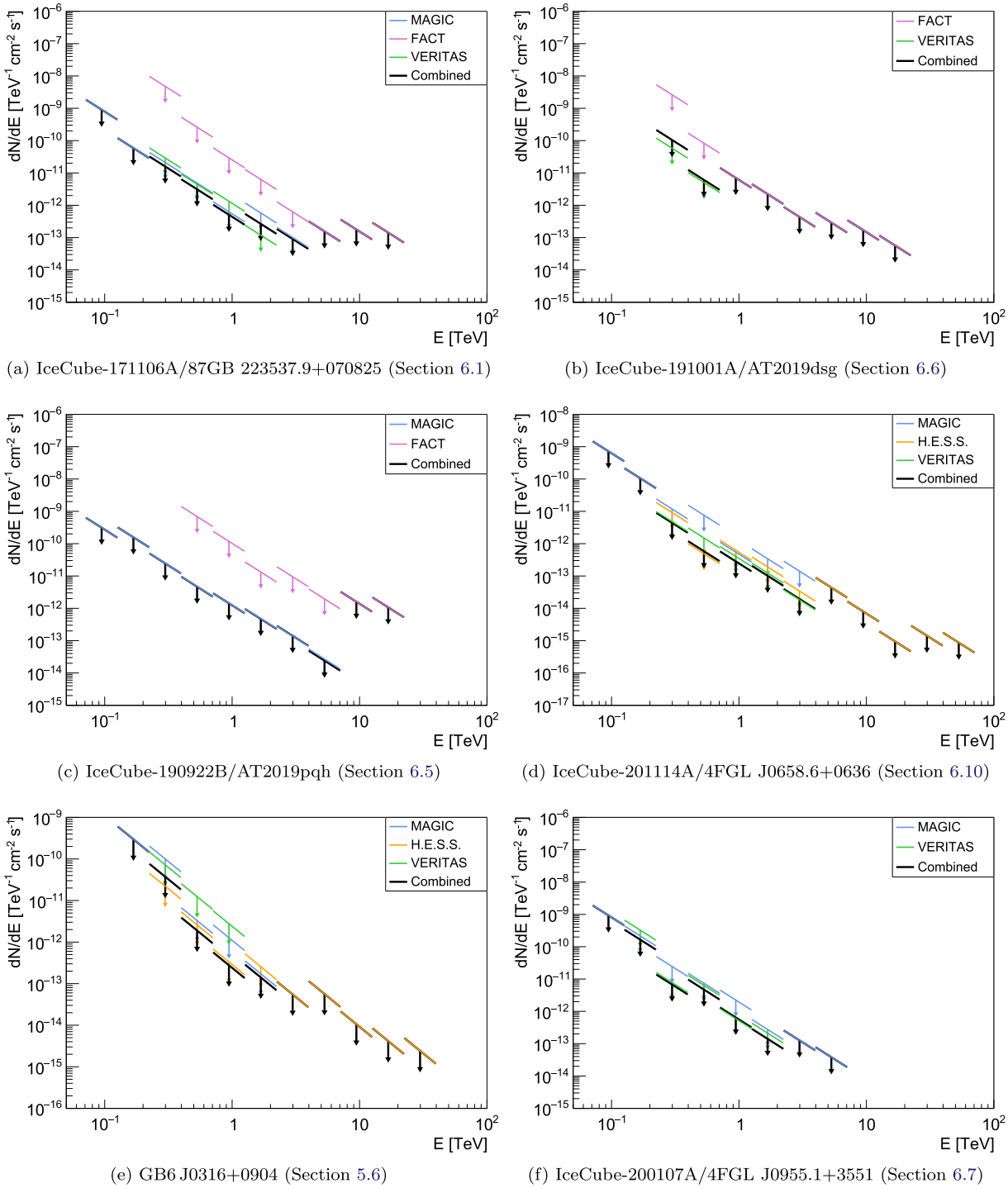

(a) IceCube-171106A/87GB 223537.9+070825 (Section 6.1)

(b) IceCube-191001A/AT2019dsg (Section 6.6)

(c) IceCube-190922B/AT2019pqh (Section 6.5)

(d) IceCube-201114A/4FGL J0658.6+0636 (Section 6.10)

(e) GB6 J0316+0904 (Section 5.6)

(f) IceCube-200107A/4FGL J0955.1+3551 (Section 6.7)

Figure 5. Combined differential-flux upper limits at 95% C.L. for sources observed by multiple IACTs.

quality data. An upper limit of $2.37 \times 10^{-11}\,\mathrm{cm^{-2}\,s^{-1}}$ was calculated for the integral flux above 110 GeV.

The source was observed 10 times by Swift-XRT between 2013 November 17, and 2019 June 6. As the first nine observations (performed between 2013 November 17 and 2016 November 12) consisted of short exposures and low count rates, we summed all of them for a total exposure of 5554 s. The summed spectrum in the 0.3−10 keV energy range can be fitted by an absorbed power-law model with a fixed $N_{\mathrm{H}} = 1.25 \times 10^{21}\,\mathrm{cm^{-2}}$ and a photon index of 1.60 ± 0.53. The corresponding unabsorbed (0.3−10 keV) flux is $(3.2 \pm 1.3) \times 10^{-13}\,\mathrm{erg\,cm^{-2}\,s^{-1}}$. The X-ray spectrum collected on 2019 June 6 can be well fitted by an absorbed power-law model with a photon index of 1.32 ± 0.35 that corresponds to an unabsorbed (0.3−10 keV) flux of $(1.2 \pm 0.4) \times 10^{-12}\,\mathrm{erg\,cm^{-2}\,s^{-1}}$. Thus, there was an increase in X-ray flux for this source on 2019 June 6, which was accompanied by a hint of hardening in the spectrum. On the same day, the source was detected ($>3\sigma$) by UVOT in the $w2$ band with a magnitude $w2 = 19.39 \pm 0.11$. Observations in the other bands resulted in upper limits ranging from 19.98 to 19.11. As such, the increase in X-ray activity coincided with an increase in the UV band (see Figure 4(a)).

5.3. PMN J2016-0903

PMN J2016-0903 is a BL Lac type object located at R.A.: 20°16′ 24.″00, decl.: −09° 03′ 32.″70 at a redshift of $z = 0.367$ (M. Ajello et al. 2022). On 2019 November 29, IceCube detected a neutrino cluster from this direction. MAGIC observed the source on the night of 2019 November 30, within a zenith-angle range of 56°−67°. The good-quality data collected cover about 0.86 hr of observation time. An upper limit on the integral flux above an energy threshold of 450 GeV was computed to be 7.40×10^{-12} cm^{-2} s^{-1}.

The source was only observed by Swift once, on 2012 December 8, with an exposure time of 1581 s. The 0.3−10 keV spectrum can be fitted with an absorbed power-law model with a fixed $N_{\rm H} = 3.97 \times 10^{21}$ cm^{-2} and a photon index of 2.69 ± 0.31. The corresponding unabsorbed flux in the 0.3−10 keV band is $(1.9 \pm 0.4) \times 10^{-12}$ erg cm^{-2} s^{-1}. The 0.1−2.4 keV flux reported in the ROSAT All Sky Survey (RASS; T. Boller et al. 2016) is 6.42×10^{-13} erg cm^{-2} s^{-1}, with an exposure of 1374 s, consistent with the Swift one. For comparison, the 0.1−2.4 keV flux estimated by Swift-XRT on 2012 December 8 is 1.36×10^{-12} erg cm^{-2} s^{-1}, a factor of 2 higher than the flux observed by ROSAT.

The measured UVOT magnitudes estimated on 2012 December 8 are $v = 17.55 \pm 0.20$, $b = 18.10 \pm 0.15$, $u = 17.02 \pm 0.10$, $w1 = 17.24 \pm 0.11$, $m2 = 17.25 \pm 0.11$, and $w2 = 17.30 \pm 0.09$.

Since there are no simultaneous Swift observations at the time of the neutrino alert, we do not compare the state of activity of the source during the neutrino event with the archival one. Thus, the SED of the source showing simultaneous MWL data (see Figure 4(b)) does not include information on the Swift flux.

5.4. OP 313

OP 313 is an FSRQ located at R.A.: 13°10′28.″66, decl: +32° 20′43.″78, with redshift $z = 0.996$ (K. Grasha et al. 2019). This source has been observed by MAGIC since 2014, though without detecting it (S. Abe et al. 2024). In 2020, IceCube issued four GFU-cluster alerts of increasing statistical significance from this region. The MAGIC telescopes observed the source on June 19, 20, and 23 with the Sum-Trigger-II analog trigger within a low zenith-angle range 16°−34°. The observations were performed in good weather conditions, providing 3.2 hr of good-quality data. Also, in this case, the source was not detected. An upper limit on the integral flux above an energy threshold of 55 GeV was computed to be 5.20×10^{-11} cm^{-2} s^{-1}. More recently, in 2023 December, the prototype Large-Sized Telescope (LST-1) achieved the first detection of OP 313 in the VHE gamma-ray band during a high state of activity of the source, marking it as the most distant AGN detected by a Cherenkov telescope (J. Cortina & CTAO LST Collaboration 2023).

The source was observed 32 times by Swift between 2007 April 3 and 2021 March 17. The 0.3−10 keV spectrum can be fitted with an absorbed power-law model with $N_{\rm H}$ fixed to 1.23×10^{20} cm^{-2}. After a period of high activity in 2007, the X-ray flux of OP 313 decreased from 2008–2014. The source exhibited renewed activity during the period from 2019 December 27 to 2020 March 21 (see Table 5). The X-ray photon index during this period is relatively hard (i.e., 1.5 −1.7) in comparison to the flat spectrum ($\Gamma \sim 2$) observed during previous low activity periods. During a similar period, increases in the optical and UV bands were also observed (see Table 6). The MWL SED is shown in Figure 4(c).

5.5. OC 457

OC 457 is an FSRQ located at R.A.: 01°36′58.″59, decl.: +4751′29.″10° at a redshift of $z = 0.86$ (A. E. Truebenbach & J. Darling 2017). On 2020 August 4, IceCube detected a neutrino cluster from this source. The source was observed by the MAGIC telescopes more than a week after the alert, on 2020 August 14 and 15, for a total of 2.5 hr of observation during moderate moonlight conditions. The observations were performed within a zenith-angle range of 22°–34°. The integral-flux upper limit above an energy threshold of 125 GeV is 1.43×10^{-11} cm^{-2} s^{-1}.

The source was observed by Swift 20 times between 2007 July 16, and 2020 August 17 (see Table 9). The 0.3–10 keV spectrum can be fitted with an absorbed power-law model with $N_{\rm H} = 1.02 \times 10^{21}$ cm^{-2} s^{-1}. Between 2007 and 2020, the source was variable in X-rays, with the flux changing by a factor of 3 and the photon index varying between 1.1 and 1.8. Interestingly, at the time of the neutrino detection, on 2020 August 5, the X-ray flux reached the minimum value observed during the 2007–2020 period. Similarly, the optical and UV magnitudes observed by UVOT on the same day are significantly dimmer than the values observed before 2020 (although not at the dimmest value observed over the entire period; see Table 10). The SED is shown in Figure 4(d).

5.6. GB6 J0316+0904

GB6 J0316+0904 is a BL Lac type object located at R.A.: 03°16′12.″733, decl: +09°04′43.″283 with redshift $z = 0.372$ (M. Stadnik & R. W. Romani 2014). It was selected as a potential target for the GFU program for all three participating IACTs. On 2021 January 15, a neutrino cluster from that region was reported.

The VERITAS telescopes were the first on target due to their automatic response and were able to collect 1.0 hr of data on the night of the alert. H.E.S.S. pointed to the source within the next 24 hr and performed 6 hr of observations in total over three consecutive nights. Due to high humidity on site, MAGIC was not able to follow up the alert until 3 days later, at which point, 1.9 hr of observations were collected.

Figures 4(e) and 5(e) show the MWL SED of the source and the combined differential-flux ULs. The VHE γ-ray upper limits were obtained by combining the data from all three IACTs (see Section 3.6).

The source was observed by Swift five times from 2009 March 9 to 2015 January 9. The 0.3−10 keV spectrum can be fitted with an absorbed power-law model with $N_{\rm H} = 1.27 \times 10^{21}$ cm^{-2}. We combined the observations that were carried out on 2011 July 3 and 4, in order to improve the statistics for the spectral fit. Results can be found in Table 7. A significant change of the X-ray flux was observed during the period from 2009–2015, indicating that the source is highly variable in X-rays. Similar high degrees of variability have been observed in the optical and UV bands (see Table 8). However, a comparison with the source activity at the time of the neutrino alert is not possible since there are no Swift observations in that period.

5.7. All-sky Alert/PMN J0325-1843

On 2019 September 19, IceCube observed a GFU-cluster through its all-sky search for time-variable point sources. This search exploits the same algorithm used to search for neutrino multiplets from known γ-ray emitters (see Section 2.1). The location of the alert is consistent with the position of PMN J0325-1843, a candidate blazar source.

On 2019 September 24, the MAGIC telescopes observed the source for a total of 2.3 hr within a zenith-angle range of 47°−51°. An upper limit on the integral flux above 250 GeV was computed to be 5.16×10^{-12}cm^{-2} s^{-1}.

The source was only observed by Swift once, on 2019 September 22, for an exposure time of 1631 s. The 0.3–10 keV spectrum can be fitted with an absorbed power-law model with $N_{\rm H} = 3.16 \times 10^{20}$ cm^{-2} and a photon index of 1.18 ± 0.48. The corresponding unabsorbed flux in the 0.3–10 keV band is $(1.0 \pm 0.4) \times 10^{-12}$ erg cm^{-2} s^{-1}. The 0.1-2.4 keV flux reported in the RASS is 2.51×10^{-13} erg cm^{-2} s^{-1}, with an exposure of 1139 s, consistent with the Swift one. The Swift-XRT observations provided a comparable flux in the 0.1–2.4 keV energy range, 2.62×10^{-13} erg cm^{-2} s^{-1} on 2019 September 22. The magnitude measured by UVOT on 2019 September 22 is $u = 19.05 \pm 0.09$. The MWL SED is given in Figure 4(f).

6. Follow-up Results on Single High-energy Neutrino Alerts

A summary of the follow-up observation campaigns of single high-energy neutrino events is listed in Table 2, while detailed information on the alerts are given in Table 17, including the event direction, energy, signalness, and FAR as well as the refined reconstruction of the events that was performed offline and reported in R. Abbasi et al. (2023c).

No VHE emission was detected from the neutrino alert directions and from the potential counterparts identified in the uncertainty region of six events. Figure 5 gives combined differential-flux upper limits for sources observed by multiple IACTs. The details of combined upper limits calculation can be found in Section 3.6.

Changes in the X-ray spectra and flux level have been observed in some of these sources, providing useful information about the sources' behavior in a broadband context and thus for modeling their SED. However, X-rays alone are not sufficient to conclusively establish a correlation between neutrino emission and a specific source.

Figure 6 shows maps of integral upper limits derived from individual observations, while Figure 7 provides the SED for the potential counterparts of the single-neutrino alerts, plotted using combined upper limits on the VHE flux as well as simultaneous MWL and archival data. While detailed SED modeling for all sources is beyond the scope of this paper, in Section 6.4 we use PKS 1502+106 as an example to discuss the potential effects as well as the limitation of our results on the current modeling work.

6.1. IceCube-171106A

Follow-up observations were carried out by FACT, MAGIC, and VERITAS.

FACT devoted a total of 19 hr of observations in following up the alert. FACT's initial observations, conducted on 2017 November 6, focused on the early reported position for the neutrino and lasted for 3.3 hr. Another 15.6 hr of observations, distributed over the following five nights, focused on updated positions for the neutrino. After removing data influenced by bad weather conditions, 4 hr on the updated position remained, covering a zenith-angle range from 21°–57°. An integral-flux upper limit above an energy threshold of 810 GeV was determined as 8.9×10^{-12} cm^{-2} s^{-1}. The FACT differential-flux upper limits are shown in Figure 5(a).

MAGIC observed the event in the direction of 87GB 223537.9+070825, on 2017 November 10, 13, 15, and 16, collecting a total of 4.5 hr of good-quality data. The observations were performed in wobble mode with a zenith-angle range of 20°−45°. The integral-flux upper limit estimated by MAGIC at the location of the source above an energy threshold of 120 GeV is 8.31×10^{-12} cm^{-2} s^{-1}.

VERITAS observed the event in the direction of the IceCube alert and collected about 2.5 hr of quality-selected observation data from 2017 November 13 to November 20, with an average zenith angle of 35.°1. Observations were performed using the standard wobble observation mode with a 0.°5 offset in each of the four cardinal directions. The integral-flux upper limit above an energy threshold of 350 GeV at the location of the FSRQ 87GB 223537.9+070825 is 1.49×10^{-12} cm^{-2} s^{-1}. An integral-flux upper-limit map and IceCube localization region are shown in Figure 6(a), and an MWL SED is shown in Figure 7(a).

6.2. IceCube-181023A

FACT followed up on the alert and observed the position of the neutrino for 1 hr on the night of 2018 October 26. Earlier observations were not possible, as during full moon, remote operations cannot be carried out for safety reasons. After data-quality selection, 0.6 hr remained, covering a zenith-angle range from 52°–60°. An integral-flux upper limit above an energy threshold of 810 GeV was determined as 1.0×10^{-11} cm^{-2} s^{-1}.

6.3. IceCube-190503A

(+0.°76, −0.°70, 90% point-spread function containment). The event was observed on 2019 May 3, by the MAGIC telescopes, which pointed in the direction of the alert position for a total observation time of 0.5 hr. The zenith-angle range of the observation is 44°−52°. An integral-flux upper limit was calculated above an energy threshold of 200 GeV. The computed value is 1.60×10^{-11} cm^{-2} s^{-1}.

6.4. IceCube-190730A / PKS 1502+106

The distant blazar PKS 1502+106 ($z = 1.84$, P. C. Hewett & V. Wild 2010) has been proposed as a potential electromagnetic counterpart to the IceCube-190730A Gold alert in several publications (e. g. F. Oikonomou et al. 2021; X. Rodrigues et al. 2021), as it is located within the 50% neutrino uncertainty region, precisely 0.°31 from the best-fit neutrino location.

On 2019 July 31, a day after the alert was issued, MAGIC observed the source for 3.1 hr with a zenith-angle range 29°−50°. Due to the high redshift of the target, the observations were performed using the Sum-Trigger-II analog stereo trigger with the aim of achieving the lowest possible energy threshold. The integral-flux upper limit computed at the location of the source, above an energy threshold of 150 GeV, is 8.09×10^{-12} cm^{-2} s^{-1}.

Swift-XRT observations performed between 2019 July 4 and July 30 found the source in a low-activity state with respect to the

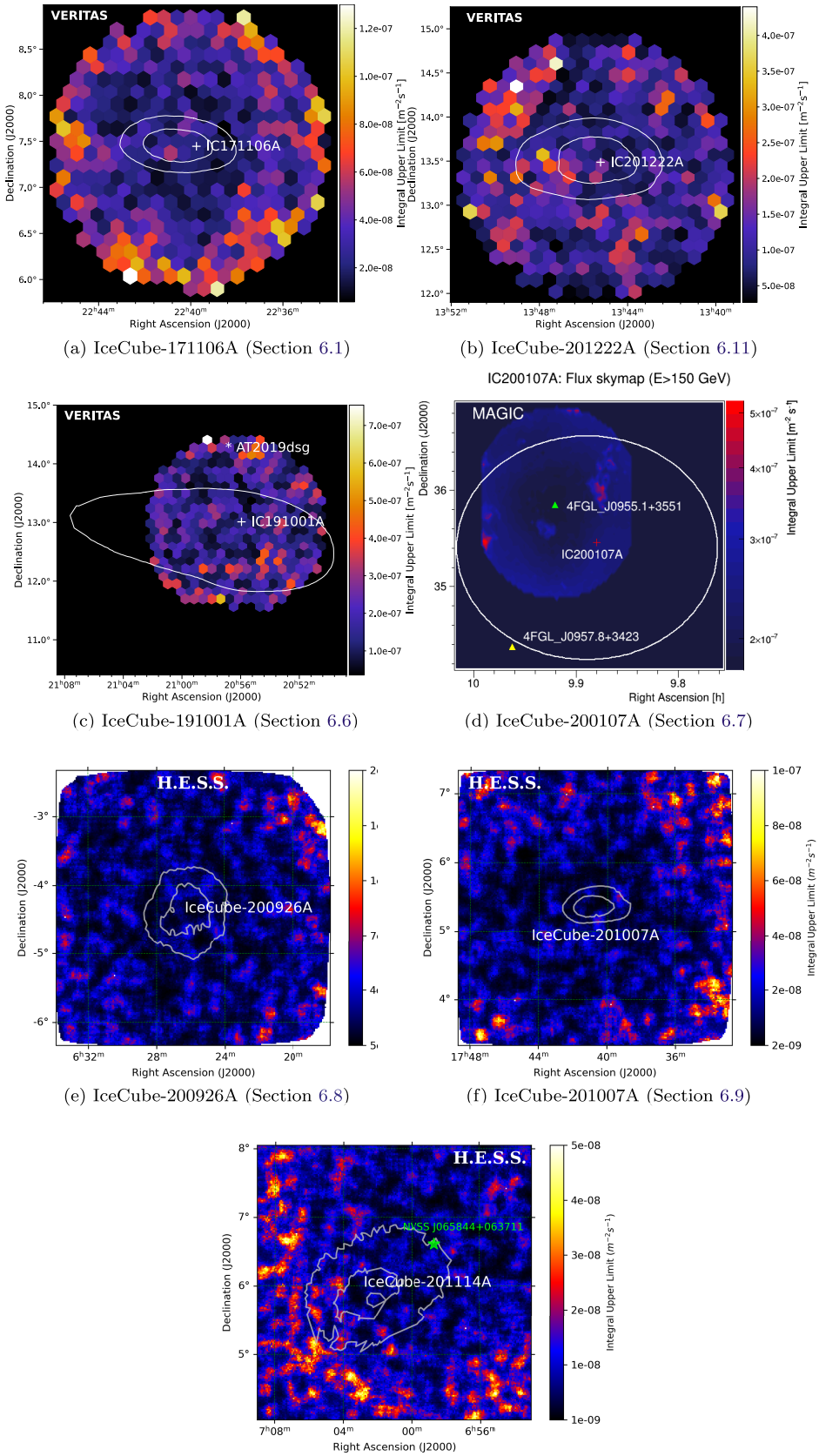

(a) IceCube-171106A (Section 6.1)

(b) IceCube-201222A (Section 6.11)

(c) IceCube-191001A (Section 6.6)

(d) IceCube-200107A (Section 6.7)

(e) IceCube-200926A (Section 6.8)

(f) IceCube-201007A (Section 6.9)

(g) IceCube-201114A (Section 6.10)

Figure 6. Integral VHE γ-ray flux upper-limit maps derived from VERITAS (panels (a), (b), and (c)), MAGIC (panel (d)), and H.E.S.S. (panels (e), (f), and (g)). The two white lines denote the 50% and 90% containment contours of the IceCube event localizations (for panels (c) and (d), only the 50% containment contours are shown). The energy thresholds used to derive the upper-limit maps are 350, 200, 138, 150, 307, 530, and 326 GeV for panels (a)–(g), respectively.

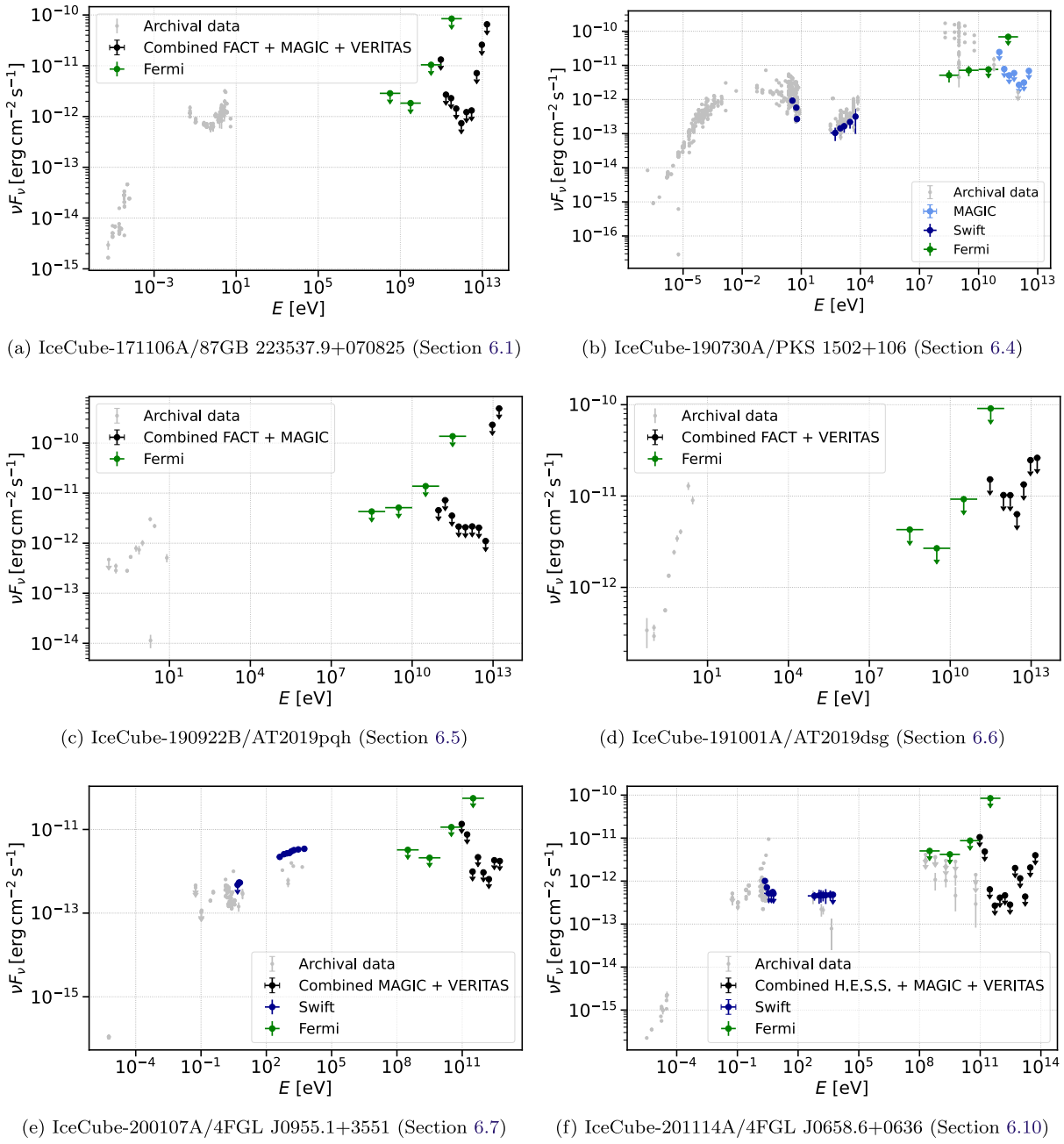

(a) IceCube-171106A/87GB 223537.9+070825 (Section 6.1)

(b) IceCube-190730A/PKS 1502+106 (Section 6.4)

(c) IceCube-190922B/AT2019pqh (Section 6.5)

(d) IceCube-191001A/AT2019dsg (Section 6.6)

(e) IceCube-200107A/4FGL J0955.1+3551 (Section 6.7)

(f) IceCube-201114A/4FGL J0658.6+0636 (Section 6.10)

Figure 7. SEDs for the potential counterparts of the single high-energy neutrino alerts. They comprise IACT ULs and simultaneous MWL data, together with archival data (from ASI ASDC; G. Stratta et al. 2011) provided for comparison.

average flux reported in the second Swift-XRT point-source (2SXPS) catalog (1.97×10^{-12} erg cm^{-2} s^{-1}; P. A. Evans et al. 2020), based on all observations carried out between 2005 January 1 and 2018 August 1 (see Table 15). In 2020, the 0.3−10 keV fluxes detected with the XRT were comparable to the average 2SXPS value. The photon index measured for the source in 2019−2020 was comparable with the average value reported in the 2SXPS catalog (i.e., 1.43) within the uncertainties.

The MWL SED resulting from this work is shown in Figure 7(b), and it is compared with models in Figure 8, as an example to discuss the potential effects as well as the limitation of our results on the current modeling work.

F. Oikonomou et al. (2021) modeled the MWL SED of PKS 1502+106 using a lepto-hadronic framework. Since the source was in a low state at the time of the neutrino detection, they used MWL data from the Wide-field Infrared Survey Explorer, Swift/UVOT, Swift-XRT, and Fermi-LAT telescopes taken between 2010 and 2014, which was a period of persistent low activity for the source. Several different locations for the emitting region were tested to explain the MWL and neutrino emission. To demonstrate how VHE γ-rays constrain the model, we choose the one that places the emitting region of PKS 1502+106 beyond the broad-line region (BLR) but inside the dust torus. In Figure 8(a), we present this model together with the VHE γ-ray ULs obtained from the MAGIC observations and MWL data.

X. Rodrigues et al. (2021) also modeled the emission of this source in a lepto-hadronic context, selecting three different emission states of the source starting from the Fermi-LAT 11

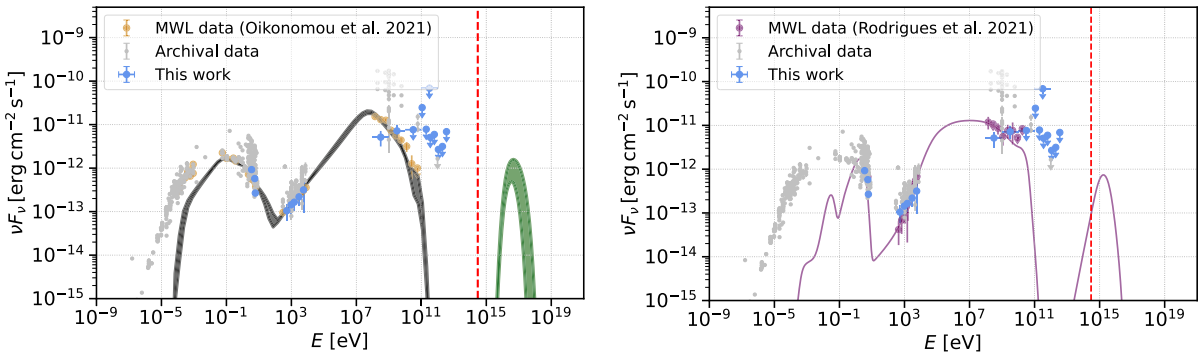

(a) Comparison with model from Oikonomou et al. (2021) in(b) Comparison with model from Rodrigues et al. (2021) in quiescent state. The black and green shaded areas correspondquiescent state. The purple solid line corresponds to the SED to the SED model and $\nu + \bar{\nu}$ all flavor from the paper respec-model from the paper, while the red dashed line corresponds tively, while the red dashed line corresponds to the IC-190730Ato IC-190730A energy.
energy.

Figure 8. Model comparison of the SED for blazar PKS 1502+106, potentially associated with the single high-energy neutrino alert IC-190730A (Section 6.4). Two different models are compared with IACT ULs and simultaneous MWL data, together with archival data (from ASI ASDC; G. Stratta et al. 2011).

yr light curve. Their model considers a single emitting region placed at the boundary of the BLR, resulting in substantial external inverse Compton emission from that region. This component dominates the hard X-ray and soft γ-ray emission, while soft X-rays and hard γ-rays are dominated by photons arising from inverse Compton scattering by pairs produced through the Bethe–Heitler process or the annihilation of VHE photons in the jet. In Figure 8(b), we show a comparison between the low state considered in X. Rodrigues et al. (2021) and the results obtained in this work.

Compared with both works, the VHE γ-ray data presented here do not provide strong constraints on either of these models. One reason could be the limited observations performed on this source. Moreover, the high-energy (HE) γ-ray data in Figures 8(a) and (b) deviate from both models, whereas the UV and X-ray data appear to be consistent with them. The inconsistency between the HE γ-ray data and the models could be because the MWL data were not taken simultaneously, although each of the periods considered coincides with a low state of activity of the source. We note that both F. Oikonomou et al. (2021) and X. Rodrigues et al. (2021) consider a long-term period of low-state activity for the source, whereas in this study, we only analyzed 1 month of Fermi data centered on the neutrino arrival time.

6.5. IceCube-190922B

Both FACT and MAGIC observed the event, collecting 1.9 hr and 2.2 hr of good-quality data, respectively.

FACT's observations started on 2019 September 22, at 23:05:26 UTC (i.e., 63 s after the alert) and lasted for 2 hr. After data-quality selection, 1.9 hr remained, covering a zenith-angle range from 35°–46°. An integral-flux upper limit above an energy threshold of 810 GeV was determined to be 1.1×10^{-11} cm^{-2} s^{-1}.

MAGIC conducted follow-up observations on 2019 September 22 and 25. The first day of observations focused on the direction of the neutrino event. The second day of observations focused on the location of the supernova candidate AT2019pqh, following its announcement by the optical telescope Zwicky Transient Facility (ZTF; E. C. Bellm et al. 2019; R. Dekany et al. 2020) on 2019 September 23, as a possible counterpart of the neutrino event (R. Stein et al. 2019). The position of this source was inside the alert error region, about $0.^{\circ}5$ shifted with respect to the neutrino direction. The integral-flux upper limit found by the MAGIC telescopes at the location of AT2019pqh, above an energy threshold of 150 GeV, is 1.25×10^{-11} cm^{-2} s^{-1}.

6.6. IceCube-191001A / AT2019dsg

Following the neutrino alert, ZTF identified the radio-emitting tidal disruption event (TDE) AT2019dsg as a possible counterpart. A TDE is a rare, transient event that occurs when a star comes sufficiently close to a supermassive black hole (SMBH) to be torn apart by tidal forces. Eventually, roughly 50% of the star's mass is captured and forms an accretion disk around the black hole. The probability of a chance coincidence between a radio-emitting TDE that is as bright as AT2019dsg in bolometric energy flux and an astrophysical neutrino event has been estimated as <0.2% (R. Stein et al. 2021).

FACT observed for a total of 5.4 hr starting on 2019 October 1, at 20:10:41, i.e., with a delay of 53 s after the alert. Of the total observation time, 1 hr was carried out in automatic mode the first night, and the remaining time was scheduled manually in the second night. After data-quality selection, 0.5 hr remained, covering a zenith-angle range of 16°–32°. An integral-flux upper limit above an energy threshold of 810 GeV was determined to be 1.9×10^{-11} cm^{-2} s^{-1}. With slightly relaxed data-quality selection cuts ($0.8 < R750_{\rm cor}/R750_{\rm ref} < 1.3$), there are 5 hr of data, covering a zenith-angle range of 16°–45°. In this case, the integral-flux upper limit above an energy threshold of 810 GeV is 4.6×10^{-12} cm^{-2} s^{-1}. Since this second choice may add a small systematic effect, we believe the true upper limit to fall in between the two values we found, possibly closer to the stricter one. For the calculation of the differential-flux upper limits, we restrict the data sample to trigger thresholds below 560 DAQ counts (moderate moonlight), leaving 3.7 hr of data.

On 2019 October 2, VERITAS performed a follow-up observation in response to the IceCube alert. The observations resulted in 40 minutes of quality-selected data taken from 02:24:00 to 04:04:48 UTC with an average zenith angle of ~20°. Observations were performed using the standard wobble observation mode with a $0.^{\circ}7$ offset in each of four cardinal directions. Assuming a photon index of 2.5, the integral-flux upper limit above an energy threshold of 138 GeV is 8.6 ×

10^{-12} cm^{-2} s^{-1}, which corresponds to 2% of the Crab Nebula flux (K. Meagher & VERITAS Collaboration 2015). An integral-flux upper-limit map and IceCube localization region are shown in Figure 6(c), and an MWL SED is shown in Figure 7(d).

6.7. IceCube-200107A / NVSS J095508+355102

The event did not pass the GOLD/BRONZE classification, but it was identified as a starting track.

This localization region contains a candidate counterpart source NVSS J095508+355102 (4FGL J0955.1+3551). This object is a blazar, located at redshift $z = 0.557$ (S. Paiano et al. 2020). The MWL SED of NVSS J095508+355102 reveals a synchrotron peak at $\sim 4 \times 10^{17}$ Hz in the rest frame (M. Karl et al. 2023), indicating that this source belongs to the rare class of extreme high-synchrotron-peak blazars. Subsequent X-ray observations revealed a flaring episode just after the detection of the neutrino (P. Giommi et al. 2020; F. Krauss et al. 2020).

The MAGIC telescopes observed the location of the source on 2020 January 17 and 18, collecting 2.7 hr of good-quality data. The observations were made in a zenith-angle range of 20°−48°. The computed value for the upper limit on the integral flux above an energy threshold of 120 GeV is 1.75×10^{-11} cm^{-2} s^{-1}. An integral-flux upper-limit map of the region observed by MAGIC is shown in Figure 6(d) together with the IceCube localization region.

VERITAS collected 9.5 hr of quality-selected data between 2020 January 29 and 2020, February 2, with an average zenith angle of $11.^{\circ}8$. Observations were performed using the standard wobble observation mode with a $0.^{\circ}5$ offset in each of four cardinal directions. The computed value for the upper limit on the integral flux above an energy threshold of 150 GeV at the location of the blazar NVSS J095508+355102 is 4.08×10^{-12} cm^{-2} s^{-1}.

In follow-up observations that were performed on 2020 January 8, Swift detected the source with the highest X-ray flux recorded in the period between 2012 and 2020. The source remained at a high X-ray flux (compared to the observations performed in 2012–2013) up to 2020 February 21 (see Table 13 and Table 14).

The MWL SED is shown in Figure 7(e). The proposed multimessenger SED models have difficulties with reconciling the observed neutrino and electromagnetic emissions. V. S. Paliya et al. (2020) explored a lepto-hadronic model with an external photon field. A larger number of possible scenarios is discussed in M. Petropoulou et al. (2020), including neutrinos being produced in the vicinity of the accreting SMBH or through interactions with photons from a possibly weak BLR. Both groups argue that the X-ray flaring event is very unlikely to be directly connected with the observed neutrino event.

6.8. IceCube-200926A

The event was observed by H.E.S.S. and MAGIC, which collected 1.3 hr and 1.0 hr of good-quality data, respectively.

H.E.S.S. observed at the direction of the neutrino event on September 27 from 02:00 UTC to 03:20 UTC with an average zenith angle of $47.^{\circ}5$. H.E.S.S. did not detect any significant emission in the ROI defined by the IceCube localization uncertainty. In Figure 6(e), we show the integral VHE γ-ray flux upper-limit map of the region covered by the H.E.S.S. observations with sufficient statistics, together with the localization contours of IceCube-200926A. The upper limit on the integral flux (above an energy threshold of 307 GeV) at the best-fit IceCube position is found to be 1.86×10^{-12} cm^{-2} s^{-1}.

The MAGIC telescopes observed at the neutrino direction on 2020 September 29, within a zenith-angle range of 38°−48°. The upper limit on the integral flux (above an energy threshold of 200 GeV) at the best-fit IceCube position is 9.78×10^{-12} cm^{-2} s^{-1}.

6.9. IceCube-201007A

The event was observed with H.E.S.S. and MAGIC, which collected 3 hr and 0.5 hr of good-quality data, respectively.

From 2020 October 8, to 2020 October 13, H.E.S.S. conducted follow-up observations of the neutrino localization region for a total of 3 hr. The zenith angles of observation ranged from 51°–60°. In Figure 6(f), we show the integral VHE γ-ray flux upper-limit map of the region covered by the H.E.S.S. observations, together with the localization contours of IceCube-200926A. The upper limit on the integral flux (above an energy threshold of 530 GeV) at the best-fit IceCube position is found to be 8.12×10^{-13} cm^{-2} s^{-1}.

The MAGIC telescopes observed the location of event IceCube-201007A on 2020 October 9, in good weather conditions. The zenith-angle range of the observations is 42°−50°. The upper limit on the integral flux (above an energy threshold of 200 GeV) at the best-fit IceCube position is found to be 2.46×10^{-11} cm^{-2} s^{-1}.

6.10. IceCube-201114A / NVSS J065844+063711

The location of the neutrino event was found to be consistent with the position of the blazar NVSS J065844+063711, also known as the Fermi source 4FGL J0658.6+0636 (R.A.: $104.^{\circ}64$, decl.: $6.^{\circ}60$). The event was observed with H.E.S.S., MAGIC, and VERITAS.

H.E.S.S. observed the region for 14.3 hr. The observation campaign was carried out from 2020 November 18 to 2020 November 25, and from 2020 December 10 to 2020 December 11. The zenith angle for observation ranged from 30°–42°. In Figure 6(g), we show the VHE γ-ray integral-flux upper-limit map of the region covered by the H.E.S.S. observations together with the localization contours of IceCube-201114A. The upper limit on the integral flux above 326 GeV at the position of NVSS J065844+063711 is found to be 5.37×10^{-13} cm^{-2} s^{-1}.

The MAGIC telescopes observed on 2020 November 16 and 17, and during the period of 2020 November 19–25. They collected 6 hr in the direction of NVSS J065844+063711. The observations were performed at a zenith angle in the range of 22°−47°. The upper limit on the integral flux above 120 GeV was computed to be 1.09e–11 cm^{-2} s^{-1}.

VERITAS collected about 7 hr of quality-selected data between 2020 November 15, and 2020 November 19, and with an average zenith angle of $31.^{\circ}1$. Observations were performed using the standard wobble observation mode with a mixture of $0.^{\circ}5$ and $0.^{\circ}7$ offset in each of four cardinal directions. The upper limit on the integral flux above an energy threshold of 200 GeV at the location of the blazar NVSS J065844+063711 is 1.37×10^{-12} cm^{-2} s^{-1}.

Swift-XRT observations carried out on 2020 November 15 indicate an increase of the X-ray flux at the time of the neutrino emission compared with previous observations performed in 2012 May (see Table 11). The source remained

at a comparable X-ray flux level up to 2020 December 11. In contrast, Swift/UVOT observations indicate that in 2020, the source was less bright in the u, $m2$, and $w2$ bands than the baseline values found in 2012 (see Table 12).

The MWL SED is shown in Figure 7(f).

6.11. IceCube-201222A

VERITAS followed up the alert on 2020 December 22, collecting 1 hr of quality-selected data taken at an average zenith angle of $39.^{\circ}2$. Observations were performed using the standard wobble observation mode with a $0.^{\circ}7$ offset in each of four cardinal directions. The upper limit on the integral flux above an energy threshold of 200 GeV at the IceCube neutrino best-fit location is 1.09×10^{-11} cm^{-2} s^{-1}. An integral-flux upper-limit map and IceCube localization region are shown in Figure 6(b).

7. Summary and Outlook

In this work, we have presented results from the neutrino ToO programs of the FACT, H.E.S.S., MAGIC, and VERITAS experiments. No associations were found between γ-ray sources and observed neutrino events. Neutrino ToO programs have evolved significantly over the years, as more has been learned about the properties of the astrophysical neutrino flux and its potential sources, and as new alert streams have been made available by IceCube (e.g., new GOLD and BRONZE single high-energy neutrino alerts and the upgraded GFU program), offering a unique opportunity to probe the possible hadronic nature of gamma-ray sources, which cannot be conclusively achieved with electromagnetic observations alone. Within this context, each IACT collaboration implemented its own observing priorities, and the resulting observations turn out to be complementary to each other (see Section 3.5). These efforts are an integral part of the current long-term science programs of the IACT observatories. The significant observation times allocated to neutrino ToO follow-ups enable the coverage of a large parameter range in terms of observed events, delay times between the neutrino event(s), and observation durations.

The IACTs conducted follow-up observations of six GFU-cluster alerts and one all-sky cluster alert from 2019–2020. The differential-flux upper limits given by the IACTs in the TeV γ-ray regime together with the X-ray observations can be used to constrain maximum contributions from photo-hadronic interactions. The combined upper limits from all IACTs increase our constraints on SED models.

Furthermore, the IACTs performed follow-up observations of 11 IceCube single high-energy neutrino events between 2017 September and 2021 January. These events have a relatively high signalness (compared to low-energy events) and small uncertainty regions $\mathcal{O}(1^{\circ})$. In addition, potential counterpart sources are found within the uncertainty region of six events. It is an ideal data sample for IACTs to search for TeV γ-ray signals from photo-hadronic interactions. Integral-flux upper-limit maps are produced to cover the entire uncertainty regions of seven IceCube single high-energy events.

The main purpose of this work is to serve as a legacy dataset. While detailed SED modeling for all sources is beyond the scope of this paper, PKS 1502+106 was used as an example to discuss the potential effects as well as the limitation of our results on the current modeling work. The VHE γ-ray data detected from the source and presented here do not provide strong constraints on either of these models, as discussed in Section 6.4. These results are a possible starting point for further modeling.

Looking to the future, the geographical distribution of the observatories in latitude has enabled full-sky coverage across the Northern and Southern Hemispheres, and their location in longitude expands the field of regard (total sky area that can be observed by the telescope) of the combined IACT network, increasing the likelihood of prompt follow-up observations in cases where the visibility from one observatory site is constrained by weather, sunlight, bright moonlight, or technical issues. This aspect is critically important to enable VHE γ-ray observations of rare transient neutrino candidate events or in the search for other time-domain or multimessenger triggers, as has been demonstrated recently by follow-up observations of gravitational-wave events (e.g., GW170817; B. P. Abbott et al. 2017) and γ-ray bursts detectable in the VHE range (see A. Berti & A. Carosi 2022 for an overview of recent detections). This underscores the value of conducting analyses combining all available IACT data as presented in this paper.

Follow-up programs are ongoing, and further analyses will prove highly beneficial in the search for VHE counterparts to neutrino events. The full adoption of common high-level data formats (e.g., "GADF"; C. Nigro et al. 2021) and analysis tools (e.g., "Gammapy"; A. Donath et al. 2023) will simplify access and enable joint analyses that combine data from multiple IACTs.

Given the absence of any clear association between multiwavelength signatures and neutrino alerts in this study, these broad searches need to continue in the future. The upcoming Cherenkov Telescope Array Observatory (CTAO) has included neutrino follow-up observations as part of the high-priority Key Science Projects to be conducted in the early years of the observatory (Cherenkov Telescope Array Consortium et al. 2019). With telescopes in both Northern and Southern Hemispheres, CTAO's significant advancement in sensitivity and full-sky coverage promise exciting breakthroughs in these searches (O. Sergijenko et al. 2022).

Further improvements are expected in the near future with the onset of science operations of the KM3NeT neutrino telescope in the Mediterranean Sea (A. Margiotta 2022), further extensions to the Gigaton Volume Detector installation in Lake Baikal (V. A. Allakhverdyan et al. 2023), and other proposed neutrino telescopes such as P-ONE (E. Resconi 2022) and TRIDENT (Z. P. Ye et al. 2022). These facilities will be able to identify more astrophysical neutrino candidate events, improve the angular resolution of the overall dataset, and, due to their location in the Northern Hemisphere, will offer a view of the Galactic Plane complementary to that provided by IceCube. The increased volume of the next-generation IceCube detector, IceCube-Gen2 (M. G. Aartsen et al. 2021), will significantly improve its sensitivity to high-energy neutrinos in the next decade, thereby improving multimessenger searches like the ones presented here.

Acknowledgments

FACT. The important contributions from ETH Zurich grants ETH-10.08-2 and ETH-27.12-1 as well as the funding by the Swiss SNF and the German BMBF (Verbundforschung Astro- und Astroteilchenphysik) and HAP (Helmoltz Alliance for Astroparticle Physics) are gratefully acknowledged. Part of this work is supported by Deutsche Forschungsgemeinschaft (DFG) within the Collaborative Research Center SFB 876

"Providing Information by Resource-Constrained Analysis," project C3. We are thankful for the very valuable contributions from E. Lorenz, D. Renker, and G. Viertel during the early phase of the project. We thank the Instituto de Astrofísica de Canarias for allowing us to operate the telescope at the Observatorio del Roque de los Muchachos in La Palma, the Max-Planck-Institut für Physik for providing us with the mount of the former HEGRA CT3 telescope, and the MAGIC collaboration for their support.

Author contributions. Within FACT, this project was led and coordinated by D. Dorner, the analysis was carried out by B. Schleicher, and both discussed the results and contributed to the manuscript. T. Bretz designed and implemented the automatic follow-up procedure in close collaboration with D. Dorner. The rest of the collaboration contributed by other means to the design, construction, and/or operation of the FACT project (telescope and everything ensuring the scientific output).

H.E.S.S. The support of the Namibian authorities and of the University of Namibia in facilitating the construction and operation of H.E.S.S. is gratefully acknowledged, as is the support by the German Ministry for Education and Research (BMBF), the Max Planck Society, the Helmholtz Association, the French Ministry of Higher Education, Research and Innovation, the Centre National de la Recherche Scientifique (CNRS/IN2P3 and CNRS/INSU), the Commissariat à l'énergie atomique et aux énergies alternatives (CEA), the U.K. Science and Technology Facilities Council (STFC), the Polish Ministry of Education and Science, agreement No. 2021/WK/06, the South African Department of Science and Innovation and National Research Foundation, the University of Namibia, the National Commission on Research, Science & Technology of Namibia (NCRST), the Austrian Federal Ministry of Education, Science and Research and the Austrian Science Fund (FWF), the Australian Research Council (ARC), the Japan Society for the Promotion of Science, the University of Amsterdam, and the Science Committee of Armenia grant 21AG-1C085. We appreciate the excellent work of the technical support staff in Berlin, Zeuthen, Heidelberg, Palaiseau, Paris, Saclay, Tübingen, and in Namibia in the construction and operation of the equipment. This work benefited from services provided by the H.E.S.S. Virtual Organisation, supported by the national resource providers of the EGI Federation.

MAGIC. We would like to thank the Instituto de Astrofísica de Canarias for the excellent working conditions at the Observatorio del Roque de los Muchachos in La Palma. The financial support of the German BMFTR, MPG, and HGF; the Italian INFN and INAF; the Swiss National Fund SNF; the grants PID2019-107988GB-C22, PID2022-136828NB-C41, PID2022-137810NB-C22, PID2022-138172NB-C41, PID2022-138172NB-C42, PID2022-138172NB-C43, PID2022-139117NB-C41, PID2022-139117NB-C42, PID2022-139117NB-C43, PID2022-139117NB-C44, CNS2023-144504 funded by the Spanish MCIN/AEI/10.13039/501100011033 and "ERDF A way of making Europe; the Indian Department of Atomic Energy; the Japanese ICRR, the University of Tokyo, JSPS, and MEXT; the Bulgarian Ministry of Education and Science, National RI Roadmap Project DO1-400/18.12.2020 and the Academy of Finland grant No. 320045 are all gratefully acknowledged. This work has also been supported by Centros de Excelencia "Severo Ochoa" y Unidades "María de Maeztu" program of the Spanish MCIN/AEI/ 10.13039/501100011033 (CEX2019-000920-S, CEX2019-000918-M, CEX2021-001131-S) and by the CERCA institution and grants 2021SGR 00426 and 2021SGR 00773 of the Generalitat de Catalunya; by the Croatian Science Foundation (HrZZ) Project IP-2022-10-4595 and the University of Rijeka Project uniri-prirod-18-48; by the Deutsche Forschungsgemeinschaft (SFB1491) and by the Lamarr-Institute for Machine Learning and Artificial Intelligence; by the Polish Ministry Of Education and Science grant No. 2021/WK/08; and by the Brazilian MCTIC, the CNPq Productivity grant 309053/2022-6 and FAPERJ grants E-26/200.532/2023 and E-26/211.342/2021.

Author contributions. E. Bernardini: PI of MAGIC Neutrino ToO proposal, supervision, paper drafting and editing. D. Miceli: production of MAGIC UL skymap. K. Satalecka: former project leader, paper drafting. I. Viale: project management, MAGIC data analysis, coordination of multiwavelength results, paper drafting and editing. M. Artero, A. Berti, H. Bökenkamp, L. Di Venere, A. Fattorini, L. Heckmann, S. Mangano, H. A. Mondal, K. Noda, S. Sakurai, S. Yoo: MAGIC data analysis. The rest of the authors have contributed in one or several of the following ways: design, construction, maintenance, and operation of the instrument(s); preparation and/or evaluation of the observation proposals; data acquisition, processing, calibration, and/or reduction; production of analysis tools and/or related Monte Carlo simulations; discussion and approval of the contents of the draft.

VERITAS. VERITAS is supported by grants from the U.S. Department of Energy Office of Science, the U.S. National Science Foundation, and the Smithsonian Institution, by NSERC in Canada, and by the Helmholtz Association in Germany. This research used resources provided by the Open Science Grid, which is supported by the National Science Foundation and the U.S. Department of Energy's Office of Science, and resources of the National Energy Research Scientific Computing Center (NERSC), a U.S. Department of Energy Office of Science User Facility operated under contract No. DE-AC02-05CH11231. We acknowledge the excellent work of the technical support staff at the Fred Lawrence Whipple Observatory and at the collaborating institutions in the construction and operation of the instrument.

IceCube. The authors gratefully acknowledge the support from the following agencies and institutions: USA—U.S. National Science Foundation-Office of Polar Programs, U.S. National Science Foundation-Physics Division, U.S. National Science Foundation-EPSCoR, U.S. National Science Foundation-Office of Advanced Cyberinfrastructure, Wisconsin Alumni Research Foundation, Center for High Throughput Computing (CHTC) at the University of Wisconsin–Madison, Open Science Grid (OSG), Partnership to Advance Throughput Computing (PATh), Advanced Cyberinfrastructure Coordination Ecosystem: Services & Support (ACCESS), Frontera and Ranch computing project at the Texas Advanced Computing Center, U.S. Department of Energy-National Energy Research Scientific Computing Center, Particle astrophysics research computing center at the University of Maryland, Institute for Cyber-Enabled Research at Michigan State University, Astroparticle physics computational facility at Marquette University, NVIDIA Corporation, and Google Cloud Platform; Belgium—Funds for Scientific Research (FRS-FNRS and FWO), FWO Odysseus and Big Science programmes, and Belgian Federal Science Policy Office (Belspo); Germany—Bundesministerium

für Bildung und Forschung (BMBF), Deutsche Forschungsgemeinschaft (DFG), Helmholtz Alliance for Astroparticle Physics (HAP), Initiative and Networking Fund of the Helmholtz Association, Deutsches Elektronen Synchrotron (DESY), and High Performance Computing cluster of the RWTH Aachen; Sweden—Swedish Research Council, Swedish Polar Research Secretariat, Swedish National Infrastructure for Computing (SNIC), and Knut and Alice Wallenberg Foundation; European Union—EGI Advanced Computing for research; Australia – Australian Research Council; Canada—Natural Sciences and Engineering Research Council of Canada, Calcul Québec, Compute Ontario, Canada Foundation for Innovation, WestGrid, and Digital Research Alliance of Canada; Denmark—Villum Fonden, Carlsberg Foundation, and European Commission; New Zealand—Marsden Fund; Japan—Japan Society for Promotion of Science (JSPS) and Institute for Global Prominent Research (IGPR) of Chiba University; Korea—National Research Foundation of Korea (NRF); and Switzerland—Swiss National Science Foundation (SNSF).

Fermi-LAT. The Fermi-LAT Collaboration acknowledges generous ongoing support from a number of agencies and institutes that have supported both the development and the operation of the LAT as well as scientific data analysis. These include the National Aeronautics and Space Administration and the Department of Energy in the United States, the Commissariat à l'Energie Atomique and the Centre National de la Recherche Scientifique / Institut National de Physique Nucléaire et de Physique des Particules in France, the Agenzia Spaziale Italiana and the Istituto Nazionale di Fisica Nucleare in Italy, the Ministry of Education,Culture, Sports, Science and Technology (MEXT), High Energy Accelerator Research Organization (KEK) and Japan Aerospace Exploration Agency (JAXA) in Japan, and the K. A. Wallenberg Foundation, the Swedish Research Council, and the Swedish National Space Board in Sweden. Additional support for science analysis during the operations phase is gratefully acknowledged from the Istituto Nazionale di Astrofisica in Italy and the Centre National d'Études Spatiales in France.

We acknowledge support by Institut Pascal at Université Paris-Saclay during the Paris-Saclay Astroparticle Symposium 2021 and 2022, with the support of the P2IO Laboratory of Excellence (program "Investissements d'avenir" ANR-11-IDEX-0003-01 Paris-Saclay and ANR-10-LABX-0038), the P2I axis of the Graduate School Physics of Université Paris-Saclay, as well as IJCLab, CEA, IPhT, IAS, OSUPS, the IN2P3 master projet UCMN, APPEC, and EuCAPT.

Fabian Schüssler acknowledges the support of the French Agence Nationale de la Recherche (ANR), under grant ANR-22-CE31-0012 (project MOTS) and support by the Programme National des Hautes Energies of CNRS/INSU with INP and IN2P3, co-funded by CEA and CNES.

This work was supported by the German Science Foundation DFG, research grant "Relativistic Jets in Active Galaxies" (FOR 5195, grant No. 443220636), and by the European Research Council, ERC Starting grant *MessMapp*, Sara Buson Principal Investigator, under contract No. 949555.

This work was performed in part under DOE contract DE-AC02-76SF00515.

Stefano Marchesi acknowledges support by the Next Generation EU funds within the National Recovery and Resilience Plan (PNRR), Mission 4—Education and Research, Component 2—From Research to Business (M4C2), Investment Line 3.1—Strengthening and creation of Research Infrastructures, Project IR0000012—"CTA+ - Cherenkov Telescope Array Plus."

Ilaria Viale and Elisa Prandini acknowledge the project "SKYNET: Deep Learning for Astroparticle Physics," PRIN 2022 (CUP: D53D23002610006).

Software: Astro-COLIBRI (P. Reichherzer et al. 2021); Astropy (Astropy Collaboration et al. 2013, 2018, 2022); gammapy (A. Donath et al. 2023); fermipy (M. Wood et al. 2018).

Data Availability

Data products presented in this paper can be downloaded via Zenodo (doi:10.5281/zenodo.17238703). The repository contains the following data products:

1. 1ES1312-423 MWL SED (Figure 3).
2. SEDs for the counterparts of the GFU-cluster alerts including IACT ULs, simultaneous MWL data, and archival data provided for comparison (Figure 4).
3. Differential-flux upper limits of each IACT and combined limits (Figure 5).
4. Fits files for the integral VHE γ-ray flux upper-limit maps (Figure 6).
5. SEDs for the potential counterparts of the single high-energy neutrino alerts (Figure 7).

Appendix A
Swift Results

Tables 3–15 provide detailed results for the Swift-XRT data and their analyses conducted on the discussed neutrino alerts.

Table 3
Logs and Fit Results of Swift-XRT Observations of 1ES 1312-423 Using a Power-law Model with N_H Fixed to Galactic Absorption

Swift ObsID	Observation Date	Net Exposure Time (s)	Photon Index (Γ)	Flux 0.3–10 keV ($\times 10^{-11}$ erg cm^{-2} s^{-1})
00031915001	2011-01-25	4772	1.77 ± 0.05	4.03 ± 0.14
00031915002	2019-03-12	1753	1.97 ± 0.08	3.77 ± 0.21
00031915003	2019-03-13	1753	1.91 ± 0.08	4.15 ± 0.25
00031915005	2019-03-15	1806	2.15 ± 0.10	4.21 ± 0.31
00031915007	2019-04-17	3142	1.89 ± 0.06	5.43 ± 0.22
00031915009	2019-04-19	3841	2.01 ± 0.05	4.14 ± 0.15

Table 4
Observed Magnitudes of 1ES 1312-423 Obtained by Swift/UVOT

Observation Date	*v* (mag)	*b* (mag)	*u* (mag)	*w*1 (mag)	*m*2 (mag)	*w*2 (mag)
2011-01-25	⋯	⋯	⋯	⋯	17.41 ± 0.06	⋯
2019-03-12	⋯	⋯	⋯	⋯	16.74 ± 0.06	⋯
2019-03-13	⋯	⋯	⋯	16.74 ± 0.06	⋯	⋯
2019-03-15	⋯	⋯	⋯	⋯	⋯	16.78 ± 0.06
2019-04-17	16.47 ± 0.06	17.15 ± 0.06	16.36 ± 0.06	16.43 ± 0.07	16.45 ± 0.07	16.57 ± 0.07
2019-04-19	16.54 ± 0.06	17.23 ± 0.06	16.56 ± 0.06	16.58 ± 0.07	16.66 ± 0.06	16.73 ± 0.07

Table 5
Logs and Fit Results of Swift-XRT Observations of OP 313 Using a Power-law Model with N_H Fixed to Galactic Absorption

Swift ObsID	Observation Date	Net Exposure Time (s)	Photon Index (Γ)	Flux 0.3–10 keV ($\times 10^{-12}$ erg cm^{-2} s^{-1})
00036384001	2007-04-03	2130	1.47 ± 0.17	4.31 ± 0.66
00036384002	2007-04-07	2793	1.52 ± 0.15	3.99 ± 0.50
00036384003	2007-06-27	465	1.63 ± 0.34	4.59 ± 1.20
00030976001	2007-07-31	852	1.82 ± 0.30	2.97 ± 0.65
00030976002	2007-08-01	4409	1.53 ± 0.15	3.09 ± 0.36
00036768001	2007-08-05	4181	1.49 ± 0.12	4.61 ± 0.43
00036768002, 00036384006	2008-05-12	7911	1.58 ± 0.11	2.58 ± 0.23
00036384007	2008-08-20	4755	1.48 ± 0.13	3.76 ± 0.40
00036384008	2009-12-12	2303	1.66 ± 0.26	1.70 ± 0.33
00036384009	2010-04-15	1975	1.47 ± 0.33	2.40 ± 0.62
00036384010, 0003638411	2011-04-17	3249	1.61 ± 0.28	1.16 ± 0.25
00036384012	2011-07-03	4722	1.90 ± 0.21	1.21 ± 0.17
00091894001	2014-05-04	3486	1.65 ± 0.16	2.72 ± 0.40
00091894004	2014-06-29	3494	1.60 ± 0.18	2.22 ± 0.30
00036384013	2019-06-20	1870	2.03 ± 0.31	1.35 ± 0.28
00036384014	2019-12-27	2035	1.55 ± 0.24	2.82 ± 0.48
00036384015	2019-12-29	1865	1.53 ± 0.23	2.79 ± 0.52
00036384016	2019-12-31	1249	1.47 ± 0.28	3.09 ± 0.69
00036384017	2020-03-11	1641	1.70 ± 0.22	3.41 ± 0.55
00036384018	2020-03-16	2238	1.67 ± 0.23	2.56 ± 0.45
00036384019	2020-03-21	2218	1.50 ± 0.22	2.85 ± 0.51
00036384020	2020-05-21	2492	1.61 ± 0.22	2.25 ± 0.38
00036384021	2020-05-25	2230	1.59 ± 0.25	2.22 ± 0.40
00036384022	2020-05-29	2048	1.70 ± 0.23	2.44 ± 0.41
00036384023	2020-06-02	2794	1.48 ± 0.23	2.36 ± 0.42
00036384024	2020-06-06	2899	1.51 ± 0.20	2.44 ± 0.39
00036384025	2020-06-10	3037	1.56 ± 0.22	2.02 ± 0.35
00036384026	2020-06-14	2737	1.68 ± 0.20	2.29 ± 0.35

Table 6
Observed Magnitudes of OP 313 Obtained by Swift/UVOT

Observation Date	v (mag)	b (mag)	u (mag)	$w1$ (mag)	$m2$ (mag)	$w2$ (mag)
2007-04-03	16.91 ± 0.08	17.39 ± 0.07	16.56 ± 0.07	16.58 ± 0.08	16.66 ± 0.08	16.96 ± 0.07
2007-04-07	17.58 ± 0.09	18.20 ± 0.08	17.25 ± 0.07	17.20 ± 0.08	17.22 ± 0.09	17.57 ± 0.07
2007-06-27	⋯	⋯	⋯	⋯	17.46 ± 0.10	⋯
2007-07-31	16.56 ± 0.16	16.98 ± 0.12	16.20 ± 0.07	16.28 ± 0.06	16.15 ± 0.14	16.66 ± 0.12
2007-08-01	16.73 ± 0.06	17.24 ± 0.06	16.45 ± 0.06	16.55 ± 0.06	16.66 ± 0.04	16.93 ± 0.06
2008-05-12	⋯	⋯	⋯	⋯	17.32 ± 0.06	⋯
2008-08-20	⋯	⋯	⋯	⋯	16.70 ± 0.06	⋯
2009-12-12	⋯	⋯	⋯	⋯	⋯	18.59 ± 0.08
2010-04-15	⋯	⋯	⋯	⋯	⋯	18.39 ± 0.08
2011-04-17	18.85 ± 0.31	19.82 ± 0.31	18.22 ± 0.14	18.12 ± 0.14	18.08 ± 0.14	18.68 ± 0.13
2011-04-17	⋯	⋯	18.40 ± 0.07	⋯	⋯	18.53 ± 0.12
2011-07-03	18.10 ± 0.15	18.71 ± 0.13	17.72 ± 0.11	17.64 ± 0.11	17.74 ± 0.11	18.21 ± 0.07
2014-05-04	18.27 ± 0.08	17.91 ± 0.10	18.03 ± 0.16	18.16 ± 0.17	19.31 ± 0.26	18.28 ± 0.25
2014-06-05	⋯	19.48 ± 0.26	18.20 ± 0.15	18.09 ± 0.15	⋯	18.57 ± 0.08
2014-06-10	>19.09	19.50 ± 0.24	19.58 ± 0.18	18.29 ± 0.16	18.08 ± 0.08	18.65 ± 0.14
2014-06-29	18.91 ± 0.33	19.79 ± 0.31	18.20 ± 0.15	18.22 ± 0.15	18.15 ± 0.17	18.50 ± 0.08
2019-06-20	16.52 ± 0.07	17.05 ± 0.07	16.31 ± 0.07	16.35 ± 0.08	16.35 ± 0.08	16.70 ± 0.07
2019-12-27	16.51 ± 0.07	16.99 ± 0.07	16.16 ± 0.06	16.35 ± 0.08	16.34 ± 0.08	16.57 ± 0.07
2019-12-29	16.52 ± 0.08	16.89 ± 0.06	16.20 ± 0.06	16.27 ± 0.08	16.27 ± 0.08	16.58 ± 0.07
2019-12-31	16.43 ± 0.07	16.80 ± 0.06	16.20 ± 0.06	16.16 ± 0.07	16.44 ± 0.08	16.87 ± 0.08
2020-03-11	⋯	⋯	⋯	15.84 ± 0.06	⋯	⋯
2020-03-16	⋯	⋯	16.08 ± 0.05	⋯	⋯	⋯
2020-03-21	⋯	⋯	⋯	⋯	⋯	16.32 ± 0.06
2020-05-21	17.18 ± 0.09	17.87 ± 0.08	17.07 ± 0.08	17.14 ± 0.09	17.17 ± 0.09	17.45 ± 0.08
2020-05-25	17.16 ± 0.09	17.76 ± 0.08	16.99 ± 0.08	17.03 ± 0.09	17.24 ± 0.10	17.52 ± 0.09
2020-05-29	17.14 ± 0.09	17.68 ± 0.08	16.94 ± 0.08	16.94 ± 0.09	16.96 ± 0.11	17.28 ± 0.08
2020-06-02	17.29 ± 0.09	17.73 ± 0.07	16.88 ± 0.07	17.00 ± 0.08	17.04 ± 0.09	17.24 ± 0.08
2020-06-06	17.28 ± 0.09	17.90 ± 0.08	17.03 ± 0.07	17.06 ± 0.09	17.16 ± 0.09	17.34 ± 0.08
2020-06-10	17.64 ± 0.11	18.08 ± 0.09	17.21 ± 0.08	17.30 ± 0.09	17.43 ± 0.10	17.72 ± 0.08
2020-06-14	17.56 ± 0.11	18.03 ± 0.09	17.37 ± 0.08	17.30 ± 0.09	17.37 ± 0.10	17.59 ± 0.08

Table 7
Logs and Fit Results of Swift-XRT Observations of GB6 J0316+0904 Using a Power-law Model with N_H Fixed to Galactic Absorption

Swift ObsID	Observation Date	Net Exposure Time (s)	Photon Index (Γ)	Flux 0.3–10 keV ($\times 10^{-12}$ erg cm^{-2} s^{-1})
00038370001	2009-03-09	2487	1.94 ± 0.10	16.0 ± 1.2
00041581001	2010-11-23	974	2.23 ± 0.85	1.17 ± 0.45
00038370002, 00038370003	2011-07-03/04	3259	2.27 ± 0.33	1.05 ± 0.23
00083407001	2015-01-09	2645	1.97 ± 0.24	2.34 ± 0.39

Table 8
Observed Magnitudes of GB6 J0316+0904 Obtained by *Swift*/UVOT

Observation Date	v (mag)	b (mag)	u (mag)	$w1$ (mag)	$m2$ (mag)	$w2$ (mag)
2009-03-09	15.91 ± 0.12	16.47 ± 0.05	15.79 ± 0.05	16.37 ± 0.06	>16.57	16.89 ± 0.07
2010-11-23	16.64 ± 0.11	17.54 ± 0.10	17.02 ± 0.11	17.59 ± 0.14	18.32 ± 0.20	18.10 ± 0.13
2011-07-03	16.38 ± 0.12	17.32 ± 0.12	16.53 ± 0.10	17.08 ± 0.12	17.74 ± 0.16	17.78 ± 0.08
2011-07-04	16.62 ± 0.13	17.10 ± 0.10	16.55 ± 0.09	17.35 ± 0.13	17.73 ± 0.11	17.73 ± 0.11
2015-01-09	17.63 ± 0.12	18.33 ± 0.12	17.81 ± 0.11	18.39 ± 0.16	18.95 ± 0.19	19.04 ± 0.15

Table 9
Log and Fitting Results of Swift-XRT Observations of OC 457 Using a Power-law Model with N_H Fixed to Galactic Absorption

Swift ObsID	Observation Date	Net Exposure Time (s)	Photon Index (Γ)	Flux 0.3–10 keV ($\times 10^{-12}$ erg cm^{-2} s^{-1})
00036759001	2007-07-16	7342	1.39 ± 0.16	2.10 ± 0.32
00036759002	2007-10-09	1306	1.12 ± 0.42	3.47 ± 1.31
00036759003	2007-10-10	3621	1.50 ± 0.22	2.21 ± 0.40
00036759004	2007-10-11	4935	1.25 ± 0.19	3.03 ± 0.51
00036188002	2007-11-22	4630	1.38 ± 0.15	3.44 ± 0.46
00036188003	2008-01-14	5472	1.30 ± 0.16	2.80 ± 0.41
00036188005	2008-02-11	4660	1.35 ± 0.23	2.60 ± 0.53
00031123001	2008-02-14	4280	1.36 ± 0.17	3.38 ± 0.49
00036188004	2008-11-18	6470	1.36 ± 0.14	2.94 ± 0.37
00036188006	2009-09-07	357	1.51 ± 0.61	3.47 ± 1.56
00036188005	2009-09-08	5162	1.32 ± 0.14	3.77 ± 0.47
00036188007	2010-02-05	4183	1.38 ± 0.18	2.71 ± 0.53
00036188008	2010-02-05	1451	1.50 ± 0.31	2.86 ± 0.70
00036188009	2011-01-28	1648	1.35 ± 0.33	2.32 ± 0.69
00036188010	2011-01-28	3501	1.42 ± 0.23	2.19 ± 0.44
00036188011	2020-08-05	1988	1.78 ± 0.44	1.12 ± 0.34
00036188012	2020-08-07	2567	1.39 ± 0.31	2.08 ± 0.53
00036188013	2020-08-11	2962	1.38 ± 0.30	1.90 ± 0.47
00036188014	2020-08-14	2647	1.69 ± 0.26	1.91 ± 0.39
00036188015	2020-08-17	2605	1.18 ± 0.38	1.35 ± 0.47

Table 10
Observed Magnitudes of OC 457 Obtained by Swift/UVOT

Observation Date	v (mag)	b (mag)	u (mag)	$w1$ (mag)	$m2$ (mag)	$w2$ (mag)
2007-07-16	…	…	…	…	…	17.21 ± 0.05
2007-11-22	14.96 ± 0.04	15.53 ± 0.04	14.94 ± 0.05	15.28 ± 0.06	15.63 ± 0.06	15.77 ± 0.06
2008-01-14	15.40 ± 0.04	16.04 ± 0.05	15.50 ± 0.05	15.85 ± 0.06	16.28 ± 0.06	16.46 ± 0.06
2008-02-14	16.23 ± 0.04	…	…	…	…	…
2008-11-18	15.83 ± 0.04	16.43 ± 0.05	15.84 ± 0.05	16.22 ± 0.06	16.55 ± 0.07	16.73 ± 0.06
2009-09-07	15.99 ± 0.11	16.96 ± 0.11	16.08 ± 0.02	16.53 ± 0.13	16.89 ± 0.20	16.94 ± 0.12
2009-09-08	16.24 ± 0.05	16.79 ± 0.05	16.18 ± 0.05	16.57 ± 0.06	16.87 ± 0.07	17.06 ± 0.06
2010-02-05	…	…	17.56 ± 0.05	…	…	18.31 ± 0.08
2010-02-05	17.62 ± 0.15	17.91 ± 0.13	17.45 ± 0.13	17.81 ± 0.14	18.10 ± 0.15	18.29 ± 0.12
2011-01-28	…	…	…	…	…	17.97 ± 0.07
2011-01-28	16.92 ± 0.09	17.46 ± 0.09	17.07 ± 0.10	17.40 ± 0.11	17.72 ± 0.13	17.84 ± 0.10
2020-08-05	18.83 ± 0.25	19.40 ± 0.22	19.20 ± 0.27	19.07 ± 0.23	19.54 ± 0.35	20.11 ± 0.33
2020-08-07	>19.04	>20.10	19.48 ± 0.31	19.58 ± 0.29	19.87 ± 0.33	>20.45
2020-08-11	18.98 ± 0.35	19.81 ± 0.26	18.87 ± 0.18	19.50 ± 0.25	19.00 ± 0.20	19.98 ± 0.27
2020-08-14	19.10 ± 0.33	19.30 ± 0.18	19.42 ± 0.27	18.98 ± 0.20	19.41 ± 0.25	19.73 ± 0.22
2020-08-17	18.76 ± 0.30	19.59 ± 0.23	19.69 ± 0.35	19.07 ± 0.20	> 19.88	19.62 ± 0.22

Table 11
Log and Fitting Results of Swift-XRT Observations of NVSS J065844+063711 Using a Power-law Model with N_H Fixed to Galactic Absorption

Swift ObsID	Observation Date	Net Exposure Time (s)	Photon Index (Γ)	Flux 0.3–10 keV ($\times 10^{-12}$ erg cm^{-2} s^{-1})
00047168001-00047168006	2012-05-01/10	4146	2.95 ± 0.65	0.80 ± 0.25
00013876001	2020-11-15	3279	1.97 ± 0.37	1.64 ± 0.35
00013876002	2020-11-18	3674	2.02 ± 0.34	1.58 ± 0.38
00013876003	2020-12-11	3062	2.41 ± 0.48	1.61 ± 0.41

Table 12
Observed Magnitudes of NVSS J065844+06371 Obtained by Swift/UVOT

Observation Date	*v* (mag)	*b* (mag)	*u* (mag)	*w*1 (mag)	*m*2 (mag)	*w*2 (mag)
2012-05-01	⋯	⋯	18.85 ± 0.13	⋯	⋯	⋯
2012-05-02	⋯	⋯	⋯	⋯	⋯	>20.09
2012-05-05	⋯	⋯	17.33 ± 0.08	⋯	⋯	⋯
2012-05-10	⋯	⋯	⋯	⋯	⋯	19.30 ± 0.24
2012-05-10	⋯	⋯	⋯	⋯	19.31 ± 0.17	⋯
2020-11-15	>18.94	>19.90	>19.53	>19.71	20.26 ± 0.29	>20.15
2020-11-18	19.22 ± 0.36	19.93 ± 0.31	18.97 ± 0.20	>19.97	>20.20	20.22 ± 0.32
2020-12-11	19.07 ± 0.34	19.94 ± 0.33	19.13 ± 0.23	18.96 ± 0.20	19.91 ± 0.33	19.71 ± 0.24

Table 13
Log and Fitting Results of Swift-XRT Observations of 4FGL J0955.1+3551 Using a Power-law Model with N_H Fixed to Galactic Absorption

Swift ObsID	Observation Date	Net Exposure Time (s)	Photon index (Γ)	Flux 0.3–10 keV ($\times 10^{-12}$ erg cm^{-2} s^{-1})
00091400002	2012-04-19	914	2.03 ± 0.24	4.51 ± 0.75
00091400006	2012-10-08	4795	1.80 ± 0.11	4.89 ± 0.39
00091400007	2012-10-10	4220	1.92 ± 0.11	4.79 ± 0.38
00091400008	2012-10-11	280	2.26 ± 0.49	5.19 ± 1.55
00091400009	2012-10-12	2382	1.96 ± 0.15	4.71 ± 0.50
00091400010	2012-10-16	1189	1.89 ± 0.24	3.75 ± 0.65
00091400011	2012-10-17	614	1.85 ± 0.36	3.10 ± 0.81
00091400012	2012-10-27	1666	1.99 ± 0.20	4.22 ± 0.57
00091400013	2012-10-30	529	2.00 ± 0.36	3.82 ± 0.96
00091400014	2012-11-01	739	2.38 ± 0.29	4.04 ± 0.74
00091400015	2012-11-22	969	2.28 ± 0.25	4.03 ± 0.65
00091400016	2012-11-23	2225	2.06 ± 0.22	3.22 ± 0.49
00091400018	2012-12-23	1611	2.13 ± 0.13	4.95 ± 0.60
00091400019	2012-12-29	704	2.08 ± 0.29	5.27 ± 1.03
00091400021	2013-01-05	1159	2.16 ± 0.18	6.64 ± 0.77
00091400022	2013-01-13	814	2.10 ± 0.22	6.03 ± 0.89
00091400023	2013-01-26	1161	1.98 ± 0.18	6.79 ± 0.84
00091400024	2013-01-29	607	1.61 ± 0.25	7.34 ± 1.40
00091400025	2013-02-01	397	1.85 ± 0.33	6.29 ± 1.43
00091400026	2013-02-06	1154	1.96 ± 0.19	6.43 ± 0.85
00091400027	2013-02-09	1216	1.84 ± 0.22	5.80 ± 0.87
00091400028	2013-02-11	252	2.94 ± 0.47	6.67 ± 1.82
00013051001	2020-01-08	2904	1.81 ± 0.10	10.81 ± 0.65
00013051002	2020-01-10	2829	1.94 ± 0.10	8.73 ± 0.63
00013051003	2020-01-11	2844	1.84 ± 0.10	9.32 ± 0.69
00013051004	2020-01-16	412	2.04 ± 0.26	9.64 ± 1.62
00013051005	2020-01-21	834	1.99 ± 0.22	7.40 ± 1.04
00013051007	2020-01-23	2592	1.92 ± 0.11	10.06 ± 0.75
00013051008	2020-01-25	1908	1.92 ± 0.13	9.35 ± 0.87
00013051010	2020-01-29	1581	1.84 ± 0.15	7.31 ± 0.80
00013051011	2020-01-30	1086	2.13 ± 0.20	6.87 ± 0.90
00013051013	2020-02-11	774	1.91 ± 0.21	9.34 ± 1.36
00013051014	2020-02-16	822	1.97 ± 0.21	9.08 ± 1.33
00013051015	2020-02-21	2155	1.86 ± 0.11	10.12 ± 0.81

Table 14
Observed Magnitudes of 4FGL J0955.1+3551 Obtained by Swift/UVOT

Observation Date	v (mag)	b (mag)	u (mag)	$w1$ (mag)	$m2$ (mag)	$w2$ (mag)
2012-04-19	⋯	⋯	19.35 ± 0.17	19.07 ± 0.25	⋯	⋯
2012-10-08	>18.50	>19.60	18.96 ± 0.08	18.52 ± 0.19	18.68 ± 0.20	18.81 ± 0.16
2012-10-10	>18.37	>19.38	18.55 ± 0.26	18.76 ± 0.26	18.60 ± 0.08	18.55 ± 0.13
2012-10-11	⋯	⋯	⋯	18.68 ± 0.19	⋯	⋯
2012-10-12	>18.45	>19.45	19.04 ± 0.10	18.88 ± 0.27	18.86 ± 0.24	19.08 ± 0.20
2012-10-16	> 18.41	>19.39	18.91 ± 0.16	18.98 ± 0.30	18.79 ± 0.27	18.75 ± 0.19
2012-10-17	>18.14	>19.21	> 18.90	18.54 ± 0.27	18.60 ± 0.28	18.85 ± 0.22
2012-10-27	⋯	>19.72	19-08 ± 0.30	18.61 ± 0.10	⋯	18.52 ± 0.17
2012-10-30	>18.16	>19.16	18.74 ± 0.36	18.74 ± 0.32	18.56 ± 0.27	18.88 ± 0.24
2012-11-01	>18.52	>19.51	18.74 ± 0.27	18.82 ± 0.26	18.38 ± 0.21	18.47 ± 0.16
2012-11-22	>17.98	>18.99	> 18.58	18.97 ± 0.36	18.56 ± 0.27	18.67 ± 0.15
2012-11-23	>18.46	>19.56	> 19.24	19.32 ± 0.30	18.59 ± 0.13	18.80 ± 0.15
2012-12-23	>18.81	>19.89	19.22 ± 0.21	18.73 ± 0.21	18.38 ± 0.18	18.38 ± 0.11
2012-12-29	>18.48	19.25 ± 0.32	18.69 ± 0.28	18.32 ± 0.22	18.17 ± 0.21	18.36 ± 0.16
2013-01-05	>18.85	19.77 ± 0.36	18.65 ± 0.21	18.48 ± 0.18	18.15 ± 0.17	18.25 ± 0.13
2013-01-13	>18.51	>19.52	18.86 ± 0.30	18.26 ± 0.20	18.25 ± 0.21	18.31 ± 0.15
2013-01-26	>18.76	>19.75	18.98 ± 0.28	18.40 ± 0.18	18.49 ± 0.19	18.53 ± 0.14
2013-01-29	>18.34	>19.34	18.87 ± 0.35	19.06 ± 0.34	18.54 ± 0.26	18.61 ± 0.19
2013-02-01	⋯	⋯	18.91 ± 0.16	⋯	⋯	18.57 ± 0.27
2013-02-06	18.64 ± 0.34	>19.74	18.91 ± 0.27	18.66 ± 0.21	18.47 ± 0.19	18.54 ± 0.15
2013-02-09	>18.77	19.64 ± 0.35	18.78 ± 0.24	18.78 ± 0.23	18.78 ± 0.21	18.52 ± 0.14
2013-02-11	⋯	>19.50	18.68 ± 0.28	18.35 ± 0.22	⋯	⋯
2020-01-08	>18.48	⋯	⋯	>18.42	18.32 ± 0.11	18.37 ± 0.09
2020-01-10	18.81 ± 0.32	19.79 ± 0.31	18.69 ± 0.19	18.58 ± 0.15	18.39 ± 0.12	18.30 ± 0.12
2020-01-11	18.98 ± 0.35	19.68 ± 0.28	18.80 ± 0.20	18.33 ± 0.15	18.43 ± 0.11	18.23 ± 0.11
2020-01-16	>17.99	>18.99	18.62 ± 0.36	18.65 ± 0.37	18.44 ± 0.30	18.53 ± 0.25
2020-01-21	>18.48	>19.50	18.50 ± 0.25	18.63 ± 0.25	18.91 ± 0.28	18.79 ± 0.20
2020-01-23	>19.19	20.02 ± 0.34	18.73 ± 0.17	18.61 ± 0.16	18.53 ± 0.15	18.61 ± 0.12
2020-01-25	19.04 ± 0.37	19.30 ± 0.22	18.81 ± 0.20	18.46 ± 0.16	18.15 ± 0.16	18.40 ± 0.12
2020-01-29	18.86 ± 0.35	19.24 ± 0.23	18.66 ± 0.20	18.83 ± 0.21	18.51 ± 0.21	18.51 ± 0.13
2020-01-30	>18.61	>19.62	18.96 ±0.31	18.28 ± 0.20	18.50 ± 0.20	18.49 ± 0.16
2020-02-11	⋯	⋯	⋯	⋯	18.36 ± 0.13	⋯
2020-02-16	⋯	⋯	⋯	18.49 ± 0.11	⋯	⋯
2020-02-21	⋯	⋯	18.69 ± 0.07	⋯	⋯	⋯

Table 15
Log and Fitting Results of Swift-XRT Observations of PKS 1502+106 Using a Power-law Model with N_H Fixed to Galactic Absorption

Swift ObsID	Observation Date	Net Exposure Time (s)	Photon Index (Γ)	Flux 0.3–10 keV ($\times 10^{-12}$ erg cm^{-2} s^{-1})
00094003011-00094003015	2019-01-03/31	5442	1.46 ± 0.26	1.14 ± 0.23
00095003001, 00095003002	2019-06-20/27	2103	1.09 ± 0.52	1.38 ± 0.65
00095003003-006, 00011493001	2019-07-04/30	4308	1.11 ± 0.37	1.10 ± 0.36
00095003007, 00095003008, 00095088001	2019-08-01/09-20	3396	1.01 ± 0.42	1.17 ± 0.43
00095003009, 00095003010	2019-12-20/27	2415	1.36 ± 0.41	1.20 ± 0.40
00095003011-00095003015	2020-01-03/31	4423	1.40 ± 0.34	0.89 ± 0.24
00095656001, 00095656002	2020-06-20/27	1673	1.54 ± 0.42	1.37 ± 0.45
00095656003-00095656006	2020-07-04/25	3888	1.61 ± 0.25	1.77 ± 0.33
00095656007, 00095656008	2020-08-01/08	1988	1.42 ± 0.33	2.12 ± 0.54
00095656009, 00095656010	2020-12-20/27	1778	1.07 ± 0.45	1.49 ± 0.64

Appendix B
IceCube Alert Properties

Table 16 provides detailed information about the GFU-cluster alerts and Table 17 provides detailed information on single high-energy neutrino alerts.

Table 16
GFU-cluster Alerts That Are Relevant to the Results of This Work

Source	Start Date	Trigger Date	ΔT (days)	p-value	Significance (σ)	FAR (yr^{-1})
1ES 1312-423	2019-03-12	2019-03-12	0.26	3.46×10^{-4}	3.4	0.02
MG1 J181841+0903	2019-01-19	2019-05-27	127.4	3.34×10^{-4}	3.3	0.1
...	2019-01-19	2019-05-27	127.7	3.39×10^{-4}	3.3	0.1
...	2019-01-19	2019-05-27	127.9	4.20×10^{-4}	3.3	0.1
...	2019-01-19	2019-06-05	136.8	1.62×10^{-4}	3.6	0.1
...	2019-01-19	2019-06-05	137.0	1.60×10^{-4}	3.6	0.1
PMN J2016-09	2019-11-29	2019-11-29	0.01	1.86×10^{-3}	3.6	0.004
OP 313	2020-02-12	2020-04-10	57.5	1.07×10^{-3}	3.1	0.05
...	2020-02-12	2020-05-01	78.8	1.18×10^{-3}	3.0	0.05
...	2020-02-12	2020-05-17	94.7	1.23×10^{-3}	3.0	0.05
...	2020-03-13	2020-08-27	166.7	1.08×10^{-3}	3.1	0.05
OC 457	2020-08-04	2020-08-04	0.3	4.20×10^{-4}	3.3	0.02
GB6 J0316+0904	2021-01-13	2021-01-15	2.3	9.80×10^{-4}	3.1	0.04
All-sky ($\alpha = 51.^{\circ}2$, $\delta = -18.^{\circ}6$)	2019-09-15	2019-09-19	3.7	7.81×10^{-6}	4.3	0.7

Note. For each alert, we provide the candidate source, the date of the first event in the cluster (Start Date), the Trigger Date, the duration of the cluster time window (ΔT), the corresponding alert pre-trials p-value and Significance (σ), and the false-alert rate (FAR).

Table 17
List of IceCube Single High-energy Neutrino Alerts Followed Up by at Least One IACT

Alert		R.A. (deg)	Decl. (deg)	Energy (TeV)	Signalness	FAR (yr^{-1})
IC-171106A	E	$340.00^{+0.70}_{-0.50}$	$+7.40^{+0.35}_{-0.25}$	230	0.75	...
...	...	$(340.14^{+0.62}_{-0.62})$	$(+7.44^{+0.30}_{-0.26})$	(1573)	(0.97)	...
IC-181023A	E	$270.18^{+2.00}_{-1.70}$	$-8.57^{+1.25}_{-1.30}$	120	0.28	...
...	...	$(270.18^{+1.89}_{-1.71})$	$(-8.42^{+1.13}_{-1.55})$	(237)	(0.15)	...
IC-190503A	E	$120.28^{+0.57}_{-0.77}$	$+6.35^{+0.76}_{-0.70}$	100	0.36	...
...	...	$(120.19^{+0.66}_{-0.66})$	$(+6.43^{+0.68}_{-0.75})$	(142)	(0.34)	...
IC-190529A[a]	H	$287.32^{+8.9}_{-8.9}$	$+78.14^{+8.9}_{-8.9}$	...	...	...
...	...	...	...	...	...	...
IC-190730A	G	$225.79^{+1.28}_{-1.43}$	$+10.47^{+1.14}_{-0.89}$	299	0.67	0.68
...	...	$(226.14^{+1.27}_{-1.98})$	$(+10.77^{+1.03}_{-1.17})$	(298)	(0.67)	...
IC-190922B	G	$5.76^{+1.19}_{-1.37}$	$-1.57^{+0.93}_{-0.82}$	187	0.50	1.33
...	...	$(5.71^{+1.19}_{-1.27})$	$(-1.53^{+0.90}_{-0.78})$	(187)	(0.50)	...
IC-191001A	G	$314.08^{+6.56}_{-2.26}$	$+12.94^{+1.50}_{-1.47}$	217	0.59	0.86
...	...	$(313.99^{+6.94}_{-2.46})$	$(12.79^{+1.65}_{-1.64})$	(218)	(0.59)	...
IC-200107A[b]	...	$148.18^{+2.20}_{-1.83}$	$+35.46^{+1.10}_{-1.22}$	...	...	...
...	...	...	...	...	...	...
IC-200926A	G	$96.46^{+0.73}_{-0.55}$	$-4.33^{+0.61}_{-0.76}$	670	0.44	0.54
...	...	$(96.46^{+0.70}_{-0.53})$	$(-4.33^{+0.60}_{-0.75})$	(670)	(0.44)	...
IC-201007A	G	$265.17^{+0.52}_{-0.52}$	$+5.34^{+0.32}_{-0.23}$	683	0.88	0.26
...	...	$(265.17^{+0.48}_{-0.48})$	$(+5.34^{+0.30}_{-0.19})$	(683)	(0.89)	...
IC-201114A	G	$105.25^{+1.28}_{-1.12}$	$+6.05^{+0.95}_{-0.95}$	214	0.56	0.92
...	...	$(105.73^{+0.92}_{-1.27})$	$(+5.87^{+1.05}_{-1.01})$	(214)	(0.56)	...
IC-201222A	G	$206.37^{+0.90}_{-0.80}$	$+13.44^{+0.55}_{-0.38}$	186	0.53	1.01
...	...	$(206.37^{+0.88}_{-0.75})$	$(+13.44^{+0.54}_{-0.34})$	(186)	(0.53)	...

Notes. A link to the corresponding GCN Circular with updated coordinates (including information regarding the initial localization) released by IceCube is provided in the alert name. The alert nature is provided: E = EHE, H = HESE, G = GOLD. For each alert, the event direction (R.A. and decl.), energy, pre-trials signalness, and false-alert rate (FAR) are provided. The values given in parentheses as a second line correspond to the offline reconstruction of direction, energy, and signalness as reported in R. Abbasi et al. (2023c). Energy and signalness estimates are not available for 200107A and 190529A, and FAR was not provided before 2019 alert stream upgrade.
[a] Retracted.
[b] The high-energy starting track was not identified as either GOLD or BRONZE.

ORCID iDs

J. Abhir https://orcid.org/0000-0001-8215-4377
A. Biland https://orcid.org/0000-0002-1288-833X
T. Bretz https://orcid.org/0000-0003-1500-6571
D. Dorner https://orcid.org/0000-0001-8823-479X
D. Elsaesser https://orcid.org/0000-0001-6796-3205
H. Ashkar https://orcid.org/0000-0002-2153-1818
M. Backes https://orcid.org/0000-0002-9326-6400
V. Barbosa Martins https://orcid.org/0000-0002-5085-8828
R. Batzofin https://orcid.org/0000-0002-5797-3386
Y. Becherini https://orcid.org/0000-0002-2115-2930
D. Berge https://orcid.org/0000-0002-2918-1824
M. Böttcher https://orcid.org/0000-0002-8434-5692
C. Boisson https://orcid.org/0000-0001-5893-1797
R. Brose https://orcid.org/0000-0002-8312-6930
F. Brun https://orcid.org/0000-0003-0770-9007
S. Casanova https://orcid.org/0000-0002-6144-9122
M. Cerruti https://orcid.org/0000-0001-7891-699X
A. Chen https://orcid.org/0000-0001-6425-5692
G. Cotter https://orcid.org/0000-0002-9975-1829
J. Damascene Mbarubucyeye https://orcid.org/0000-0002-4991-6576
A. Djannati-Ataï https://orcid.org/0000-0002-4924-1708
G. Fontaine https://orcid.org/0000-0002-6443-5025
S. Funk https://orcid.org/0000-0002-2012-0080
J.F. Glicenstein https://orcid.org/0000-0003-2581-1742
M. Jamrozy https://orcid.org/0000-0002-0870-7778
B. Khélifi https://orcid.org/0000-0001-6876-5577
Nu. Komin https://orcid.org/0000-0003-3280-0582
R. Konno https://orcid.org/0000-0003-1892-2356
D. Kostunin https://orcid.org/0000-0002-0487-0076
G. Kukec Mezek https://orcid.org/0000-0001-8461-1922
M. Lemoine-Goumard https://orcid.org/0000-0002-4462-3686
J.-P. Lenain https://orcid.org/0000-0001-7284-9220
A. Luashvili https://orcid.org/0000-0003-4384-1638
J. Mackey https://orcid.org/0000-0002-5449-6131
V. Marandon https://orcid.org/0000-0001-9077-4058
G. Martí-Devesa https://orcid.org/0000-0003-0766-6473
R. Marx https://orcid.org/0000-0002-6557-4924
A. Mitchell https://orcid.org/0000-0003-3631-5648
L. Mohrmann https://orcid.org/0000-0002-9667-8654
E. Moulin https://orcid.org/0000-0003-4007-0145
J. Niemiec https://orcid.org/0000-0001-6036-8569
S. Panny https://orcid.org/0000-0001-5770-3805
R.D. Parsons https://orcid.org/0000-0003-3457-9308
G. Pühlhofer https://orcid.org/0000-0003-4632-4644
M. Punch https://orcid.org/0000-0002-4710-2165
G. Rowell https://orcid.org/0000-0002-9516-1581
B. Rudak https://orcid.org/0000-0003-0452-3805
V. Sahakian https://orcid.org/0000-0003-1198-0043
M. Sasaki https://orcid.org/0000-0001-5302-1866
H.M. Schutte https://orcid.org/0000-0002-1769-5617
M. Senniappan https://orcid.org/0000-0001-6734-7699
J.N.S. Shapopi https://orcid.org/0000-0002-7130-9270
S. Spencer https://orcid.org/0000-0001-5516-1205
S. Steinmassl https://orcid.org/0000-0002-2865-8563
T. Tanaka https://orcid.org/0000-0002-4383-0368
A.M. Taylor https://orcid.org/0000-0001-9473-4758
C. van Eldik https://orcid.org/0000-0001-9669-645X
S.J. Wagner https://orcid.org/0000-0002-7474-6062
A. Wierzcholska https://orcid.org/0000-0003-4472-7204
M. Zacharias https://orcid.org/0000-0001-5801-3945
A.A. Zdziarski https://orcid.org/0000-0002-0333-2452
S. Abe https://orcid.org/0000-0001-7250-3596
J. Abhir https://orcid.org/0000-0001-8215-4377
A. Aguasca-Cabot https://orcid.org/0000-0001-8816-4920
I. Agudo https://orcid.org/0000-0002-3777-6182
S. Ansoldi https://orcid.org/0000-0002-5613-7693
L. A. Antonelli https://orcid.org/0000-0002-5037-9034
A. Arbet Engels https://orcid.org/0000-0001-9076-9582
C. Arcaro https://orcid.org/0000-0002-1998-9707
K. Asano https://orcid.org/0000-0001-9064-160X
A. Babić https://orcid.org/0000-0002-1444-5604
C. Bakshi https://orcid.org/0009-0007-1843-5386
U. Barres de Almeida https://orcid.org/0000-0001-7909-588X
J. A. Barrio https://orcid.org/0000-0002-0965-0259
L. Barrios-Jiménez https://orcid.org/0009-0008-6006-175X
I. Batković https://orcid.org/0000-0002-1209-2542
J. Becerra González https://orcid.org/0000-0002-6729-9022
W. Bednarek https://orcid.org/0000-0003-0605-108X
E. Bernardini https://orcid.org/0000-0003-3108-1141
A. Berti https://orcid.org/0000-0003-0396-4190
C. Bigongiari https://orcid.org/0000-0003-3293-8522
A. Biland https://orcid.org/0000-0002-1288-833X
O. Blanch https://orcid.org/0000-0002-8380-1633
G. Bonnoli https://orcid.org/0000-0003-2464-9077
Ž. Bošnjak https://orcid.org/0000-0001-6536-0320
E. Bronzini https://orcid.org/0000-0001-8378-4303
I. Burelli https://orcid.org/0000-0002-8383-2202
A. Campoy-Ordaz https://orcid.org/0000-0001-9352-8936
A. Carosi https://orcid.org/0000-0001-8690-6804
R. Carosi https://orcid.org/0000-0002-4137-4370
M. Carretero-Castrillo https://orcid.org/0000-0002-1426-1311
A. J. Castro-Tirado https://orcid.org/0000-0002-0841-0026
D. Cerasole https://orcid.org/0000-0003-2033-756X
G. Ceribella https://orcid.org/0000-0002-9768-2751
Y. Chai https://orcid.org/0000-0003-2816-2821
A. Chilingarian https://orcid.org/0000-0002-2018-9715
A. Cifuentes https://orcid.org/0000-0003-1033-5296
J. L. Contreras https://orcid.org/0000-0001-7282-2394
J. Cortina https://orcid.org/0000-0003-4576-0452
S. Covino https://orcid.org/0000-0001-9078-5507
G. D'Amico https://orcid.org/0000-0001-6472-8381
P. Da Vela https://orcid.org/0000-0003-0604-4517
F. Dazzi https://orcid.org/0000-0001-5409-6544
A. De Angelis https://orcid.org/0000-0002-3288-2517
B. De Lotto https://orcid.org/0000-0003-3624-4480
M. Delfino https://orcid.org/0000-0002-9468-4751
C. Delgado Mendez https://orcid.org/0000-0002-7014-4101
F. Di Pierro https://orcid.org/0000-0003-4861-432X
R. Di Tria https://orcid.org/0009-0007-1088-5307
L. Di Venere https://orcid.org/0000-0003-0703-824X
D. Dominis Prester https://orcid.org/0000-0002-9880-5039
A. Donini https://orcid.org/0000-0002-3066-724X
D. Dorner https://orcid.org/0000-0001-8823-479X
M. Doro https://orcid.org/0000-0001-9104-3214
D. Elsaesser https://orcid.org/0000-0001-6796-3205
J. Escudero https://orcid.org/0000-0002-4131-655X

L. Fariña https://orcid.org/0000-0003-4116-6157
L. Foffano https://orcid.org/0000-0002-0709-9707
L. Font https://orcid.org/0000-0003-2109-5961
Y. Fukazawa https://orcid.org/0000-0002-0921-8837
S. Gasparyan https://orcid.org/0000-0002-0031-7759
M. Gaug https://orcid.org/0000-0001-8442-7877
J. G. Giesbrecht Paiva https://orcid.org/0000-0002-5817-2062
N. Giglietto https://orcid.org/0000-0002-9021-2888
F. Giordano https://orcid.org/0000-0002-8651-2394
P. Gliwny https://orcid.org/0000-0002-4183-391X
N. Godinović https://orcid.org/0000-0002-4674-9450
R. Grau https://orcid.org/0000-0002-1891-6290
D. Green https://orcid.org/0000-0003-0768-2203
J. G. Green https://orcid.org/0000-0002-1130-6692
D. Hadasch https://orcid.org/0000-0001-8663-6461
A. Hahn https://orcid.org/0000-0003-0827-5642
T. Hassan https://orcid.org/0000-0002-4758-9196
L. Heckmann https://orcid.org/0000-0002-6653-8407
D. Hrupec https://orcid.org/0000-0002-7027-5021
R. Imazawa https://orcid.org/0000-0002-0643-7946
D. Israyelyan https://orcid.org/0000-0002-5804-6605
I. Jiménez Martínez https://orcid.org/0000-0003-2150-6919
J. Jormanainen https://orcid.org/0000-0003-4519-7751
D. Kerszberg https://orcid.org/0000-0002-5289-1509
P. M. Kouch https://orcid.org/0000-0002-9328-2750
H. Kubo https://orcid.org/0000-0001-9159-9853
J. Kushida https://orcid.org/0000-0002-8002-8585
M. Láinez https://orcid.org/0000-0003-3848-922X
A. Lamastra https://orcid.org/0000-0003-2403-913X
E. Lindfors https://orcid.org/0000-0002-9155-6199
S. Lombardi https://orcid.org/0000-0002-6336-865X
F. Longo https://orcid.org/0000-0003-2501-2270
R. López-Coto https://orcid.org/0000-0002-3882-9477
M. López-Moya https://orcid.org/0000-0002-8791-7908
A. López-Oramas https://orcid.org/0000-0003-4603-1884
S. Loporchio https://orcid.org/0000-0003-4457-5431
P. Majumdar https://orcid.org/0000-0002-5481-5040
M. Makariev https://orcid.org/0000-0002-1622-3116
M. Mallamaci https://orcid.org/0000-0003-4068-0496
G. Maneva https://orcid.org/0000-0002-5959-4179
M. Manganaro https://orcid.org/0000-0003-1530-3031
S. Mangano https://orcid.org/0000-0001-5872-1191
S. Marchesi https://orcid.org/0000-0001-5544-0749
M. Mariotti https://orcid.org/0000-0003-3297-4128
M. Martínez https://orcid.org/0000-0002-9763-9155
P. Maruševec https://orcid.org/0000-0002-6748-4615
A. Mas-Aguilar https://orcid.org/0000-0002-8893-9009
D. Mazin https://orcid.org/0000-0002-2010-4005
D. Miceli https://orcid.org/0000-0002-2686-0098
J. M. Miranda https://orcid.org/0000-0002-1472-9690
R. Mirzoyan https://orcid.org/0000-0003-0163-7233
E. Molina https://orcid.org/0000-0003-1204-5516
H. A. Mondal https://orcid.org/0000-0001-7217-0234
A. Moralejo https://orcid.org/0000-0002-1344-9080
T. Nakamori https://orcid.org/0000-0002-7308-2356
C. Nanci https://orcid.org/0000-0002-1791-8235
V. Neustroev https://orcid.org/0000-0003-4772-595X
M. Nievas Rosillo https://orcid.org/0000-0002-8321-9168
C. Nigro https://orcid.org/0000-0001-8375-1907
K. Nilsson https://orcid.org/0000-0002-1445-8683
K. Nishijima https://orcid.org/0000-0002-1830-4251
K. Noda https://orcid.org/0000-0003-1397-6478
S. Nozaki https://orcid.org/0000-0002-6246-2767
J. Otero- Santos https://orcid.org/0000-0002-4241-5875
S. Paiano https://orcid.org/0000-0002-2239-3373
D. Paneque https://orcid.org/0000-0002-2830-0502
J. M. Paredes https://orcid.org/0000-0002-1566-9044
M. Peresano https://orcid.org/0000-0002-7537-7334
M. Persic https://orcid.org/0000-0003-1853-4900
F. Podobnik https://orcid.org/0000-0001-6125-9487
P. G. Prada Moroni https://orcid.org/0000-0001-9712-9916
E. Prandini https://orcid.org/0000-0003-4502-9053
M. Ribó https://orcid.org/0000-0002-9931-4557
J. Rico https://orcid.org/0000-0003-4137-1134
T. Saito https://orcid.org/0000-0001-6201-3761
F. G. Saturni https://orcid.org/0000-0002-1946-7706
K. Schmitz https://orcid.org/0000-0002-9883-4454
F. Schmuckermaier https://orcid.org/0000-0003-2089-0277
J. Sitarek https://orcid.org/0000-0002-1659-5374
V. Sliusar https://orcid.org/0000-0002-4387-9372
D. Sobczynska https://orcid.org/0000-0003-4973-7903
A. Stamerra https://orcid.org/0000-0002-9430-5264
J. Strišković https://orcid.org/0000-0003-2902-5044
D. Strom https://orcid.org/0000-0003-2108-3311
M. Strzys https://orcid.org/0000-0001-5049-1045
Y. Suda https://orcid.org/0000-0002-2692-5891
M. Takahashi https://orcid.org/0000-0002-0574-6018
R. Takeishi https://orcid.org/0000-0001-6335-5317
P. Temnikov https://orcid.org/0000-0002-9559-3384
T. Terzić https://orcid.org/0000-0002-4209-3407
A. Tutone https://orcid.org/0000-0002-2840-0001
S. Ubach https://orcid.org/0000-0002-6159-5883
J. van Scherpenberg https://orcid.org/0000-0002-6173-867X
M. Vazquez Acosta https://orcid.org/0000-0002-2409-9792
S. Ventura https://orcid.org/0000-0001-7065-5342
I. Viale https://orcid.org/0000-0001-5031-5930
C. F. Vigorito https://orcid.org/0000-0002-0069-9195
V. Vitale https://orcid.org/0000-0001-8040-7852
I. Vovk https://orcid.org/0000-0003-3444-3830
F. Wersig https://orcid.org/0009-0006-1828-6117
M. Will https://orcid.org/0000-0002-7504-2083
T. Yamamoto https://orcid.org/0000-0001-9734-8203
A. Acharyya https://orcid.org/0000-0002-2028-9230
P. Bangale https://orcid.org/0000-0002-3886-3739
J. T. Bartkoske https://orcid.org/0000-0002-9675-7328
W. Benbow https://orcid.org/0000-0003-2098-170X
J. H. Buckley https://orcid.org/0000-0001-6391-9661
Y. Chen https://orcid.org/0009-0001-5719-936X
M. Errando https://orcid.org/0000-0002-1853-863X
Q. Feng https://orcid.org/0000-0001-6674-4238
S. Filbert https://orcid.org/0000-0002-2636-4756
L. Fortson https://orcid.org/0000-0002-1067-8558
A. Furniss https://orcid.org/0000-0003-1614-1273
W. Hanlon https://orcid.org/0000-0002-0109-4737
O. Hervet https://orcid.org/0000-0003-3878-1677
C. E. Hinrichs https://orcid.org/0000-0001-6951-2299
J. Holder https://orcid.org/0000-0002-6833-0474
T. B. Humensky https://orcid.org/0000-0002-1432-7771
W. Jin https://orcid.org/0000-0002-1089-1754
M. N. Johnson https://orcid.org/0009-0008-2688-0815

P. Kaaret https://orcid.org/0000-0002-3638-0637
D. Kieda https://orcid.org/0000-0003-4785-0101
T. K. Kleiner https://orcid.org/0000-0002-4260-9186
N. Korzoun https://orcid.org/0000-0002-4289-7106
M. J. Lang https://orcid.org/0000-0003-4641-4201
M. Lundy https://orcid.org/0000-0003-3802-1619
G. Maier https://orcid.org/0000-0001-9868-4700
M. J. Millard https://orcid.org/0000-0001-7106-8502
P. Moriarty https://orcid.org/0000-0002-1499-2667
R. Mukherjee https://orcid.org/0000-0002-3223-0754
W. Ning https://orcid.org/0000-0002-6121-3443
R. A. Ong https://orcid.org/0000-0002-4837-5253
A. Pandey https://orcid.org/0000-0003-3820-0887
M. Pohl https://orcid.org/0000-0001-7861-1707
J. Quinn https://orcid.org/0000-0002-4855-2694
K. Ragan https://orcid.org/0000-0002-5351-3323
D. Ribeiro https://orcid.org/0000-0002-7523-7366
I. Sadeh https://orcid.org/0000-0003-1387-8915
L. Saha https://orcid.org/0000-0002-3171-5039
R. Shang https://orcid.org/0000-0002-9856-989X
D. Tak https://orcid.org/0000-0002-9852-2469
J. Valverde https://orcid.org/0000-0002-8090-6528
D. A. Williams https://orcid.org/0000-0003-2740-9714
S. L. Wong https://orcid.org/0000-0002-2730-2733
S. Buson https://orcid.org/0000-0002-3308-324X
R. Abbasi https://orcid.org/0000-0001-6141-4205
M. Ackermann https://orcid.org/0000-0001-8952-588X
S. K. Agarwalla https://orcid.org/0000-0002-9714-8866
J. A. Aguilar https://orcid.org/0000-0003-2252-9514
M. Ahlers https://orcid.org/0000-0003-0709-5631
J.M. Alameddine https://orcid.org/0000-0002-9534-9189
S. Ali https://orcid.org/0009-0001-2444-4162
K. Andeen https://orcid.org/0000-0001-9394-0007
C. Argüelles https://orcid.org/0000-0003-4186-4182
S. N. Axani https://orcid.org/0000-0001-8866-3826
X. Bai https://orcid.org/0000-0002-1827-9121
A. Balagopal V. https://orcid.org/0000-0001-5367-8876
S. W. Barwick https://orcid.org/0000-0003-2050-6714
V. Basu https://orcid.org/0000-0002-9528-2009
J. J. Beatty https://orcid.org/0000-0003-0481-4952
J. Becker Tjus https://orcid.org/0000-0002-1748-7367
J. Beise https://orcid.org/0000-0002-7448-4189
C. Bellenghi https://orcid.org/0000-0001-8525-7515
S. BenZvi https://orcid.org/0000-0001-5537-4710
E. Bernardini https://orcid.org/0000-0003-3108-1141
E. Blaufuss https://orcid.org/0000-0001-5450-1757
L. Bloom https://orcid.org/0009-0005-9938-3164
S. Blot https://orcid.org/0000-0003-1089-3001
J. Y. Book Motzkin https://orcid.org/0000-0001-6687-5959
C. Boscolo Meneguolo https://orcid.org/0000-0001-8325-4329
S. Böser https://orcid.org/0000-0002-5918-4890
O. Botner https://orcid.org/0000-0001-8588-7306
J. Böttcher https://orcid.org/0000-0002-3387-4236
B. Brinson https://orcid.org/0000-0001-9128-1159
M. A. Campana https://orcid.org/0000-0003-4162-5739
K. Carloni https://orcid.org/0000-0003-3859-3748
J. Carpio https://orcid.org/0000-0003-0667-6557
S. Chattopadhyay https://orcid.org/0009-0006-1352-2248
D. Chirkin https://orcid.org/0000-0003-4911-1345
B. A. Clark https://orcid.org/0000-0003-4089-2245
A. Coleman https://orcid.org/0000-0003-1510-1712
D. A. Coloma Borja https://orcid.org/0000-0003-0007-5793
J. M. Conrad https://orcid.org/0000-0002-6393-0438
D. F. Cowen https://orcid.org/0000-0003-4738-0787
C. De Clercq https://orcid.org/0000-0001-5266-7059
J. J. DeLaunay https://orcid.org/0000-0001-5229-1995
D. Delgado https://orcid.org/0000-0002-4306-8828
P. Desiati https://orcid.org/0000-0001-9768-1858
K. D. de Vries https://orcid.org/0000-0002-9842-4068
G. de Wasseige https://orcid.org/0000-0002-1010-5100
T. DeYoung https://orcid.org/0000-0003-4873-3783
J. C. Díaz-Vélez https://orcid.org/0000-0002-0087-0693
S. DiKerby https://orcid.org/0000-0003-2633-2196
D. Durnford https://orcid.org/0000-0002-6608-7650
M. A. DuVernois https://orcid.org/0000-0002-2987-9691
A. Eimer https://orcid.org/0009-0002-6308-0258
P. Eller https://orcid.org/0000-0001-6354-5209
D. Elsässer https://orcid.org/0000-0001-6796-3205
H. Erpenbeck https://orcid.org/0000-0001-6319-2108
W. Esmail https://orcid.org/0000-0002-0097-3668
P. A. Evenson https://orcid.org/0000-0001-7929-810X
A. R. Fazely https://orcid.org/0000-0002-6907-8020
A. Fedynitch https://orcid.org/0000-0003-2837-3477
C. Finley https://orcid.org/0000-0003-3350-390X
L. Fischer https://orcid.org/0000-0002-7645-8048
D. Fox https://orcid.org/0000-0002-3714-672X
A. Franckowiak https://orcid.org/0000-0002-5605-2219
P. Fürst https://orcid.org/0000-0002-7951-8042
J. Gallagher https://orcid.org/0000-0001-8608-0408
E. Ganster https://orcid.org/0000-0003-4393-6944
A. Garcia https://orcid.org/0000-0002-8186-2459
E. Genton https://orcid.org/0009-0003-5263-972X
A. Ghadimi https://orcid.org/0000-0002-6350-6485
C. Glaser https://orcid.org/0000-0001-5998-2553
T. Glüsenkamp https://orcid.org/0000-0002-2268-9297
S. J. Gray https://orcid.org/0000-0003-2907-8306
S. Griffin https://orcid.org/0000-0002-0779-9623
S. Griswold https://orcid.org/0000-0002-7321-7513
K. M. Groth https://orcid.org/0000-0002-1581-9049
D. Guevel https://orcid.org/0000-0002-0870-2328
C. Günther https://orcid.org/0009-0007-5644-8559
P. Gutjahr https://orcid.org/0000-0001-7980-7285
C. Ha https://orcid.org/0000-0002-9598-8589
C. Haack https://orcid.org/0000-0003-3932-2448
A. Hallgren https://orcid.org/0000-0001-7751-4489
L. Halve https://orcid.org/0000-0003-2237-6714
F. Halzen https://orcid.org/0000-0001-6224-2417
A. Haungs https://orcid.org/0000-0002-9638-7574
J. Häussler https://orcid.org/0009-0003-5552-4821
K. Helbing https://orcid.org/0000-0003-2072-4172
J. Hellrung https://orcid.org/0009-0006-7300-8961
F. Henningsen https://orcid.org/0000-0002-0680-6588
N. Heyer https://orcid.org/0000-0001-9036-8623
C. Hill https://orcid.org/0000-0003-0647-9174
S. Hori https://orcid.org/0009-0007-2644-5955
M. Hostert https://orcid.org/0000-0002-9584-8877
W. Hou https://orcid.org/0000-0003-3422-7185
T. Huber https://orcid.org/0000-0002-6515-1673
K. Hultqvist https://orcid.org/0000-0003-0602-9472
K. Hymon https://orcid.org/0000-0002-4377-5207
W. Iwakiri https://orcid.org/0000-0002-0207-9010

S. Jain https://orcid.org/0009-0000-7455-782X
O. Janik https://orcid.org/0009-0007-3121-2486
M. Jeong https://orcid.org/0000-0003-2420-6639
M. Jin https://orcid.org/0000-0003-0487-5595
N. Kamp https://orcid.org/0000-0001-9232-259X
D. Kang https://orcid.org/0000-0002-5149-9767
W. Kang https://orcid.org/0000-0003-3980-3778
A. Kappes https://orcid.org/0000-0003-1315-3711
T. Karg https://orcid.org/0000-0003-3251-2126
M. Karl https://orcid.org/0000-0003-2475-8951
A. Karle https://orcid.org/0000-0001-9889-5161
M. Kauer https://orcid.org/0000-0003-1830-9076
J. L. Kelley https://orcid.org/0000-0002-0846-4542
A. Khatee Zathul https://orcid.org/0000-0002-8735-8579
A. Kheirandish https://orcid.org/0000-0001-7074-0539
J. Kiryluk https://orcid.org/0000-0003-0264-3133
S. R. Klein https://orcid.org/0000-0003-2841-6553
Y. Kobayashi https://orcid.org/0009-0005-5680-6614
A. Kochocki https://orcid.org/0000-0003-3782-0128
R. Koirala https://orcid.org/0000-0002-7735-7169
H. Kolanoski https://orcid.org/0000-0003-0435-2524
T. Kontrimas https://orcid.org/0000-0001-8585-0933
C. Kopper https://orcid.org/0000-0001-6288-7637
D. J. Koskinen https://orcid.org/0000-0002-0514-5917
P. Koundal https://orcid.org/0000-0002-5917-5230
M. Kowalski https://orcid.org/0000-0001-8594-8666
T. Krishnan https://orcid.org/0000-0002-3237-3114
K. Kruiswijk https://orcid.org/0009-0002-9261-0537
A. Kumar https://orcid.org/0000-0002-8367-8401
N. Kurahashi https://orcid.org/0000-0003-1047-8094
N. Lad https://orcid.org/0000-0001-9302-5140
C. Lagunas Gualda https://orcid.org/0000-0002-9040-7191
M. Lamoureux https://orcid.org/0000-0002-8860-5826
M. J. Larson https://orcid.org/0000-0002-6996-1155
F. Lauber https://orcid.org/0000-0001-5648-5930
J. P. Lazar https://orcid.org/0000-0003-0928-5025
K. Leonard DeHolton https://orcid.org/0000-0002-8795-0601
A. Leszczyńska https://orcid.org/0000-0003-0935-6313
J. Liao https://orcid.org/0009-0008-8086-586X
Y. T. Liu https://orcid.org/0009-0007-5418-1301
L. Lu https://orcid.org/0000-0003-3175-7770
F. Lucarelli https://orcid.org/0000-0002-9558-8788
W. Luszczak https://orcid.org/0000-0003-3085-0674
Y. Lyu https://orcid.org/0000-0002-2333-4383
J. Madsen https://orcid.org/0000-0003-2415-9959
E. Magnus https://orcid.org/0009-0008-8111-1154
E. Manao https://orcid.org/0009-0002-6197-8574
S. Mancina https://orcid.org/0009-0003-9879-3896
A. Mand https://orcid.org/0009-0005-9697-1702
I. C. Mariş https://orcid.org/0000-0002-5771-1124
S. Marka https://orcid.org/0000-0002-3957-1324
Z. Marka https://orcid.org/0000-0003-1306-5260
I. Martinez-Soler https://orcid.org/0000-0002-0308-3003
R. Maruyama https://orcid.org/0000-0003-2794-512X
J. Mauro https://orcid.org/0009-0005-9324-7970
F. Mayhew https://orcid.org/0000-0001-7609-403X
F. McNally https://orcid.org/0000-0002-0785-2244
K. Meagher https://orcid.org/0000-0003-3967-1533
M. Meier https://orcid.org/0000-0002-9483-9450
L. Merten https://orcid.org/0000-0003-1332-9895
T. Montaruli https://orcid.org/0000-0001-5014-2152
R. W. Moore https://orcid.org/0000-0003-4160-4700
M. Moulai https://orcid.org/0000-0001-7909-5812
T. Mukherjee https://orcid.org/0000-0002-0962-4878
R. Naab https://orcid.org/0000-0003-2512-466X
J. Necker https://orcid.org/0000-0003-0280-7484
L. Neste https://orcid.org/0000-0002-4829-3469
H. Niederhausen https://orcid.org/0000-0002-9566-4904
M. U. Nisa https://orcid.org/0000-0002-6859-3944
K. Noda https://orcid.org/0000-0003-1397-6478
A. Obertacke https://orcid.org/0000-0002-2492-043X
V. O'Dell https://orcid.org/0000-0003-0903-543X
J. Osborn https://orcid.org/0000-0002-2924-0863
E. O'Sullivan https://orcid.org/0000-0003-1882-8802
H. Pandya https://orcid.org/0000-0002-6138-4808
N. Park https://orcid.org/0000-0002-4282-736X
E. N. Paudel https://orcid.org/0000-0001-9276-7994
L. Paul https://orcid.org/0000-0003-4007-2829
C. Pérez de los Heros https://orcid.org/0000-0002-2084-5866
M. Plum https://orcid.org/0000-0001-8691-242X
B. Pries https://orcid.org/0000-0003-4811-9863
L. Pyras https://orcid.org/0000-0003-1146-9659
C. Raab https://orcid.org/0000-0001-9921-2668
N. Rad https://orcid.org/0000-0002-5204-0851
Z. Rechav https://orcid.org/0000-0002-7653-8988
A. Rehman https://orcid.org/0000-0001-7616-5790
E. Resconi https://orcid.org/0000-0003-0705-2770
C. D. Rho https://orcid.org/0000-0002-6524-9769
W. Rhode https://orcid.org/0000-0003-2636-5000
L. Ricca https://orcid.org/0009-0002-1638-0610
B. Riedel https://orcid.org/0000-0002-9524-8943
M. Rongen https://orcid.org/0000-0002-7057-1007
A. Rosted https://orcid.org/0000-0003-2410-400X
C. Rott https://orcid.org/0000-0002-6958-6033
T. Ruhe https://orcid.org/0000-0002-4080-9563
J. Saffer https://orcid.org/0000-0002-0040-6129
D. Salazar-Gallegos https://orcid.org/0000-0002-9312-9684
A. Sandrock https://orcid.org/0000-0002-6779-1172
G. Sanger-Johnson https://orcid.org/0000-0002-4463-2902
M. Santander https://orcid.org/0000-0001-7297-8217
S. Sarkar https://orcid.org/0000-0002-3542-858X
H. Schieler https://orcid.org/0000-0002-2637-4778
S. Schindler https://orcid.org/0000-0001-5507-8890
L. Schlickmann https://orcid.org/0000-0002-9746-6872
F. Schlüter https://orcid.org/0000-0002-5545-4363
F. G. Schröder https://orcid.org/0000-0001-8495-7210
L. Schumacher https://orcid.org/0000-0001-8945-6722
S. Sclafani https://orcid.org/0000-0001-9446-1219
L. Seen https://orcid.org/0009-0004-9204-0241
M. Seikh https://orcid.org/0000-0002-4464-7354
S. Seunarine https://orcid.org/0000-0003-3272-6896
P. A. Sevle Myhr https://orcid.org/0009-0005-9103-4410
R. Shah https://orcid.org/0000-0003-2829-1260
N. Shimizu https://orcid.org/0000-0001-6857-1772
B. Skrzypek https://orcid.org/0000-0002-0910-1057
D. Soldin https://orcid.org/0000-0003-3005-7879
P. Soldin https://orcid.org/0000-0003-1761-2495
G. Sommani https://orcid.org/0000-0002-0094-826X
G. M. Spiczak https://orcid.org/0000-0002-0030-0519
C. Spiering https://orcid.org/0000-0001-7372-0074
J. Stachurska https://orcid.org/0000-0002-0238-5608

T. Stezelberger https://orcid.org/0000-0003-2676-9574
T. Stuttard https://orcid.org/0000-0001-7944-279X
G. W. Sullivan https://orcid.org/0000-0002-2585-2352
I. Taboada https://orcid.org/0000-0003-3509-3457
S. Ter-Antonyan https://orcid.org/0000-0002-5788-1369
M. Thiesmeyer https://orcid.org/0009-0003-0005-4762
W. G. Thompson https://orcid.org/0000-0003-2988-7998
J. Thwaites https://orcid.org/0000-0001-9179-3760
K. Tollefson https://orcid.org/0000-0001-9725-1479
S. Toscano https://orcid.org/0000-0002-1860-2240
A. K. Upadhyay https://orcid.org/0000-0003-1957-2626
A. Vaidyanathan https://orcid.org/0000-0001-6591-3538
N. Valtonen-Mattila https://orcid.org/0000-0002-1830-098X
J. Valverde https://orcid.org/0000-0002-8090-6528
J. Vandenbroucke https://orcid.org/0000-0002-9867-6548
N. van Eijndhoven https://orcid.org/0000-0001-5558-3328
J. van Santen https://orcid.org/0000-0002-2412-9728
S. Verpoest https://orcid.org/0000-0002-3031-3206
J. Villarreal https://orcid.org/0000-0001-9690-1310
A. Wang https://orcid.org/0009-0006-9420-2667
E. H. S. Warrick https://orcid.org/0009-0006-3975-1006
C. Weaver https://orcid.org/0000-0003-2385-2559
A. Y. Wen https://orcid.org/0009-0009-4869-7867
C. Wendt https://orcid.org/0000-0001-8076-8877
N. Whitehorn https://orcid.org/0000-0002-3157-0407
C. H. Wiebusch https://orcid.org/0000-0002-6418-3008
L. Witthaus https://orcid.org/0009-0000-0666-3671
M. Wolf https://orcid.org/0000-0001-9991-3923
J. P. Yanez https://orcid.org/0000-0002-5373-2569
Y. Yao https://orcid.org/0000-0002-4611-0075
S. Yoshida https://orcid.org/0000-0003-2480-5105
F. Yu https://orcid.org/0000-0002-5775-2452
S. Yu https://orcid.org/0000-0003-0035-7766
T. Yuan https://orcid.org/0000-0002-7041-5872
A. Zegarelli https://orcid.org/0000-0003-1497-3826
S. Zhang https://orcid.org/0000-0002-2967-790X
P. Zhelnin https://orcid.org/0000-0003-1019-8375
F. D'Ammando https://orcid.org/0000-0001-7618-7527

References

Aartsen, M. G., et al. 2013, Sci, 342, 1242856
Aartsen, M. G., Abraham, K., Ackermann, M., et al. 2016, JInst, 11, P11009
Aartsen, M. G., Ackermann, M., Adams, J., et al. 2017a, JInst, 12, P03012
Aartsen, M. G., Ackermann, M., Adams, J., et al. 2017b, APh, 92, 30
Aartsen, M. G., Ackermann, M., Adams, J., et al. 2018a, Sci, 361, eaat1378
Aartsen, M. G., et al. 2018b, Sci, 361, 147
Aartsen, M. G., et al. 2020a, PhRvL, 124, 051103
Aartsen, M. G., et al. 2020b, PhRvL, 125, 121104
Aartsen, M. G., et al. 2021, JPhG, 48, 060501
Abbasi, R., et al. 2021a, PhRvD, 104, 022002
Abbasi, R., Ackermann, M., Adams, J., et al. 2021b, JInst, 16, P07041
Abbasi, R., et al. 2022a, Sci, 378, 538
Abbasi, R., Ackermann, M., Adams, J., et al. 2022b, ApJ, 928, 50
Abbasi, R., Ackermann, M., Adams, J., et al. 2023a, ApJ, 951, 45
Abbasi, R., Ackermann, M., Adams, J., et al. 2023b, Sci, 380, 1338
Abbasi, R., Ackermann, M., Adams, J., et al. 2023c, ApJS, 269, 25
Abbasi, R., Ackermann, M., Adams, J., et al. 2024, PhRvD, 110, 022001
Abbasi, R., et al. 2025, PoS, 501, 1
Abbott, B. P., et al. 2017, ApJL, 848, L12
Abdollahi, S., Acero, F., Ackermann, M., et al. 2020, ApJS, 247, 33
Abe, H., et al. 2022, MNRAS, 517, 4736
Abe, S., Abhir, J., Abhishek, A., et al. 2024, MNRAS, 535, 1484
Acero, F., Ackermann, M., Ajello, M., et al. 2015, ApJS, 218, 23
Ageron, M., Aguilar, J. A., Al Samarai, I., et al. 2012, APh, 35, 530
Aharonian, F., Akhperjanian, A. G., Bazer-Bachi, A. R., et al. 2006, A&A, 457, 899
Ahlers, M., & Halzen, F. 2018, PrPNP, 102, 73
Ahnen, M. L., Ansoldi, S., Antonelli, L. A., et al. 2017, APh, 94, 29
Ajello, M., Atwood, W. B., Baldini, L., et al. 2017, ApJS, 232, 18
Ajello, M., Baldini, L., Ballet, J., et al. 2022, ApJS, 263, 24
Albert, A., Alves, S., André, M., et al. 2024, JCAP, 2024, 042
Aleksić, J., Ansoldi, S., Antonelli, L. A., et al. 2016a, APh, 72, 76
Aleksić, J., Ansoldi, S., Antonelli, L. A., et al. 2016b, APh, 72, 61
Aleksić, J., MAGIC Collaboration, et al. 2012, APh, 35, 435
Allakhverdyan, V. A., et al. 2023, PhRvD, 107, 042005
Anderhub, H., Backes, M., Biland, A., et al. 2013, JInst, 8, P06008
Ansoldi, S., Antonelli, L. A., Arcaro, C., et al. 2018, ApJL, 863, L10
Arbet-Engels, A., Baack, D., Balbo, M., et al. 2021, A&A, 647, A88
Arnaud, K. A. 1996, ASPC, 101, 17
Astropy Collaboration, Robitaille, T. P., Tollerud, E. J., et al. 2013, A&A, 558, A33
Astropy Collaboration, Price-Whelan, A. M., Sipőcz, B. M., et al. 2018, AJ, 156, 123
Astropy Collaboration, Price-Whelan, A. M., Lim, P. L., et al. 2022, ApJ, 935, 167
Atoyan, A., & Dermer, C. D. 2001, PhRvL, 87, 221102
Atwood, W. B., Abdo, A. A., Ackermann, M., et al. 2009, ApJ, 697, 1071
Ballet, J., Burnett, T., Digel, S., & Lott, B. 2020, arXiv:2005.11208
Barthelmy, S. D., Barbier, L. M., Cummings, J. R., et al. 2005, SSRv, 120, 143
Bayer, M., Dumm, J., Larson, K., Montaruli, T., & Steele, D. 2007, JPhCS, 60, 300
Beck, M., Arbet-Engels, A., Baack, D., et al. 2019, ICRC , 36, 630
Bellm, E. C., Kulkarni, S. R., Graham, M. J., et al. 2019, PASP, 131, 018002
Berge, D., Funk, S., & Hinton, J. 2007, A&A, 466, 1219
Berti, A., & Carosi, A. 2022, Galaxies, 10, 67
Biland, A., Bretz, T., Buß, J., et al. 2014, JInst, 9, P10012
Blaufuss, E., Kintscher, T., Lu, L., & Tung, C. F. 2019, ICRC, 358, 1021
Boller, T., Freyberg, M. J., Trümper, J., et al. 2016, A&A, 588, A103
Boscolo Meneguolo, C., Bernardini, E., Mancina, S., et al. 2024, ICRC, 38, 1500
Breeveld, A. A., Curran, P. A., Hoversten, E. A., et al. 2010, MNRAS, 406, 1687
Bretz, T. 2019, APh, 111, 72
Bretz, T., & Dorner, D. 2010, in Astroparticle, Particle and Space Physics, Detectors and Medical Physics Applications, ed. C. Leroy et al. (Singapore: World Scientific), 681
Bretz, T., Biland, A., Buss, J., et al. 2013, ICRC, 33, 3024
Burrows, D. N., Hill, J. E., Nousek, J. A., et al. 2005, SSRv, 120, 165
Buson, S., Tramacere, A., Pfeiffer, L., et al. 2022, ApJL, 933, L43
Cardelli, J. A., Clayton, G. C., & Mathis, J. S. 1989, ApJ, 345, 245
Cash, W. 1979, ApJ, 228, 939
Cerruti, M., Zech, A., Boisson, C., et al. 2019, MNRAS, 483, L12
Cherenkov Telescope Array Consortium, Acharya, B. S., Agudo, I., et al. 2019, Science with the Cherenkov Telescope Array (Singapore: World Scientific Publishing Co.)
Cogan, P. 2007, ICRC, 3, 1385
Cortina, J. & CTAO LST Collaboration 2023, ATel, 16381, 1
Dazzi, F., Schweizer, T., Ceribella, G., et al. 2021a, ITNS, 68, 1473
Dazzi, F., Schweizer, T., Ceribella, G., et al. 2021b, ITNS, 68, 1473
de Naurois, M., & Rolland, L. 2009, APh, 32, 231
de Menezes, R., Fermi-LAT, H.E.S.S., et al. 2022, PoS, 395
Dekany, R., Smith, R. M., Riddle, R., et al. 2020, PASP, 132, 038001
Dermer, C. D., Ramirez-Ruiz, E., & Le, T. 2007, ApJ, 664, L67
Donath, A., Terrier, R., Remy, Q., et al. 2023, A&A, 678, A157
Dorner, D., Ahnen, M. L., Bergmann, M., et al. 2015, arXiv:1502.02582
Dorner, D., Arbet-Engels, A., Baack, D., et al. 2019, ICRC, 36, 665
Dwek, E., & Krennrich, F. 2013, APh, 43, 112
Evans, P. A., Beardmore, A. P., Page, K. L., et al. 2009, MNRAS, 397, 1177
Evans, P. A., Page, K. L., Osborne, J. P., et al. 2020, ApJS, 247, 54
Fomin, V. P., Stepanian, A. A., Lamb, R. C., et al. 1994, APh, 2, 137
Garrappa, S., Buson, S., Franckowiak, A., et al. 2022, ICRC, 37, 956
Gehrels, N., Chincarini, G., Giommi, P., et al. 2004, ApJ, 611, 1005
Giommi, P., Glauch, T., & Resconi, E. 2020, ATel, 13394, 1
Grasha, K., Darling, J., Bolatto, A., Leroy, A. K., & Stocke, J. T. 2019, ApJS, 245, 3
HESS Collaboration, Abramowski, A., Acero, F., et al. 2013, MNRAS, 434, 1889
Hewett, P. C., & Wild, V. 2010, MNRAS, 405, 2302
HI4PI Collaboration, Ben Bekhti, N., Flöer, L., et al. 2016, A&A, 594, A116
Hill, J., Burrows, D., Nousek, J., et al. 2004, SPIE, 5165, 217

Hoischen, C., Füßling, M., Ohm, S., et al. 2022, A&A, 666, A119
Holder, J., Atkins, R. W., Badran, H. M., et al. 2006, APh, 25, 391
Holder, J., (VERITAS Collaboration), et al. 2006, APh, 25, 391
Karl, M., Padovani, P., & Giommi, P. 2023, MNRAS, 526, 661
Kintscher, T. 2019, KM3NeT Town Hall Meeting, 1, 1, https://indico.cern.ch/event/848390/contributions/3614228/attachments/1964044/3265348/2019_12_18_Marseille_IC 2.pdf
Kintscher, T. 2020, PhD thesis, Humboldt-Universität zu Berlin, Mathematisch-Naturwissenschaftliche Fakultät https://edoc.hu-berlin.de/items/3dc2f42e-293f-4fa5-a067-c698e23da060
Knoetig, M. L., Biland, A., Bretz, T., et al. 2013, ICRC, 33, 1132
Krauss, F., Gregoire, T., Fox, D. B., Kennea, J., & Evans, P. 2020, ATel, 13395, 1
Lundberg, J., Conrad, J., Rolke, W., & Lopez, A. 2010, CoPhC, 181, 683
Mahlke, M., Bretz, T., Adam, J., et al. 2017, ICRC, 301, 612
Maier, G., & Holder, J. 2017, ICRC, 301, 747
Mao, L. S. 2011, NewA, 16, 503
Margiotta, A. 2022, arXiv:2208.07370
Meagher, K. & VERITAS Collaboration 2015, ICRC, 34, 792
Moretti, A., Campana, S., Mineo, T., et al. 2005, SPIE, 5898, 360
Nigro, C., Hassan, T., & Olivera-Nieto, L. 2021, Univ, 7, 374
Oikonomou, F., Petropoulou, M., Murase, K., et al. 2021, JCAP, 2021, 082
Paiano, S., Falomo, R., Padovani, P., et al. 2020, MNRAS, 495, L108
Paliya, V. S., Böttcher, M., Olmo-García, A., et al. 2020, ApJ, 902, 29
Paoletti, R., Cecchi, R., Corti, D., et al. 2007, ITNS, 54, 404
Park, N., et al. 2015, ICRC, 34, 771
Parsons, R., & Hinton, J. 2014, APh, 56, 26
Petropoulou, M., Oikonomou, F., Mastichiadis, A., et al. 2020, ApJ, 899, 113
Poole, T. S., Breeveld, A. A., Page, M. J., et al. 2008, MNRAS, 383, 627
Reichherzer, P., Schüssler, F., Lefranc, V., et al. 2021, ApJS, 256, 5
Reimer, A., Böttcher, M., & Buson, S. 2019, ApJ, 881, 46
Resconi, E. 2022, ICRC, 37, 24
Rodrigues, X., Gao, S., Fedynitch, A., Palladino, A., & Winter, W. 2019, ApJL, 874, L29
Rodrigues, X., Garrappa, S., Gao, S., et al. 2021, ApJ, 912, 54
Rolke, W. A., López, A. M., & Conrad, J. 2005, NIMPA, 551, 493
Roming, P. W. A., Kennedy, T. E., Mason, K. O., et al. 2005, SSRv, 120, 95
Santander, M. 2016, ICRC, 236, 785
Santander, M. 2017, in Proc. of 38th Int. Conf. on High Energy Physics—PoS (ICHEP2016), 282 (Trieste: SISSA), 85
Santander, M., Dorner, D., Dumm, J., Satalecka, K., & Schüssler, F. 2017, ICRC, 301, 618
Santander, M. & VERITAS Collaboration 2016, in Proc. of the 38th Int. Conf. on High Energy Physics (ICHEP2016) (Trieste: SISSA), 85
Santander, M., VERITAS Collaboration, Dorner, D., et al. 2017, ICRC, 301, 618
Schlafly, E. F., & Finkbeiner, D. P. 2011, ApJ, 737, 103
Schleicher, B., Arbet-Engels, A., Baack, D., et al. 2022, ICRC, 37, 760
Schmuckermaier, F., Gaug, M., Fruck, C., et al. 2022, JPCS, 2398, 012011
Schmuckermaier, F., Gaug, M., Fruck, C., et al. 2023, A&A, 673, A2
Schüssler, F., Ashkar, H., Backes, M., et al. 2019, ICRC, 36, 787
Schüssler, F., Backes, M., Balzer, A., et al. 2017, ICRC, 301, 653
Sergijenko, O., Brown, A., Fiorillo, D., et al. 2022, ICRC, 37, 975
Stadnik, M., & Romani, R. W. 2014, ApJ, 784, 151
Stein, R., Franckowiak, A., Kowalski, M., & Kasliwal, M. 2019, ATel, 13125, 1
Stein, R., Velzen, S. v., Kowalski, M., et al. 2021, NatAs, 5, 510
Stratta, G., Capalbi, M., Giommi, P., et al. 2011, arXiv:1103.0749
Truebenbach, A. E., & Darling, J. 2017, ApJS, 233, 3
Wood, M., Caputo, R., Charles, E., et al., 2018 Fermipy: Fermi-LAT data analysis package, Astrophysics Source Code Library, ascl:1812.006
Ye, Z. P., Hu, F., Tian, W., et al. 2022, arXiv:2207.04519
Zanin, R., Carmona, E., Sitarek, J., et al. 2013, ICRC, 33, 2937